POLITECNICO DI TORINO

Master's Degree in Biomedical Engineering

Master's Degree Thesis

Dual drug inhibitors loaded on a nanotheranostics and biomimetic platform for the synergistic treatment of pancreatic ductal adenocarcinoma

Supervisor
Prof. Valentina Cauda
Co-supervisor
Dr. Sugata Barui

Candidate
Rocío María García Montero

Academic Year 2021/2022

March, 2022

Abstract

Rapid growth in bionanotechnologies towards the improvement of therapeutic strategies against cancer relies on the development of nanomedicine products, such as nanoparticles (NPs). NPs have enormous therapeutic potential for treating tumours, as they represent a way of preparing multifunctional platforms, achieving sophisticated targeting strategies, enhancing drug delivery, attenuating drug toxicity on healthy organs, and protecting drugs from rapid clearance. Furthermore, the use of multifunctional theranostic nanocarriers allows the simultaneous diagnosis and therapy of cancer, in conjunction with the co-delivery of drugs for combination therapies. However, challenges in the development of optimized NPs have to be addressed: their toxicological characterization, in terms of biocompatibility and immunogenicity, their stability in biological media, and their targeting selectivity are current limitations to overcome, to fulfil safety requirements and enhance site-specific delivery.

This Master's Thesis work is inserted in a project funded by the European Community under Grant Marie Skłodowska-Curie Actions. It focuses on the development of a nanotheranostics and biomimetic NPs-based platform loaded with dual drug inhibitors for the synergistic diagnosis and treatment of one of the most lethal and resistant types of cancer, pancreatic ductal adenocarcinoma. The developed nanoconstruct consists of a core of zinc oxide nanocrystals doped with the rare earth element gadolinium. The advantage of using this kind of nanocrystals relies on its low intrinsic toxicity and strong resistance to microbes, as well as its magnetic properties, enabling it to work as a contrast agent in magnetic resonance imaging (MRI) for diagnostic purposes. The functionalization of the nanocrystal surface with oleic acid and amino-propyl groups permits a fair stabilization in water-based media, the covalent labelling with fluorescent dyes, and the physical adsorption of two hydrophobic therapeutic agents, namely Sorafenib and Vismodegib. Finally, a lipid bilayer coating is provided on the nanocrystal-drug ensemble. This lipid bilayer not only enhances the biostability of the nanoconstruct but also allows the incorporation of a pancreatic cancer target peptide, CKAAKN, to address the tumour site. All these components of the nanoconstruct concur to the preparation of a multifunctional theranostic nanoplatform, able to address the tumour microenvironment by active tar-

geting of some crucial signal pathways, with the consequent site-specific delivery of the above-mentioned drugs. The nanoplatforms obtained are characterized in terms of chemical structure and composition, morphology, dimension, and zeta potential. Their performance is tested in terms of cytotoxicity, cellular uptake, and apoptotic events, on two pancreatic cell lines (specifically BxPC-2 and a metastatic one, AsPC-1).

The preliminary in vitro results indicate that the dual drug-loaded nanoconstructs increased the treatment efficacy compared to their free drug counterparts, proving to be a feasible multimodal theranostic approach that deserves further research.

GRAPHICAL ABSTRACT

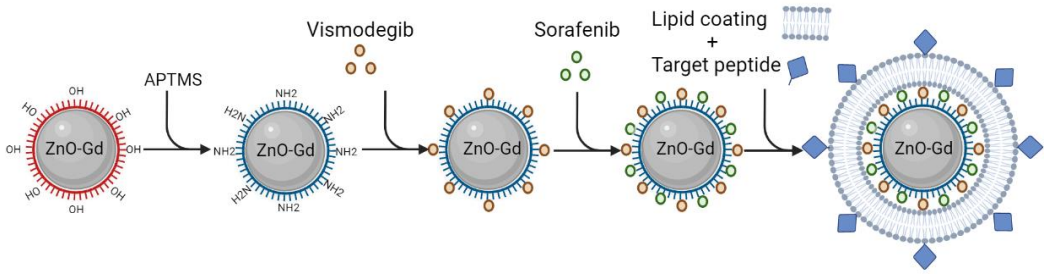

Figure 0.1: Dual drug-loaded nanoconstructs. Synthesis, functionalization, drug loading process and lipidic coating with an active targeting peptide

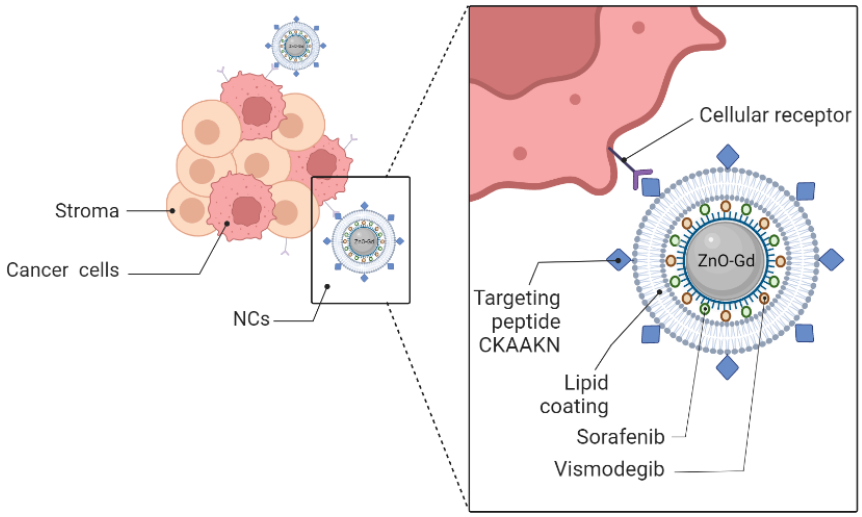

Figure 0.2: Active targeting by the interaction of CKAAKN peptide with tumour cells

Contents

List of Figures

List of Tables

1 State of the Art

1.1 Pancreatic Cancer

Cancer is a group of diseases developed by the uncontrolled growth and spread of abnormal cells, that can cause mortality if not treated [1]. The causes of cancer are not yet completely elucidated. However, risk factors have been classified into two categories; potentially modifiable risk factors include excess body weight and tobacco and alcohol use, while not modifiable factors are represented by age and inherited genetic mutations, among others.

Pancreatic cancer (PC) is a highly fatal malignancy, which is increasingly becoming a common cause of cancer mortality [2]; in the next 20 to 30 years, it is projected to become the second leading cause of cancer death in the United States [1]. According to the American Cancer Society, in 2022, an estimated 62,210 new cases of pancreatic cancer will be diagnosed in the USA and 49,830 people will die from the disease.

More than 90% of PC cases are developed in the exocrine tissue, being pancreatic ductal adenocarcinoma (PDAC) the most common type of PC. 5-year survival rate at the time of diagnosis is 11% in the USA, and near 80–85% of patients present either metastatic or unresectable disease [2]. Even for people diagnosed with local disease (represented by 13% of cases), the 5-year survival rate is only 42% [3].

Three are the main obstacles to the improvement of outcomes in PDAC patients: diagnosis in early stages of the disease are not yet able to be performed, high resistance to various therapeutic strategies is developed, and in case of surgical resection in early localized disease, the risk of PC recurrence continues to be high.

Patients typically present with advanced disease due to lack of or vague symptoms when the cancer is still localised. Indeed, early stages of PC do not present specific signs and symptoms, making screening tests difficult to be developed, diminishing the possibility to reduce mortality caused by this disease. When diagnosed at later stages, the prognosis is poor, as the possibility of cancer spreading to other districts of the body are higher, and therefore the disease becomes more difficult to treat.

1.1.1. Overview

The tumour microenvironment (TME) of PC is characterized by fibrous and connective growth, namely desmoplasia, showing the presence of both stromal and immune cells, and a dense extracellular matrix (ECM), as depicted in Figure 1.1. Pancreatic cancer stroma plays a major role in illness development, as it regulates vascularization, tumour growth, metastasis, drug responsiveness, and immune landscape. Indeed, the cells of the stroma, namely cancer-associated fibroblasts (CAFs), can promote PC progression and dampen the chemotherapeutic response. The bulk of the tumour mass is represented by ECM, which consists of a dense network of different types of proteins, proteoglycans, and enzymes. One important component is hyaluronic acid (HA), a glycosaminoglycan. It causes an increased interstitial pressure, which leads to vascular collapse and reduced tumour perfusion, limiting the accessibility of chemotherapeutic agents to cancer cells [4].

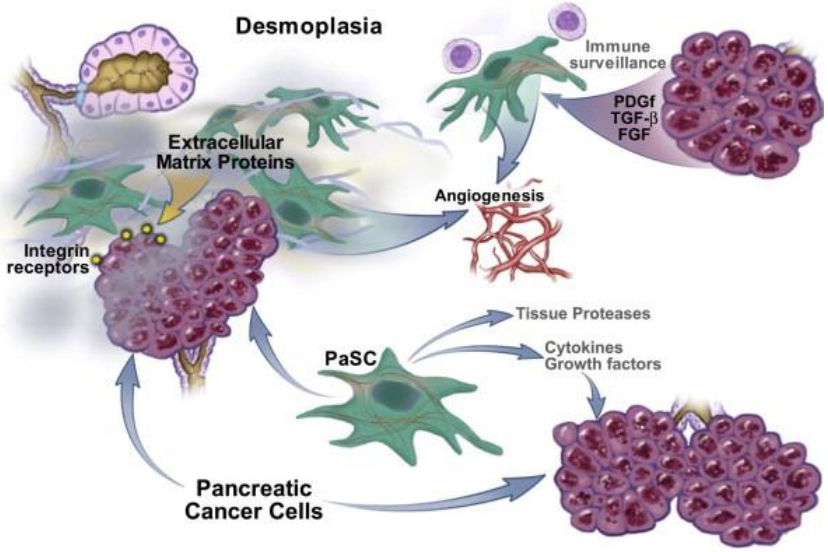

Figure 1.1: Desmoplasia in Pancreatic Cancer

PC is highly hypoxic in comparison with the healthy surrounding tissue. This is due to the desmoplastic environment of the tumour, which limits the availability of oxygen and nutrients in cancer cells. This hypoxic environment characteristic makes it difficult to use antiangiogenic therapy, as results would only worsen the situation, promoting cancer stem cell enrichment, invasion and metastasis, and promoting chemoresistance.

Pancreatic Cancer is characterized by genetic mutations and its development depends on the TME. Hedgehog Pathway (Hh) is a prominent signal-

ling pathway, which is related to high proliferation of the tumour and reduced survival rate, as it is responsible for the development of desmoplasia in the tumour site.

The importance of addressing not only tumour tissue but also the stromal environment for successful treatment of PC was demonstrated in 2018 by Jun Zhao et. al. In this work, the use of multifunctional nanoparticles loaded with two different drugs was proposed. Cyclopamine (CPA) addressed the stroma-producing CAFs, and paclitaxel (PTX) inhibited tumour proliferation. The main aim was to increase the microvessel density, reducing the matrix stiffness and thus alleviating hypoxia, in order to modulate the stroma. Results obtained were promising as animal survival was extended, promoting the development of this type of multifunctional nanoconstructs for drug delivery.

Drugs that address the Hedgehog signal pathway are termed SHH inhibitors. Their therapeutic action presents the inconvenience of generating the loss of collagenous ECM, which can lead to a more invasive and metastatic tumour, as they induce the epithelial-mesenchymal transition to tumour cells, thus provoking failure of the treatment.

Consequently, in this study, the doses of SHH inhibitors were regulated in order to permit the beneficial effects of their actions, without suffering from the drawbacks on the TME and the worsening of the cancer disease [5]. Preclinical studies highlighted that radical stromal depletion via Hedgehog deletion, using SHH inhibitors, resulted in more aggressive, poorly differentiated, and highly vascularized tumours, together with proven beneficial effects such as the depletion of cancer stem cells and the sensitization of tumour cells to radiotherapy.

As a consequence, the importance of modulating rather than totally suppressing the tumour microenvironment was taken as a key concept to pursue. Results obtained suggested that limiting some stromal components rather than completely eliminating them may help to gradually allow therapeutic agents to reach tumours without risking enhancing metastases formation.

Pancreatic cancer vascular structure is characterized by heterogeneous blood perfusion, due to tortuous chaotically organized vessels, vascular compression, reduced blood flow in some regions, causing low extracellular pH and hypoxia. As flow stasis is developed, the vascular endothelial growth factor (VEGF) release is upregulated, thus creating a vicious cycle.

The importance of administrating anti-VEGF drugs in this kind of tumour, tuning their dose, was highlighted by an article in the Journal of Clinical Oncology, published in 2013. The normalization of the vascular structure was hypothesized to play a key role; paradoxically needing functional blood vessels that would permit the entrance and delivery of the therapeutics, like anti-VEGF drugs, that would then destruct such vessels used. [6]

It is therefore crucial not to target a single deregulated pathway, as it can be inefficient owing to redundant signalling and complex crosstalk. More than one of the TME components have to be addressed to have a chance to defeat this kind of cancer. Therefore, a combination of druggable key signalling compartments needs to be identified and targeted. To do so, and to reach the tumour site more effectively, tuneable nanodevices can be developed, for overcoming the limitations of traditional cancer therapies.

1.1.2.Traditional therapies

As previously said, one of the main reasons for pancreatic cancer's high lethality is the lack of early diagnosis. Once diagnosed, traditional treatment options include surgery, radiation therapy, and chemotherapy. They may relieve symptoms, improve a bit the quality of life of the patient, and/or extend survival, but seldom produce a cure. [3].

Surgery represents the only treatment that offers curative potential [2]. Resection techniques include total pancreatectomy, distal pancreatectomy plus splenectomy and pancreaticoduodenectomy [7]. However, fewer than 20% of patients are diagnosed with early-onset PC, and are therefore candidates for surgery, because cancer has usually spread beyond the pancreas at diagnosis, developing metastatic disease and showing poor performance.

For those who do undergo surgery, adjuvant treatment with chemotherapy (and sometimes radiation) may lower the risk of recurrence and might help people live longer [3]. Studies have shown that after radical resection, adjuvant chemotherapy can significantly improve disease-free survival and overall survival of patients with PC [7], being Gemcitabine a well-known and widely used chemotherapy agent, which represents generally the first choice of treatment. On the other hand, radiation therapy uses X-rays to destroy or damage cancer cells, making them unable to proliferate. Radiotherapy is mainly used in patients with locally advanced PC [7]. However, the main drawback is that the surrounding tissue is greatly damaged.

For advanced disease, chemotherapy (sometimes along with a targeted therapy drug) or immunotherapy might be used. Clinical trials are testing several new targeted agents and immunotherapies.[3]

1.2 Theranostic platforms

Theranostic approaches have attracted great interest in recent times. They are strategies that combine diagnosis and therapy, allowing the simultaneous detection of targets in real-time, the monitoring of drug distribution, and the evaluation of therapeutic responses, reducing side effects and providing bigger therapeutic windows.

Synergistic therapeutic effects can be reached by the use of nanotechnology-assisted cancer theranostics, or cancer nanotheranostics. These systems present many unique advantages; oncotherapy and diagnosis can be developed due to specific optical properties of some nanocarriers, real-time imaging can generate guided therapy of the disease, and the platforms' properties can be tuned to develop specific interaction with biological processes [8].

The development of nanoparticle-based transport platforms for co-delivery of diagnosis agents and therapeutic drugs is going through rapid development. Nanoparticles are characterized by a large surface area/volume ratio, in a small size of the particle (1-100nm), demonstrating high drug-loading capacities. Therefore, the co-carry of different therapeutic drugs, the loading of imaging/diagnosis agents, and the tuning of their optical and magnetic properties are possible; always guaranteeing easy blood circulation, and the possibility of being modified to allow the internalization into the cells.

Furthermore, some nanomaterials have unique physicochemical properties that allow their behaviour as imaging agents themselves, thus representing a promising strategy to overcome the early diagnosis limitation, also helping to reduce the quantity of time between the detection of the tumour and the beginning of the therapy.

The main goal in their development is the reaching of the target tumour site. To this end, the Nanoconstruct has to be able to circulate for long periods into the patient's body, without being eliminated by biological processes, and to reach such specific site. Targeting ligands can be introduced on nanoparticles, including aptamers, antibodies and different peptides. The specific recognition between ligands and the receptors on the surface of tumour tissues can improve the targeting efficiency. On the other hand, the

inhibition of the biological clearance by the patients' systems, and the enhanced circulation time into the bloodstream are two milestones to reach.

1.2.1.Passive targeting

Passive targeting permits the deposit of the drug-carrier structures at a specific site as a result of physicochemical factors. Aberrant molecular and fluid transport dynamics are induced by abnormal vessels in tumour tissues. Colloidal size drug delivery systems, resembling nanoparticles, are favourably gathered into solid tumours. Nanoparticles able of evading reticuloendothelial system capture, because of their specific size and surface fulfilled requirements, can travel in the bloodstream and passively accumulate in the targeted tumour surrounding, following their well-known enhanced permeability and retention (EPR) effects [9]; which is due to the enlarged vascular permeability together with the defective lymphatic drainage of fast-growing tumours, as depicted in Figure 1.2.

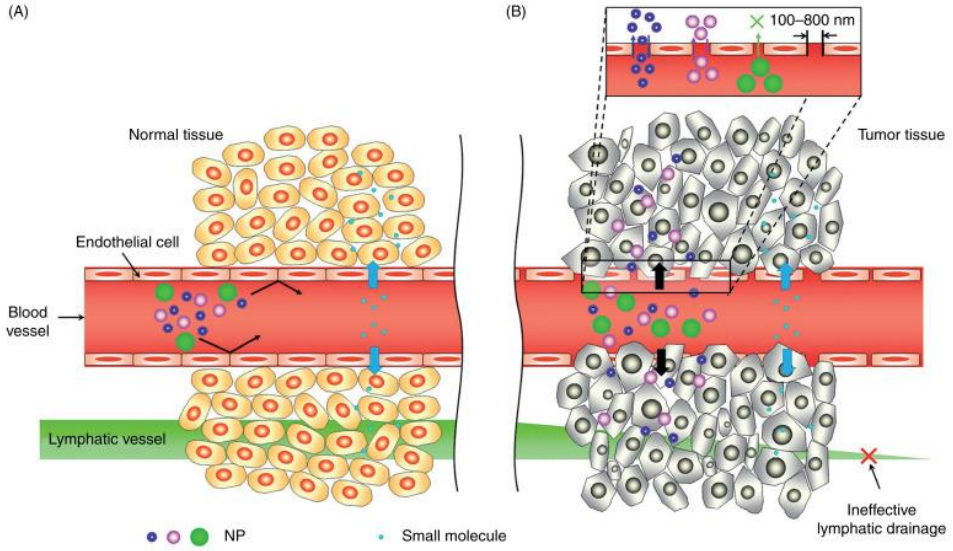

Figure 1.2: Scheme of Enhanced Permeability and Retention effect[10].

The surface modification of the nanoparticles with the addition of polyethylene glycol (PEG) has been identified to defend the nanosystems from developing immunogenic responses while circulating in the body, developing cytotoxic and inflammatory effects that can carry to cell death. Thanks to this PEG coating, the nonspecific adsorption of serum proteins is reduced, opsonization along with clearance by the reticuloendothelial system (RES) are diminished, as well as the instantaneous clearance of the particles.

Immunogenic response can also be reduced by the coating of the NPs with cell membranes' resembling constructs, i.e. synthetic or biologically derived lipid bilayers. This approach aims at preventing the formation of aggregates while facilitating the uptake of the NCs into the cells by membrane fusion. However, as no chemical bonds between the NPs and the lipids are developed, the risk of detachment of the coating is high.

The EPR effect is highly dependent on the type of tumour, and its developed leaky vasculature. In the case of Pancreatic Ductal Adenocarcinoma (PDAC), the dense tumour stroma present has the effect of lowering the EPR effect, and thus the performance of the nanoconstructs in the treatment of the tumour. Therefore, Lui et al. suggested transcytosis as a major mechanism for drug delivery in the case of PDAC. To this end, the functionalization of the nanoconstructs with tumour-specific integrins' receptors is considered an optimal approach for the enhancement of their cancer cell uptake [11].

1.2.2. Active targeting

For the specific recognition of cancerous cells, and the limitation of the damages provoked on the surrounding healthy cells, active targeting strategies are developed. A targeting moiety (e.g. ligand, antibody, peptide) has to be introduced onto the nanoparticle system to aim at specific receptors present in cancer cell biology, which may be highly upregulated, in comparison to the healthy surrounding cells and tissues.

By doing so, nanoparticles will be able to recognize and bind to target cells through ligand-receptor interactions. Bound nanoparticles can be internalized before the drug is released inside the cell, resulting in less off-target drug release compared to passively targeted systems [12].

These types of functionalizations can be carried out with different types of signalling molecules, such as peptides, antibodies, oligonucleotides and DNA-containing complexes. Their action is depicted in Figure 1.3.

Peptides represent the mainly exploited tool for active targeting, due to their high resistance to thermal treatments and pH variations. Besides, their steric hindrance has no particular impact on the nanoconstruct's size. Therefore, some types of NCs, such as ZnO nanocrystals were demonstrated to have an increased targeting agent potential. They allow the decoration, in multiple binding sites of their surface, with peptides of different types simultaneously, thus representing a highly performant tool to this aim.[13]

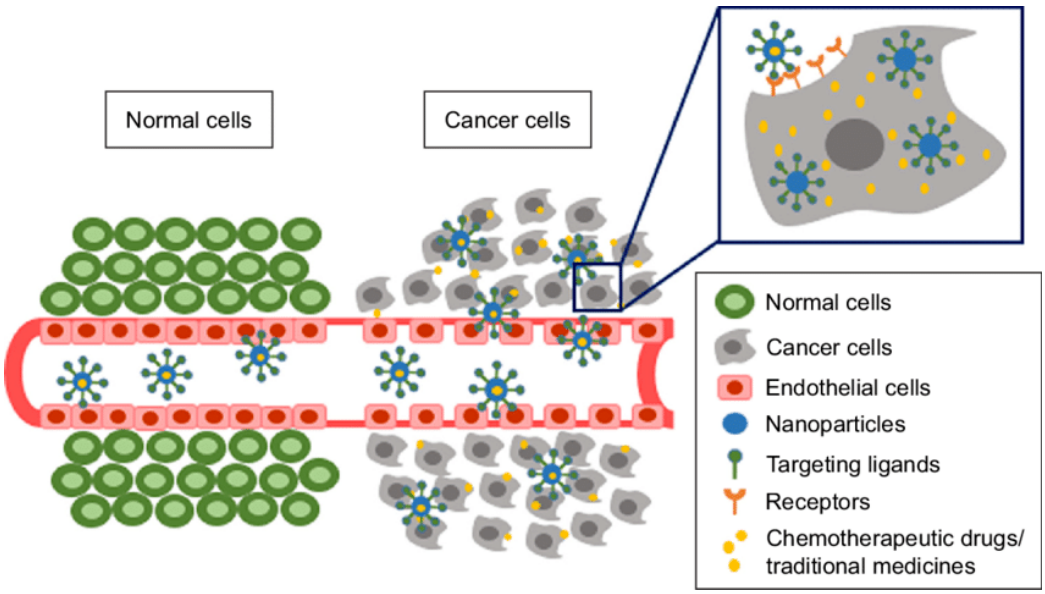

Figure 1.3: Scheme of active targeting strategy

1.2.3. Drug delivery systems

Nanoparticle-based drug delivery provides appealing opportunities for safer and more effective cancer treatment. Their use could minimize the collateral side effects of cancer therapies, by reducing the overall amount of drugs used, and the repercussion on healthy surrounding tissues, targeting only the specific sites of cancer cells.

Organic materials can be used as nanocarrier systems for drug delivery, represented by dendrimers, liposomes, and albumin, among others. Liposomes present a high biocompatibility and encapsulation capacity of both hydrophilic, inside the aqueous core, and hydrophobic, within the lamellae, drugs. Disadvantages of this type of nanocarriers include the slow drug release and hydrophilic drug leakage, along with the limited shelf life in the solution. For an increased circulation time in the bloodstream, and to improve the immunogenicity of the nanoconstructs, "stealth" liposomes were developed. They consist of the coating of the liposome surface, using hydrophilic polymers such as Poliethylene Glycol (PEG) or chitosan [14].

On the other hand, Inorganic nanocarriers have acquired an interest in cancer drug delivery, as their properties include a large surface/area ratio, which permits high drug loading capacity, bioavailability and biocompatibility, and controlled drug release. However, their main drawback when aiming to the delivery in the tumour microenvironment is represented by their poor stability and high aggregation in biological fluids [15]. This type of

nanocarriers includes mesoporous silica, magnetic and metal oxide nanoparticles, and quantum dots.

Zinc Oxide nanoparticles are especially attractive for cancer drug delivery due to their intrinsic properties which demonstrate high potential for effective treatment development [16].

1.3 Zinc-Oxide Nanocrystals (ZnO NCs)

This Master's Thesis work aim was the development of a nanoconstruct consisting of a core of Zinc oxide (ZnO) Nanocrystals. Nanoscaled ZnO has peculiar physical and chemical properties, showing promising prospects for biomedical applications, such as anticancer, drug delivery, antibacterial, and diabetes treatment; anti-inflammation; wound healing; and bioimaging [16]. As Zinc exists extensively in all body tissues, ZnO NPs, with such small particle sizes, can be easily absorbed by the body, thus demonstrating low toxicity and high biocompatibility. They have superior antibacterial and antimicrobial properties, and their pH-sensitivity properties assure an effective endosomal release. ZnO was then taken as a potential candidate for the generation of nanotheranostics platforms.

Wurtzite's (B4) crystalline structure is obtained when exploiting ZnO as a nanomaterial. This is a consequence of the more stable configuration at environment conditions. Its form is represented in Figure 1.4, showing two interpenetrating hexagonal closed pack(hcp) sublattices. Properties such as piezoelectricity are developed because of the particular disposition of the different atoms that conform the structure, whereas optical properties include a wide band gap, equal to 3.37 eV, improving the suitability for theranostic applications.

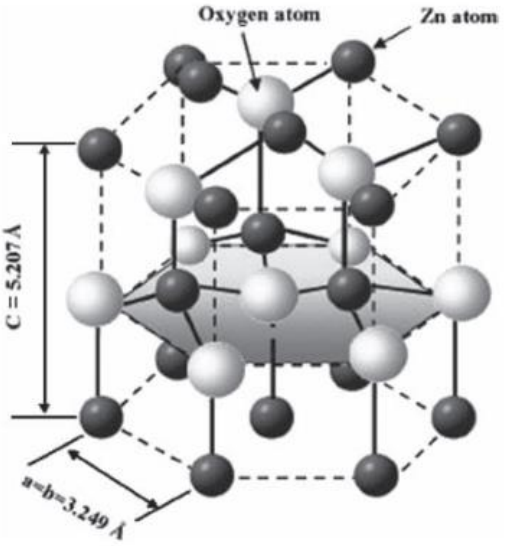

Figure 1.4: Scheme of ZnO Nanocrystals' wurtzite crystalline structure

1.3.1. Chemical Synthesis

The development of a controlled structure of the NPs is essential for the development of biological activities of the Nanoparticles, as they are dependent on their size distribution and morphology, surface chemistry and particle reactivity in solution.

Stable ZnO NPs preparation methods include the chemical precipitation method, sol-gel method, solid-state pyrolytic method, solution-free mechanochemical method, and biosynthesis method.

Sol-Gel is a chemical precipitation method, which permits obtaining mono or polycrystalline materials, such as colloids or powders. It consists of using a highly purified zinc forerunner such as zinc acetate, zinc nitrate or zinc sulfate and a precipitator solution, such as sodium hydroxide or ammonium hydroxide. Using this technique, obtaining ZnO NPs is a simple and easily controlled process.

Typically, these reactions, whose advantages are the use of non-toxic solvents and low synthesis temperatures, occur through the following reaction steps:

$$Zn^{2+} + 2OH^{-} \rightarrow Zn(OH)_2$$

$$Zn(OH)_2 + 2OH^{-} \rightarrow Zn(OH)^{2-}_4$$

$$Zn(OH)^{2-}_4 \rightarrow ZnO + H_2O + 2OH^{-}$$

1.3.2.Structural properties

Biomedical research has been actively promoted by the use of Zinc Oxide Nanocrystals (ZnO NCs). These nanoparticles have particular structural, physical, optical and chemical properties, that are not present in bulk dimensions of the material. The chemical reactivity of the surface of the particles increase, because larger number of constituting atoms are exposed to the surface. Also the area/volume ratio is increased.
ZnO NCs have low toxic properties, and can be used for biomedical applications, because of their capacity of being internalized by cells. This phenomenom occurs thanks to the EPR effect, which allows the permeation and retention of this type of particle into the sites of the tumour, when exhibiting nanoscale dimensions, i.e. diameter between 50 and 200 nm. Particular attentions thus need to be taken to the parameters that tune the preparation and synthesis process of this particular material, as NCs obtained need to have a controlled shape, size and dispersity. The precursor typess and concentrations, types of solvent, types of capping molecule, reaction time and temperature are parameters to be set for obtaining such specific properties.
As capping molecules remains into the created Nanocrystal, and in order to compute biomedical processes, they need to express low cytotoxicity and high solubility in reaction media. Different capping agents were investigated, and it has been seen that they can improve the NCs size distribution and medium-long term stability.
ZnO when nanodimensioned is demonstrated to have a toxic nature towards different bacterial systems, which means that ZnO NCs can be exploited for antibacterial applications. ZnO dissolution is enhanced thus releasing zion ions which increases the number of ROS, activating the apoptosis signalling pathway, inducing the death of bacteria.
It has been clearly exhibited that the design parameters for the NCs systems define the properties of the constructs, enabling the maximization of the therapeutic capabilities and enhancing their biomedical application properties.

1.3.3.Cytotoxicity

Both the capability of ZnO NCs to induce oxidative stress by the generation of reactive oxygen species (ROS)[17] and the release of Zn^{2+} ions, play a major role in the strong cytotoxic effects on cells. These aspects make ZnO a compound of election for cancer treatment.

ROS generated by the excitation of an electron, which passes from the valence to the conduction band; a reaction with water molecules takes place, and the result is the generation of hydroxyl and peroxide radicals, as follows:

$$^{*}O_2 + H^{+} \rightarrow HO_{2}^{*}$$

$$HO_{2}^{*} + H^{+} + e^{-} \rightarrow H_2O_2$$

The generation and accumulation of ROS at an intracellular level cause protein denaturation and DNA damage, as well as cell membrane damage, all due to the increase of oxidative stress conditions. When all these processes take place, cells go through apoptosis or autophagy, destructing themselves[18].

On the other hand, Zinc ions are involved in many cellular processes and do not exhibit intrinsic toxicity when present in low concentrations. Concentrations of intracellular Zinc ions are constantly regulated by zinc-transporting and zinc-sequestering proteins. When internalized into the cells, specifically into low pH environments such as lysosomes and endosomes, ZnO NCs dissolve and release Zinc ions in high quantities. This causes homeostasis to be disrupted and a lot of processes are affected, being the most significant the mitochondrial damage, which results in the loss of protein activity balance, causing the activation of cell apoptotic pathways [16].

Extracellular release effects have not been yet elucidated, thus making it important in each case to assess and control the dissolution rate of the compound when exposed to extracellular media. Improvements can be achieved through the functionalization and the doping of the ZnO NCs. [18]

1.3.4.Doping of ZnO-NCs with Gadolinium

Biomedical applications of ZnO NCs can be enhanced by the doping process, which consists of modifying the host's properties by inserting specific ions into the crystal lattice. This modification can potentially be exploited for the design of multifunctional platforms as it improves not only the magnetic and optical properties of the pure element but also the piezoelectric ones.

Specifically, ZnO doping was carried out in precedence with transition metal dopant ions and rare-earth ions. Manganese (Mn) makes part of the first category. When ZnO NCs were doped with this material, room temperature ferromagnetic properties were demonstrated, together with the devel-

oped ability to work as Diluted Magnetic Semiconductor (DMS). Furthermore, antibacterial activity was increased, and cytotoxicity was not diminished, as ROS production was enhanced by the dopant's presence.

Gadolinium, instead, is a rare earth ion. Doping of ZnO with this element permitted an increase in photocatalytic effects and the enhancement of optical properties.

Iron doped ZnO NCs exhibited improved electrochemical behaviours, as well as enhanced optical and magnetic properties.

The main aim of this Master Thesis work was the development of a ZnO-based nanotools for theranostic purposes. Pristine ZnO-Ncs have the potential for their use in biomedical applications because of their intrinsic properties for therapeutic purposes. However, their properties regarding diagnosis can be yet enhanced, and for this end, Gd-doped ZnO NPs were developed. Gadolinium was proved to be a magnetic resonance imaging (MRI) contrast agent, thus making it possible to diagnose cancer also when located deep in the retroperitoneal cavity, by tracking the drug-loaded nanoparticles when they are aimed at pancreatic cancer.

1.3.5.Surface functionalization

Nanomaterials-based nanomedicine is lately becoming a potentially effective alternative to traditional cancer therapies, through their high drug delivery capacity and easily surface modification.

Modification of the surface can be both physical and chemical, and properties such as electrostatic characteristics, agglomeration processes and solubility and stability of the platform can be improved, therefore enhancing the NPS effectiveness.

Functionalization could be defined as the coating or capping of the ZnO NCs' surface, including for example the exposure of specific functional groups, which can carry improvements in drug loading and molecule binding capacities, targeting capabilities, stability in solution and internalization rate in cells [19].

Imaging properties can also be enhanced and if combined with an active and specific targeting strategy and a therapeutic activity, efficient nanotheranostics platforms can be obtained.

Multiple studies have developed functionalized ZnO NCs, for overcoming agglomeration problems, preserving water solubility and enhancing probes/drugs bioconjugate attachment and drug delivery[20].

To date, the modification and functionalization of ZnO nanoparticles were carried out employing different capping agents or polymeric compounds.

P. Saravanan et. al. exploited the reaction between 3-aminopropyltriethoxysilane (APTS) and the hydroxyl groups on the nano ZnO surface, for the introduction of reactive -NH_2 groups onto it. Results obtained showed a reduced agglomeration of the functionalized NCs, and enhanced spherical morphology and mono-dispersity with respect to pristine NCs, improving also their suspension stability. The final aim of this study was the attachment of inorganic fillers to the NCs surface, which was successfully obtained by hydrogen bonds. [21]

Liao et al. also aimed at the development of amine-functionalized surfaces, in this case of ZnO nanosheets. They exploited monoethanolamine (MEA), which possesses a hydroxyl (-OH) group for covalent attachment on ZnO, and a primary amine (-NH_2) group to endow the amine-functionalized surface. The final aim of the work was the enhanced photocatalytic activity for CO_2 reduction, which was greatly enhanced [22]

For maximizing the therapeutic efficiency of ZnO NCs, immobilization of drugs on their surface is the main goal. Recently, a multi-step functionalization process was evaluated. In this study, a Polyglycerol (PG) layer was grafted to the ZnO NPs, which is then coupled with arginine-glycine-aspartate (RGD) peptide. The following encapsulation of the anti-cancer drug Doxorubicin hydrochloride (DOX) was permitted by the previously mentioned functionalization. In this case, PG coating reduced the aggregation of NPs, and the treatment results showed interesting performance of the drug-loaded NCs towards the target tumour cells, having an active targeting and enhanced therapeutic effects, thus damaging the cancer tissue [23].

Functionalization can be therefore described as an important step to improve NCs' theranostic potential, increasing their stability in biological media, improving the drug loading and releasing capacities and specific targeting endeavours.

Nonetheless, the main limitation is yet to be overcome. Functionalization carries with it an increase in the absolute surface charge, thus increasing the immunogenicity of the construct, as it can be easily recognized by the patient's immune system. To surmount this drawback, a biomimetic coating approach can be developed, in order to reduce the capacity of the immune system to recognize the nanoplatforms. Indeed, the biocompatible coating

was proved to not affect the anticancer action of ZnO NPs but further increase the targeting effects against cancer cells and improve the safety against normal cells [16].

1.3.6.Phospholipidic coating

One of the main challenges in the correct development of nanoconstructs is to guarantee their biocompatibility, colloidal stability in aqueous solution and specific cell targeting functions. Nano-biointerfaces are therefore proposed as important candidates for the coating of inorganic NPs' surfaces, consisting of lipid molecules that present a hydrophobic and a hydrophilic region. NPs' coating reduces cytotoxic effects, avoids immunogenic or thrombogenic responses, and improves stability towards aggregation. [24]

The possibility of combining different amphiphilic functional molecules for the creation of the shell that coats the NPs brings further flexibility to the nanoconstructs' functionalities.

Recent studies investigated the design of lipid-coated silica NPs loaded with four drugs against the pancreatic ductal adenocarcinoma, and tests on cells were carried out. The lipid coating was composed by a mixture of 1,2-Distearoyl-sn-glycero-3-phosphocholine (DSPC), cholesterol and 1,2-distearoyl-sn-glycero-3-phosphoethanolamineN-[methoxy(polyethyleneglycol)-2000] (DSPE-PEG2000). Results showed increased stability of the NPs towards aggregation, strong reduction of drug toxicity in healthy tissues and an improved and favourable NPs internalization[24][25].

Other studies were developed to assess the use of coated NPS for the treatment of lymphatic metastatic tumours. 6-mercaptopurine (6-MP) drug-loaded ZnO NPs were encapsulated into a lipidic shell and administered to both healthy and cancer cells. A more effective drug release was shown by the lipid-coated NPs, as they displayed enhanced biocompatibility and higher cell internalization levels compared to uncoated ones. [26][27]

Most recently, an extremely valuable biomaterial, namely exosomes, is considered to be exploited as a shell for biomimetic coating. Exosomes are membrane-bound extracellular vesicles (EVs) derived from the fusion of the cell membrane with multivesicular bodies. They play an important role in cell-to-cell communication and transport of molecules and are released by different types of cells into the extracellular environment. They are therefore

considered as highly attractive coating shells for nanocarriers for drug delivery, as they present not only elevated biocompatibility but also represent non-invasive diagnostic biomarkers.[28]

Nevertheless, in-depth studies are yet needed in order to obtain an efficient method for large scale reproducibility of engineered exosomes production and purification, which would lead to the possibility of retaining these elements as an effective option from a clinical point of view.[29]

Y.T. Sato et. al investigated the possibility of exploiting the freeze-thaw method to obtain hybrid membranes derived from the fusion of exosomes membranes with liposomes, which were then used as potential nanocarriers. In vitro tests confirmed the potential use of exosomes for the development of therapeutic nanoconstructs.[30]

Altogether the above-mentioned scientific cases demonstrate that lipid coating strongly improved in-vitro results, enhancing also the stability in circulation and improving the biocompatibility of the constructs.

1.4 NCs as Drug Carriers

The main objective of this Master Thesis work is the development of a nanotheranostics platform containing a zinc oxide core with enhanced drug delivery capabilities, able to perform pancreatic tumour targeted therapeutic activity, disturbing its microenvironment, while also working as a magnetic resonance contrast agent.

ZnO NCs functionalization and drug loading techniques are analyzed to reach the most suitable strategy to be applied in the current work.

1.4.1. Single Drug loading

In recent years, the possibility of incorporating specific molecules and drugs into ZnO nanoconstructs has been widely investigated. Table 1.1 report some examples.

Drug	Cells	Year	Ref
Doxorubicin	Human glioblastoma (U87MG) cell	2019	[31]
Camptothecin	A549 cells	2019	[32]
Curcumin	MDA-MB-231 cells	2020	[33]

Table 1.1: Drug loading of ZnO NCs[34]

Several studies used ZnO NPs as potential drug delivery systems (DDSs) for the delivery of Doxorubicin or Curcumin in cancer cells.

Recently in 2019, Yang et al. [31] synthesized DDSs for targeted cancer therapy, using ZnO NPs conjugated with arginine-glycineaspartate (RGD) peptide. DOX was loaded onto ZnONPs surface via a metal-DOX complex formation. Human glioblastoma (U87MG) cells present an integrin receptor that is overexpressed, and RGD develops a peptide attachment, binding with it for targeted activity. The nanocarrier was uptaken by the cancer cells and pH-responsive drug release took place. Results showed higher cytotoxicity compared to non-targeted nanocarriers and free DOX.

Also in 2019, Li et al. [32] developed N-acetyl-L-cysteine conjugated ZnO NPs for loading and delivery of camptothecin. The drug was linked to the ZnO NP surface via covalent conjugation. The drug-loaded nanocomposites exhibited higher cytotoxicity in A549 cells as compared with the free drug in a synergistic manner.

In 2020, Ghaffar et al. [33] developed N-succinyl chitosan functionalized ZnO NPs (CS-ZnO) nanoconstruct, for the efficient loading of curcumin. The delivery was pH-responsive. Curcumin was loaded into the CS-ZnO via ester bond formation between carboxylic groups on N-succinyl CS-ZnO and hydroxylic groups on curcumin. When exposed to low pH conditions, the amide and ester bond suffered hydrolysis, and simultaneous swelling of chitosan was developed, thus releasing the curcumin. The drug-loaded CS-ZnO NPs exhibited a higher apoptosis degree in cancerous cells as compared with free curcumin, whereas no toxicity was observed in normal cells.

1.4.2.Dual Drug Loading

To date, dual drug loading into ZnO NPs was only reported once, by Tan et al. [35]. This approach was used to propose a protocol method that permits the encapsulation of Sorafenib and Vismodegib, the two hydrophobic drugs used in this Master Thesis work. Consequently, and due to the lack of literature on the specific binomial ZnO/dual drug loading, the following paragraph gives an overview of the current state of the art of nanocarriers developed for dual-drug delivery, to highlight similarities or possible protocols that could be developed also on ZnO NCs.

The following Table 1.2, nominates different studies that evidenced the synergistic effect of the different nanocarried-dual-drugs on cancer cells, thus sharing common points with the current study.

Carrier	Drugs	Year	Ref
Porous silicon (pSi) microparticles	Daunorubicin (DNR) and Dexamethasone (DEX)	2018	[36]
PLGA and PEG-PLGA Polymeric Nanoparticles	Sorafenib and Doxorubicin	2018	[37]
Chitosan nanoparticles	Quercetin and 5-fluorouracil	2015	[38]

Table 1.2:Dual drug loading studies and references

Dual drug release in 3D pancreatic cell culture was carried out for the first time by the development of a nanocarrier which aimed to address the multiple issues of pancreatic cancer, such as the development of multidrug resistance, presence of cancer stem cells, development of a stromal barrier and a hypoxic environment due to hypo-perfusion [38]. The authors obtained a 3D culture of MiaPaCa2 cells (human pancreatic cancer cell line). The drugs were quercetin (hydrophobic) and 5-fluorouracil (5-FU, slightly polar), and they were used together for the first time, loaded in chitosan NPs. A significant dose-dependent reduction in the cell viability was observed. A decrease in cell viability was enhanced by the delivery of the cytotoxic agent since free drugs did not show such a cytotoxic effect. Quercetin showed to augment the cytotoxic effects of 5-FU. The 3D cultures also suffered from death events, in contrast with their controls, thus confirming a synergistic cytotoxic action against cancer cells. The system was hypothesized to be effective also in solid tumours, as the effective results were also demonstrated in 3D cultures. This is a major milestone to reach. The outcome confirmed the potential of the synergistic dual drug activity on complex models.

A recent study performing dual-drug loading on ZnO was recently published[65]. The drugs were Doxorubicin (DOX) and phenylsulfonyl furoxan (PSF). The nanoconstruct consisted of 2,3-Dimethylmaleic anhydride (DMMA)-decorated ZnO NPs with DOX and PSF loaded and was tested in vitro on human gastric carcinoma cells (SGC7901) and human gastric carcinoma drug-resistant cells (SGC7901/ADR) and in vivo on BALB/c mice (an albino, laboratory-bred strain of the house mouse). DMMA was used to overcome the repulsion between the negatively charged nanoparticles and the tumours' cell membrane. The amino-terminated ZnO NPs were synthesized, then DOX was encapsulated by forming a coordination bond between DOX and Zn2+ ions. In addition, PSF as a NO (nitric oxide) donor was conjugated to the particle via amide bonding. After DMMA decoration, a

charge-reversal property was given through the hydrolyzation of the amine bonding connecting DMMA and ZnO as pH lowered from 7.5 to 6.5. The nanoconstructs obtained were applied on both in-vitro and in-vivo models.

EPR effect caused an increased concentration of Zinc in the tumour than in other body parts. The concentration decrease of nanospheres in the tumour was slower, showing enhanced retention.

This study shows the overcoming of ZnO limitations, such as short time circulation, thanks to the charge-reversal activity given by DMMA, which increased the chances of permeating the tumour by prolonging blood circulation and favouring then cell uptake. The synergistic anticancer efficacy of multiple agents was validated and was even improved by the effect of Zn2+ ions released from the dissolution of ZnO once inside cancer cells.

1.4.3. Considerations

From the bibliographic research here reported, it can be hypothesized that simultaneous delivery of two drugs carries advantages in terms of enhanced therapeutic action, and the use of a target ligand can be proposed as one of the most efficient ways of increasing the delivery selectivity.

Dual drug inhibitors that were chosen to be uploaded into the nanoconstructs are represented by Sorafenib and Vismodegib.

Sorafenib is a vascular endothelial growth factor (VEGF) inhibitor, considered to have a potent effect on tumour angiogenesis and neovascularization in various solid tumours, while Vismodegib is an inhibitor of Hh signalling that acts by antagonizing the protein Smoothened (SMO), thereby preventing downstream transcriptional activation of genes involved in cell proliferation and survival.

Thus, it is hypothesized that with synergistic approaches it is possible to improve the efficacy of the anti-angiogenic therapy if VEGFR kinase inhibitor will be administered simultaneously with a stromal depleting agent known to increase perfusion and vascular promotion. Even though this combination therapy can create potent and lethal interactions between tumour-specific signalling and anti-angiogenic processes, the efficacy of these therapeutic approaches remains affected by limited targeted delivery and sometimes by their low bioavailability and high hydrophobicity. For these reasons, there is a need for molecularly targeted and smart drug carriers.

Therefore, in the present Thesis, for the first time, VEGFR kinase inhibitor & HH pathway inhibitor will be dual-loaded onto a theranostic nanoconstruct to deplete tumour stroma, normalize tumour vascularity and show synergism to evaluate the improvements in pancreatic cancer treatment.

1.5 In-vitro assays

As the main goal of the biomimetic dual drug-loaded nanoconstructs developed is the application on pre-clinical and clinical levels, tests on healthy and cancer cells need to be carried out. Cytotoxicity and internalization rates are assessed, and in-depth analyses of the type of mechanisms of cell death are checked.

1.5.1. Cytotoxicity and cell viability assays

The measurement of cytotoxicity and cell viability represents an important point to be considered when analyzing a nanoconstruct in vitro. They permit us to understand the different mechanisms of action that can cause cell death. The need for sensitive, reliable, fast and easy methods to assess cellular death has led to the development of several standard assays. A classification of such methods can be described as follow:

1. Luminometric assays: ATP and real-time viability assays.
2. Colourimetric assays: WST-1, WST-8, MTT, MTS, SRB, LDH, NRU, and crystal violet assays;
3. Dye exclusion assays: Trypan blue, eosin, Congo red, erythrosine B assays;
4. Fluorometric assays: CFDA-AM and alamarBlue assays;

Luminometric assays consist of the evaluation of cells viability after the administration of the reagent. To this aim, a luminometric microplate reader is used. The most commonly used technique is the ATP assay; it exploits the catalysis reaction of the enzyme luciferase into luciferin, when ATP is present. The intensity of the luminescent signal produced is dependent on the ATP concentration, and therefore healthy cells, in the sample, thus determining cell viability.

Colorimetric assays determine the cells' metabolic activity and viability by exploiting specific reagents, which are then analyzed by spectrophotometric analyses. WST-1 Assay consists of the administration of tetrazolium

salts into the culture media. These salts are cleaved to soluble formazan by cellular enzymes, through the activity of mitochondrial dehydrogenases, when they are alive. An expansion in the number of viable cells results in an increase in the overall mitochondrial activity in the sample, which in turn increases the amount of formazan dye formed. Quantification of the formazan dye produced by metabolically active cells can be done using a scanning UV-Vis multiwell spectrophotometer. The Cell Proliferation Reagent WST-1 is designed to be used for quantification of cell proliferation, growth, viability, and chemosensitivity in cell populations using the 96-well-plate format. It is therefore widely used for the measurement of cell proliferation in response to growth factors, cytokines and nutrients, the assessment of growth-inhibitory antibodies and physiological mediators, and the analysis of cytotoxic and cytostatic compounds, such as anti-cancer drugs and other pharmaceutical compounds, as the nanoconstructs developed in this work.

Dye exclusion assays present the main advantage of consisting in a simple staining process; however, the main limitation is represented by the challenge of examining multiple samples. This experiment is generally carried out in cell suspensions; it consists of the interaction of the dyes with the dead cells, following the exclusion of living cells. Trypan Blue is a well-known dye exclusion assay. This dye is not able to interact with living cells that present an intact membrane, as it presents a highly negative charge and is repelled. Instead, after interacting with the cytoplasm of dead cells, the dye becomes blue. Cell viability is determined as a percentage of the total number of cells per unit volume.

Fluorometric assays allow the evaluation of cell viability through flow cytometry of fluorescence microscopy. The sensibility of the method is increased with respect to colorimetric assays. The alamarBlue assay technique consists of the administration into the culture media of a non-fluorescent blue dye, namely resazurin. Living cells' mitochondria transform resazurin into resorufin, increasing the blue colour of the culture media and making it fluorescent, being the latter proportional to the cell viability.

1.5.2.Cellular uptake

Internalization tests have to be carried out in order to assess the correct theranostics effects of the obtained nanoplatforms. Cellular uptake is generally evaluated with two main procedures, namely fluorescence microscopy and Fluorescence-Activated Cell Sorting (FACS) analyses.

Fluorescence Microscopy estimates the cellular internalization by the specific recognition and collection of a signal produced by a fluorescent dye. The labelling of different materials can be carried out; Nanoparticles, exosomes, liposomes and also specific molecules can be linked to different dyes for their recognition. The instrument emits an exciting signal, and the fluorescence signal generated by the fluorophore as a response is collected and processed. The results of this kind of experiment are qualitative and are obtained by the contrasting labelling of the cellular membranes and the elements to be internalized. In-vitro internalization can be detected by the colocalization of both different fluorophores. The uptake process can be evaluated in real-time and, as it is a non-invasive technique, it permits the realization of different hypotheses of cellular internalization mechanisms.

FACS analyses consist of a quantitative method that allows the distinction of specific light scattering and fluorescence characteristics of indicators, which are related to distinct cell populations. This method permits obtaining data from individual cells of particular interest, which need to be strongly attached to a fluorescent element, that can be also internalized, permitting its detection through flow cytometry. The technique allows the quantification of the number of cells in the total population that contains the specific element. Therefore, the uptake of any specifically marked element can be detected and evaluated, so it can be used for the evaluation of the internalization of Nanoparticles as long as they are marked with fluorescent dyes. The quantification process includes the setting of an untreated cell population, namely a healthy cell population that represent the phenotypic status and permits the definition of a baseline fluorescence of the whole population. After the background condition is set, cells with internalized NPs run inside the instrument, and the signal measured should be higher in intensity if the construct has been uptaken. FACS is a very useful technique for the measurements of uptake of different elements such as NPs, liposomes, liposomes-coated NPs, or other theranostic nanoconstructs, like those performed at the TrojanNanoHorse Lab where this Master Thesis work was developed.[29]

1.5.3.Cell death detection

Apoptosis and necrosis are two different mechanisms of cell death. Apoptosis occurs autonomously and naturally, involving the activation of a metabolic cascade complementary to mitosis. It is a regulated and programmed process. On the other hand, necrosis is an accidental and passive cell death,

which is caused by irreparable mechanical trauma created by external stimuli. The outcome of treatment is to be measured not only taking into account the quantity of living and dead cells, but also the causes of the latter, as this detail can give crucial information on the mechanism of action of the developed treatment. Besides, the investigation of after-death cell communication pathways can be pivotal in the understanding of the biological environment.

Through the years, the techniques utilized to carry out these assays evolved. Recently, special kits have been developed for the evaluation of a cellular population in terms of the amount of necrotic and apoptotic components. These techniques exploit different physical properties, as can be the absorption of light or fluorescent emission. One example is the use of Annexin V dye. During apoptotic processes, cells expose phosphatidylserines to the outside layer of their membrane. These components bound with Annexin V, making recognizable the apoptotic cell population. Another dye, propidium iodide, links to the DNA derived from necrotic cells which is released as a consequence of autolysis, characteristic of this type of cell death, therefore identifying the necrotic cell population. Therefore, real-time detection of both fluorescence and luminescence signals, with the use of a plate reader or flow cytometry analysis, can allow the discrimination between the two cell death processes and their quantification in terms of the whole population.

2 Materials and Methods

2.1 Synthesis of Oleic Acid stabilized ZnO Nanocrystals

The synthesis of both undoped and gadolinium doped nanocrystals was carried out following a wet chemical co-precipitation method, as previously described in the literature [39]. The synthesis setup is shown in Figure 2.1.

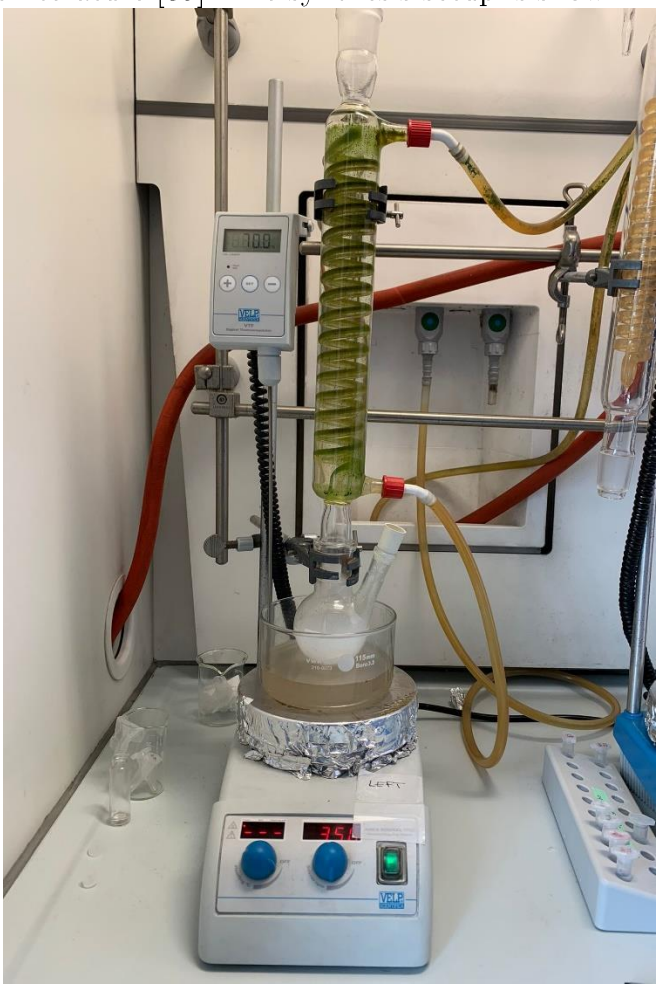

Figure 2.1: Setup for the synthesis of nanocrystals

2.1.1. Ol-ZnO nanocrystals' synthesis

For the synthesis of undoped oleate-stabilized zinc oxide nanocrystals (NCs-undoped), 0.5268 g of zinc acetate dihydrate ($Zn(CH3COO)2 \cdot 2H2O$) (2.4 mmol), stored in dry and vacuum conditions to avoid moisture, were dissolved into 40 ml of absolute ethanol in a 100 ml round-bottom flask. Subsequently, 140 µl of oleic acid were added. The reaction flask was then

placed under a chemical hood, mounted to a refrigeration column, and immersed in a silicon oil heating bath, set to 70ºC, under constant stirring (VELP Scientifica ARE Hot plate stirrer) at 350 rpm.

After reaching the fixed temperature, and when moisture was detectable, a Tetramethylammonium hydroxide (TMAH) solution was rapidly added to the reaction mixture, always under vigorous stirring. Such solution consisted of 0.522 g of TMAH firstly dissolved into 1.052 ml of bidistilled water, with the consecutive addition of 10 ml of absolute ethanol. The so-obtained colloidal solution evolved from transparent to white.

After 5 minutes of stirring, the reaction was interrupted; the flask was removed from its setup, 40 ml of ice-cold (0 - 4ºC) ethanol were quickly added, and the vessel was put in an ice bath for further cooling.

The resulting undoped nanocrystals were put into two 50 ml falcon and collected by centrifugation (at 10000 RCF for 5 minutes). The reaction's supernatant was discarded, and 30 ml of fresh ethanol were added to redisperse the pellet, generating a suspension that was then vortexed and immersed into an ultrasound bath, to improve the disaggregation process.

Lastly, NCs-undoped underwent two washing steps through the concatenation of centrifugations and resuspension steps by sonication and vortexing.

2.1.2. Gd-doped Ol-ZnO nanocrystals' synthesis

For the doping of nanocrystals, the above-mentioned procedure was carried out, with the addition of Gadolinium(III) acetate hydrate ($Gd(CH3COO)3 \cdot H2O$, molecular weight 334.38 g/mol) at the beginning of the reaction to the flask. The desired molar ratio of zinc acetate dehydrate and the dopant was 1:0,12, thus 0.0963 g of $Gd(CH3COO)3 \cdot H2O$ were added to the starting solution containing 0.5268 g of $Zn(CH3COO)2 \cdot 2H2O$ and 40 ml of ethanol. The reaction process was invariable concerning the protocol previously elucidated, except for the time of stirring, which was incremented from 5 to 15 minutes. Identically to the NCs-undoped reaction, the colloidal suspension changed from transparent to white colour, after the addition of the TMAH solution.

2.2 Amino-propyl functionalization of Ol-ZnO NCs

For the development of the nanoconstructs, the freshly synthesized nanocrystals (NCs) had to be functionalized to expose amino-propyl groups (-NH_2) on their surface, to permit a fair stabilization in water-based media,

the covalent labelling with fluorescent dyes, and the physical adsorption of hydrophobic therapeutic agents.

Firstly, the nanocrystals' suspensions obtained had to be characterized in terms of their concentration. One Eppendorf tube for each sample was weighted 5 times, and the average of the measures was taken. After 10 minutes of sonication, and vigorous vortexing, 500µl of each colloidal suspension were put into the corresponding Eppendorf tubes, which remained open to dry up under the hood for two days. After the total evaporation of the ethanol, the tubes were weighed again five times and the average weight was computed. The concentration of the samples (mg/ml) was calculated as the difference in weight between the loaded and the empty tubes, multiplied by a factor of 2.

Once the NCS-unfunc were synthesized, and their concentration was evaluated, the functionalization process was implemented. The setup used for the purpose, and its corresponding parts, are depicted in Figure 2.2: Setup for functionalization with amino groups.

The functionalization solution was obtained by incorporating the precise volume of colloidal suspension that corresponded to 40 mg of NCs-undoped, into a round bottom flask containing the amount of Ethanol needed to bring the final suspension to a 2,5 mg/ml concentration. The flask was then mounted to a refrigeration column and put into a silicon oil heating bath, set at 70^{o}C. After some minutes, and when condensation appeared visible in the flask walls, 12,5 µl of (3-Aminopropyl)trimethoxysilane (APTMS, 179.29 g/mol, 1.027 g/ml) were added.

The reaction was carried out for 6 hours. A continuous flow of nitrogen (N_2) was provided through the attachment of an inflating tube into one of the flask's necks. The others were sealed with grease. The purpose of this flow was to avoid direct contact of the solution with oxygen, which could cause the auto-polymerization of APTMS. The volume of the suspension was constantly supervised, to prevent excessive evaporation of ethanol.

After the 6 hours of process, the flask was taken away from the setup, to allow the cooling of the suspension. After it arrived at room temperature, the whole sample was put into a 15 ml falcon tube and centrifuged at 10000 RCF for 10 minutes. The supernatant was removed, and 5 ml of ethanol were added to resuspend the pellet, followed by sonication to favour the

redispersion of the NCs. Lastly, two washing steps were performed, to eliminate any trace of the reagent. The first one, just after the redispersion process, and the second one, the day after.

Once again, the concentration of the functionalized ZnO-Gd Nanocrystals (NCs) was evaluated, using the previously explained protocol of weighting.

Figure 2.2: Setup for functionalization with amino groups

2.3 Characterization of Ol-ZnO NCs

All following procedures of characterization were developed in order to evaluate that the quality criteria previously reported by the author were fulfilled. Knowing the concentration of the samples, Nanocrystals were analyzed before and after their amino-functionalization and also when being subjected to the dual drug uptake, which will be explained in section 2.4.5.

Analyses included the utilization of the Dynamic Light Scattering instrument for the assessment of Size distribution and Z-Potential, the Field Emission Scanning Electron Microscope (FESEM), for the evaluation of the morphology, X-Ray Diffractometry (XRD), for analysis of the crystalline structure, and Fourier-transform infrared spectroscopy (FTIR) to check the chemical composition.

2.3.1. Dynamic Light Scattering – Size

Size measurements of the obtained samples were carried out with a process called Dynamic Light Scattering (DLS), using the Zetasizer Nano ZS90 (Malvern Instruments, Worcestershire, UK) particle characterization system, which components are detailed in Figure 2.3.

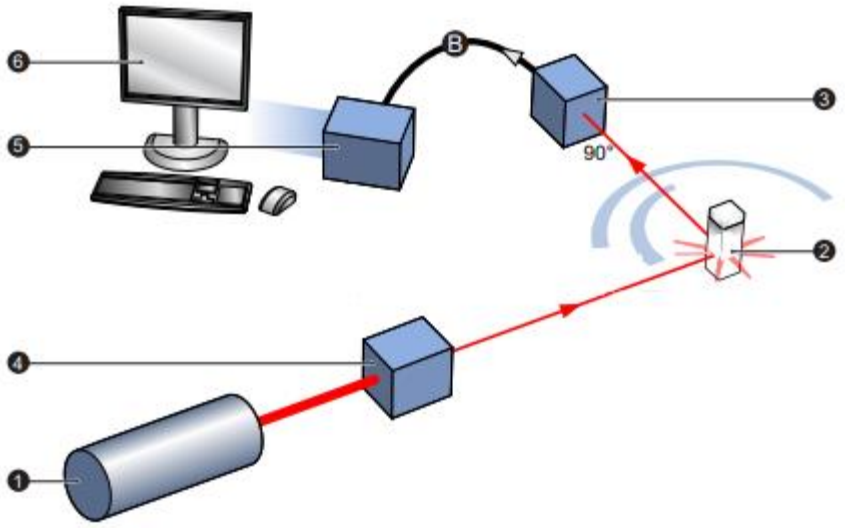

Figure 2.3: Scheme of Zetasizer Nano ZS90 component

Dynamic Light Scattering is a technique based on the Brownian motion of dispersed nanoparticles. When in suspension, Nanoparticles suffer continuous collisions with the liquid molecules in which they are contained. Small particles move quickly, while larger ones develop slower movements.

The hydrodynamic size of a particle is related to such speed by the Stokes-Einstein equation, as follows:

$$D = \frac{k_B T}{6\pi\eta R_H}$$

Where D is the translational diffusion coefficient, k_B is the Boltzmann constant, T is temperature, and η and R_H are the viscosity and the hydrodynamic radius, respectively.

When a monochromatic beam of light, i.e. laser, hits a sample containing dispersed particles of different sizes into a cuvette, the light gets scattered in all directions. Due to constructive or destructive interference by the surrounding particles, this phenomenon produces intensity fluctuations in the scattered light, which is detected at an angle of 90^{o} in the used instrument.

Over time the signal is collected and used to determine the diffusion coefficient. Afterwards, the Stokes-Einstein equation is used to obtain the hydrodynamic diameter, namely the corresponding size of a sphere that diffuses at the same speed as the nanoparticles being measured, comprising the particle and the bounded ions on its surface.

DLS analyses depend on many factors, such as the size of the particle core, the surface structures present, the particles' suspension concentration, and the types of ions in the medium. The diffusion coefficient of the particles is determined to study their stability, as it gives information regarding the aggregation over time.

Size measurements were developed using two different solvents, ethanol and bidistilled water, in order to understand if the behaviour of the NCs differed in each situation.

The stock solution of each type of NCs was sonicated for 10 minutes and then vigorously vortexed for complete homogenization. Then the precise amount of solution needed for the obtention of 100 µg of each type of NCs was collected and put into different Eppendorf tubes. For the ethanol dispersed samples, the amount of solvent needed to reach a total of 1ml was added, and a sample of 100 µg/ml concentration was obtained. For the NCs in water, the NCs collected were centrifugated at 14000 RCF for 10 minutes, and a pellet was obtained by removing the ethanol supernatant. Subsequently, 1 ml of bidistilled water was added and mixed for the obtention of the same concentration of 100 µg/ml.

Both suspensions were then sonicated for 10 minutes and were put, each at a time, into a 1 ml cuvette (DTS0012, Figure 2.4) to perform the DLS size analysis. The measurements were carried out 3 times, in order to calculate an average and plot the corresponding graph.

Figure 2.4: Picture of DTS0012 cuvette for DLS size measurement.

2.3.2.Zeta Potential measurements

Zeta potential analyses were carried out using the same instrument as for the DLS experiments. This instrument determines the Electrophoretic Mobility by performing an electrophoresis experiment, measures the velocity of the particles using the Laser Doppler Velocimetry (LDV), and then applies the Henry equation to obtain the Zeta potential.

Since the surface of the nanoparticles presents a net charge, the distribution of the counter ions present on the surrounding interfacial region tends to concentrate close to it, forming an Electrical Double Layer (EDL), represented in Figure 2.5. This layer consists of two different parts; an inner region, the Stern layer, where ions present strong boundaries, and an outer region, the Diffuse layer, where they are weakly attached. A notional boundary is created within this diffuse layer where the particle and the surrounding ions form a stable entity, termed the slipping plane. The Z-potential is the potential that exists at this boundary, and it is an indicator of the stability of the colloidal system. It is measured by the application of an electric field between two electrodes, which attract the charged particles towards the electrode of opposite charge, forcing them to move across the electrolyte. Viscous forces tend to oppose this movement, and when equilibrium is reached, a constant velocity, which can be referred to as the particle's Electrophoretic mobility (μ_e), can be calculated as shown in the following equation:

$$\mu_e = \frac{V}{E}$$

being V the particle's velocity (µm/s), and E the electric field strength (Volt/cm).

Once obtained this value, Henry equation can be applied to calculate the zeta potential as:

$$\mu_e = \frac{2\ \varepsilon\ \mathrm{z}\ \mathrm{f(Ka)}}{3\eta}$$

where ε indicates the dielectric constant, z the Zeta potential, f(Ka) is Henry's function (generally used values are 1.5 or 1.0) and η is the viscosity at experimental temperature.

Electrophoretic measurements of zeta potential are largely affected by the pH of the dispersant. They are therefore generally carried out under moderate electrolyte concentration conditions, in aqueous media. In this case, all the measurements were performed at neutral pH, with the samples dispersed in bi-distilled water at room temperature.

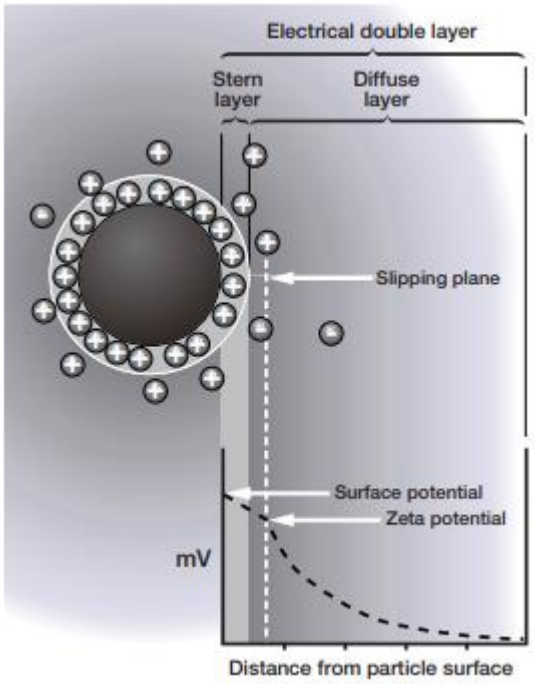

Figure 2.5: Scheme of nanoparticle's Z-potential and charge surface

Right after the DLS measurements in water were obtained, 750 µl of the used sample were collected and put into another specific cuvette (DTS1070, Figure 2.6) for the measurement of the zeta potential. Special care needed to be taken to avoid the formation of air bubbles. The analysis was also carried out 3 times, and the average value and graphs were therefore obtained.

Figure 2.6: Picture of DTS1070 cuvette for Z-potential measurements.

2.3.3.X-Ray Diffractometry (XRD)

X-Ray Diffraction is a rapid, non-destructive analytical technique, primarily used to identify the phases of a crystalline material, providing also information regarding unit cell dimensions and the atomic structure of the sample. This method is based on the constructive interference of monochromatic X-rays and the sample containing crystalline structures. The incident X-ray energy (λ) has the same order of magnitude as the spacing between the crystal planes which permits the measurement of the lattice spacing, or distance between the atoms, by a special interference effect called diffraction.
The experiment consists of enlightening the sample with a collimated and monochromatic X-ray beam, while the tube and detector move synchronously, recording and plotting all information obtained. Elastic scattering occurs when X-rays encounter an atom whose electrons absorb the beam energy and re-emit it as a new X-ray containing the same energy as the original one. The interference between the emitted and the re-emitted X-rays can be either constructive or destructive. In this last case, the signal is destroyed. When constructive interference occurs, the signal is amplified and the process is called diffraction. It arises at very specific angles between the incident and scattered beam (θ) and can give information on the lattice spacing or distance between the crystal planes.
Bragg's Law equation (Figure 2.7) relates the wavelength of electromagnetic radiation (λ), multiplied by a integer n, to the diffraction angle (θ) and the lattice spacing, or the distance between two adjacent planes in the crystal (d), as follows:

$$n\lambda = 2\ d\ sin\ (\theta)$$

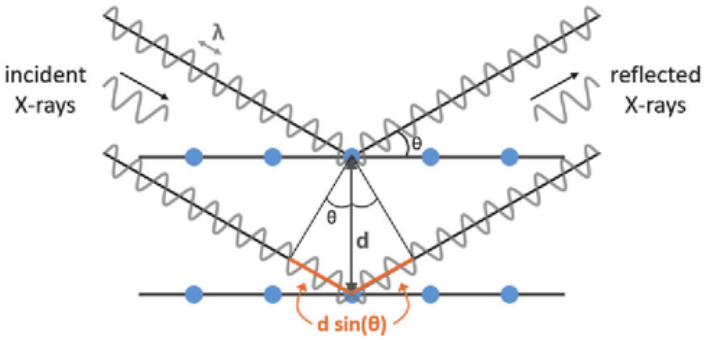

Figure 2.7: Scheme of Bragg's Law for XRD analyses

Samples were prepared by taking the corresponding suspension volume to obtain 1 mg of NCs and putting it in Eppendorf tubes. They were then centrifuged at 14000 RCF for 10 minutes, the supernatant was removed and 50µl of pure ethanol was added for resuspending the pellets. Little pieces of silicon wafer were cut in dimensions of approximately 1cm x 1cm and used as a substrate for the measurements, and one as a control. The samples were collected in aliquots of 10 µl and put onto the silicon wafer. Once the drop dried up, the process was repeated until the formation of a thin film with the deposition of the complete sample. X-Ray Diffraction analyses were performed by a Panalytical X'Pert PRO diffractometer in Bragg-Brentano configuration, equipped with a CuKα monochromatic radiation ($\lambda = 1.54059$ Å) as X-ray source. Each silicon wafer was put on the sample holder and collocated into the dedicated housing of the instrument for the measurement process.

2.3.4.Fourier-Transform Infrared Spectroscopy (FTIR)

Fourier-transform infrared spectroscopy (FTIR) analyses were performed using the NICOLET 5700 FTIR spectrometer. The aim was to study the chemical composition of the NCs and afterwards to assess the drug uploading process.

FTIR spectroscopy is an analytical technique based on the absorption phenomena that occurs when the sample is exposed to infrared radiation; a part of the incident radiation suffers from reflection, and a larger portion passes through the sample. The absorbed radiation is converted into vibrational and/or rotational energy depending on the molecule or chemical structure that it encounters, which will produce a unique spectral fingerprint.

A detector collects the transmitted light. The resulting signal is elaborated and presented as a spectrum, which is considered the molecular fingerprint

of the sample. The instrument has a central component, called the interferometer, where the IR beam enters and is deviated towards a beamsplitter. A moving and a static mirror receive the split beams and reflect them again to the beamsplitter where interference is caused. The resulting ray is directed to the sample.

Fast measurements can be acquired with this technique and by the use of the interferometer, as spectral information of all wavelengths is simultaneously acquired.

A control sample is needed, as environmental influences can affect the measurements. Therefore a naked silicon wafer, without sample deposited on it is evaluated; the instrument calculates the Fourier Transform, and the spectrum obtained is used as reference.

The preparation of the samples was developed as explained for the XRD measurements, in paragraph 322.3.3. All obtained sample substrates and the control substrate were then scanned 64 times in the [4000-400] cm^{-1} range. The spectrum was obtained by calculating the mean value, using a resolution of 2 cm^{-1}. For the obtention of the transmission spectrum, the sample spectra were divided by the reference spectrum, in order to remove the background signal.

2.3.1. Field Emission Scanning Electron Microscope (FESEM)

Field emission scanning electron microscopy (FESEM) was performed to analyze the topographical and elemental properties of the NCs. The instrument used was FESEM Merlin (Zeiss) coupled with an X-Ray detector for EDS analysis.

FESEM technique consists of the scanning of a surface using a focused high and low-energy electron beam, which results in magnified high-resolution images of such surface. The source of emitted electrons is a sharp small-sized tungsten tip, which is put into a high electric field. Because of the size and shape of the source, electrons are generated using low voltages and are directed to hit the sample. Secondary electrons are created by this interaction (whose velocity and angle are dependent on the surface they encounter) are collected by a detector, the produced electric signal is processed and amplified to be then converted into a clear image.

2.4 Drug Uptake

2.4.1. Drugs' Characteristics

The aim of this Master's Thesis was the development of an innovative nanoconstruct, which would contain two inhibitor drugs: Sorafenib (Sigma-Aldrich, molecular weight 464.82 g/mol) and Vismodegib (AstaTech, Inc., molecular weight 421.3 g/mol). Their chemical structure is depicted in Figure 2.8.

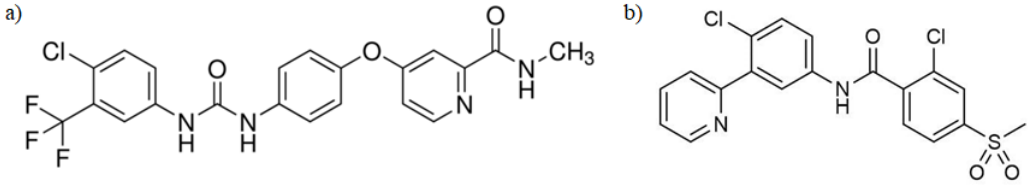

Figure 2.8: Sorafenib (a) and Vismodegib (b) chemical structure.

As both drugs are considered hydrophobic, different solvents were used to perform the drug adsorption on the NCs. Sorafenib was diluted in ethanol (EtOH), while Vismodegib in Dimethyl Sulfoxide (DMSO).

2.4.2. UV-Vis Spectroscopy

UV-Vis spectroscopy is a quantitative technique that measures how much light, in the ultraviolet and visible range, is absorbed by a chemical substance. The resulting absorbance value (A), in arbitrary units, can then be used for the calculation of the concentration (c) of the sample, expressed in M, by means of the Lambert-Beer Law; where ε is the molar absorption coefficient, of units $M^{-1}cm^{-1}$, and l is the optical path length, in cm, as:

$$A = \varepsilon cl$$

Analyses were performed with the Thermo Scientific Multiskan, coupled with FC Thermo Scientific Skanit Software. The instrument consists of a tungsten halogen lamp that emits light in the ultraviolet and visible range. When the beam hits the sample, part of the light is absorbed while another portion is transmitted, diffracted and collected by a photodetector. The software then interprets the data and the absorbance values in the specified range of wavelengths are plotted into a spectrograph.

The calibration curve can be obtained by the subsequent analysis of various known concentrations of samples, using the same specific wavelength. The curve is then linearly fitted, the equation of the line with its intercept (q) and slope (p) values are calculated.

This fitted curve permits the calculation of the concentration (CONC) of a specific sample, by measuring its absorbance (ABS) at the same wavelength of the creation of the curve and applying the equation of the line. The expression of the equation in terms of these values results as follows:

$$y = m \cdot x + q \rightarrow ABS = m \cdot CONC + q$$

Therefore, the direct equation for the calculus of the samples' concentration is:

$$CONC = (ABS\text{-}q)/m$$

2.4.3.Drug's Calibration Curves

For the performance of the drugs' uptake analyses and the evaluation of the drug released in cell culture media, calibration curves needed to be calculated for each drug in each solvent. For this matter, in each case, a spectrograph was obtained and the wavelength that presented the peaks of absorbance was taken as reference for the construction of the curves and the following measurements of the samples.

Both Sorafenib and Vismodegib were analyzed in their respective solvent, being ethanol and DMSO respectively, and in cell culture media (RPMI). Stock solutions were obtained for all drug/solvent combinations. Standard samples were prepared to start from each stock solution and make serial dilutions. For Sorafenib in ethanol, the stock solution corresponded to a concentration of 5mM. In the case of Vismodegib in DMSO, the concentration was 10 mM.

In both cases, the initial stock was obtained by diluting the solutions to a 1mM stock. From this solution, serial dilution by a factor of 10 was performed. 200 µl aliquots were obtained for each concentration, reaching a minimum of 0.01 µM, by diluting 20 µl of the previous solution into 180 µl of solvent each time, as seen in Figure 2.9.

From the above-mentioned standards, and for completing the set of dilutions, 500, 250 and 125 µM samples were obtained from the stock sample.

From each standard, an aliquot of 100 µl was taken and put into a synthetic quartz glass (QG) microplate (96 wells, Hellma Analytics) and measures were performed with the instruments described in paragraph 2.4.2. The absorbance spectrum was obtained in a range from 200 to 800 nm.

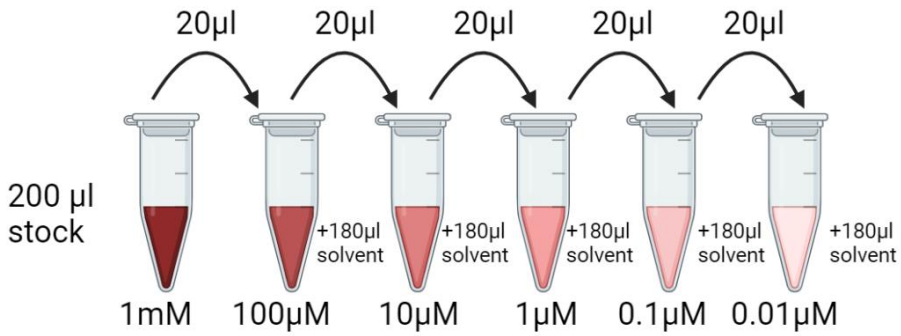

Figure 2.9: Serial dilutions from 1mM drug solution stock

2.4.4.Single Drug Uptake

The following procedures were performed for Sorafenib in Ethanol and for Vismodegib in DMSO. From the original stock samples, 1mM solutions were obtained by dilution and used as new stock solutions.

Firstly, 5 Eppendorf tubes were filled with the corresponding volume of colloidal suspension to obtain 100 µg of amino-propyl functionalized ZnO-Gd nanocrystals (NCs) in each. The drug adsorption was assessed for each tube at different time steps (from 1 to 6 hours, except for the 5^{th} timepoint).

All samples were centrifuged at 14000 RCF for 10 minutes, ethanol as removed, obtaining a pellet, which was resuspended in 200 µl of 1mM drug solution and mixed. A clean magnet was inserted into each tube, and the samples were put onto a stirrer plate at 200 rpm.

After the completion of each time step, the corresponding sample was analyzed; the magnet was removed, centrifugation at 14000 RCF for 10 minutes was performed, and the supernatant was collected and put into a separate Eppendorf tube.

For the absorbance analysis, the obtained supernatant had to be diluted in different proportions, as the instrument reaches saturation for high molarities; 1:2 for Vismodegib in DMSO, and 1:4 for Sorafenib in ethanol. The procedure is depicted in Figure 2.10. Afterwards, 3 aliquots of 100 µl of each diluted supernatant were collocated in different wells of the quartz microplate and the absorbance reading was carried out, using the established wavelength. Concentration calculation was subsequently performed using the equation obtained from the calibration curve. Two control solutions were also analyzed; a negative control, consisting of the solvent (DMSO or ethanol) alone, for the obtention of the background, and a positive control consisting of the stock of 1mM solution of drug diluted in the same ratio of the corresponding samples.

The raw samples' reading was adjusted using both controls. Firstly, all data obtained (samples and stock) was normalized with respect to the negative control, so the absorbance of the background was subtracted. The obtained absorbance was then converted into concentration values, using m and q of the calibration curve. The amount of drug adsorbed was determined by the subtraction of the samples' concentration to that of the drug stock solution (positive control); this concentration was then described in µg of drug per mg of NCs, by knowing the molecular weight of the drug, the volume of supernatant, and the weight of NCs in the tube.

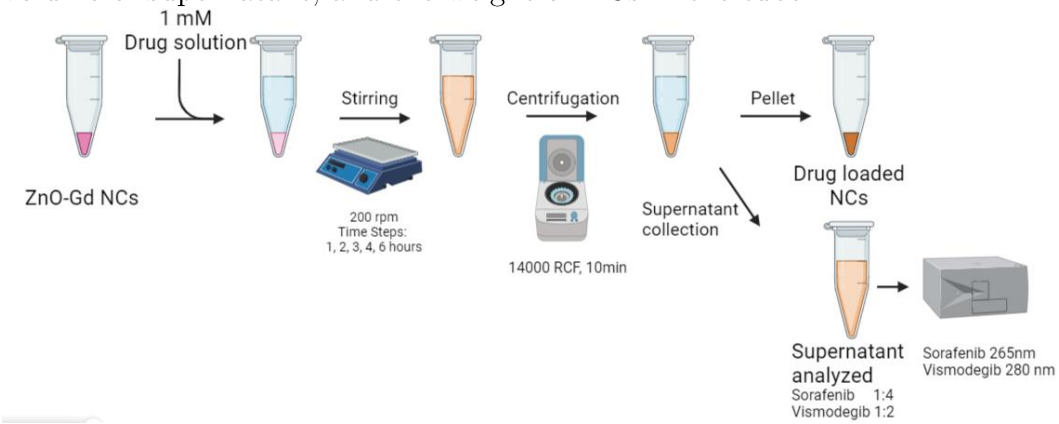

Figure 2.10: Protocol for drug uptake for each drug and respective solvent.

2.4.5. Dual Drug Uptake

Previous studies performed by members of the research team regarding several optimization processes and uptake studies in different orders, made it possible to obtain a dual-drug protocol for the uptake of Vismodegib in DMSO, followed by Sorafenib in ethanol.

100 µg of NCs were collected in an Eppendorf tube. A pellet was obtained after centrifugation at 14000 RCF for 10 minutes and ethanol removal. It was then redispersed into 200 µl (2:1 ratio of µl per µg of NCs) of 1mM Vismodegib in DMSO solution. The whole was mixed with the pipette and vigorously vortexed. A little magnet was inserted and 3.5 hours of magnetic stirring at 200 rpm were performed.

The obtained Vismodegib-loaded NCs were then centrifuged (14000 RCF, 10 minutes), and the supernatant was collected for uptake analysis; 170 µl were diluted in the appropriate quantity of DMSO to obtain a 500 µM sample (1:2 dilution, so the addition of 170 µl of DMSO). 3 microplate wells were filled with aliquots of 100 µl each, for absorbance reading and concentration calculus, following the normalization procedures explained in paragraph 2.4.4.

Afterwards, the Vismodegib-loaded NCs pellet was dispersed in 200 µl of Sorafenib in ethanol solution (1mM), by manual mixing and vortexing. A clean magnet was introduced and samples were put to stirring for 2 hours at 200 rpm. After such, the supernatant was collected, using the same previously described protocol of centrifuge, and 100 µl were diluted by a 1:4 factor, obtaining a 250 µM concentration, for the absorbance reading and uptake analysis. (Figure 2.11).

The obtained dual drug-loaded NCs were used for preliminary studies and for cell treatments. The pellets resulting from the centrifuge post-uptake were kept at -20°C overnight before being coated with a lipidic shell, for the successive development of the nanoconstructs.

When nanoconstructs were used for cell treatments, all above-mentioned processes were carried out in sterile conditions, under a biological hood.

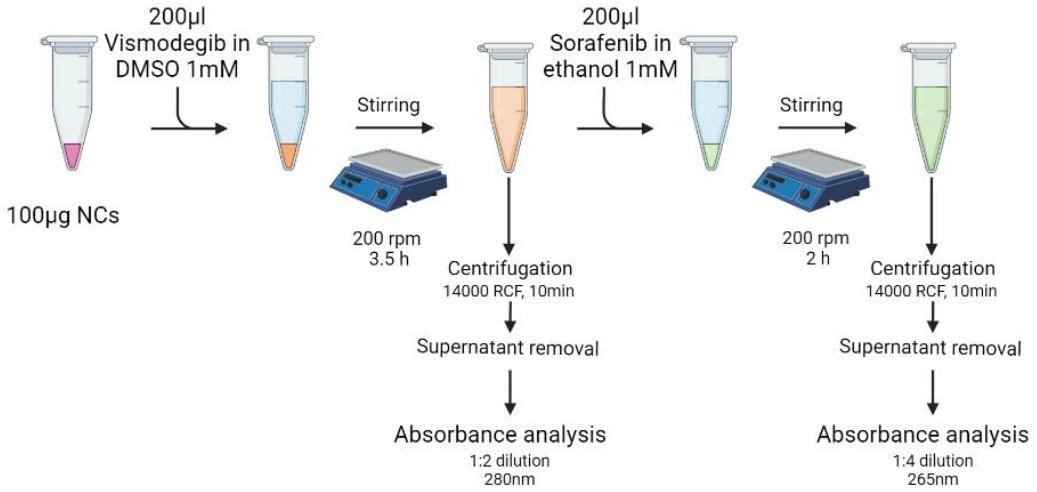

Figure 2.11: Protocol for dual drug uptake of Vismodegib and Sorafenib.

2.5 Nanoconstruct Design

The aim of this Master's Thesis work was the development of an innovative dual-drug loaded nanoconstruct with enhanced biostability and prolonged bloodstream circulation, low cytotoxicity and low aggregation between NCs, ensuring a specific action towards the target cells.

To reach these goals, drug-loaded amino-functionalized ZnO-Gd nanocrystals (NCs) were coated by a bilayer lipid coating, making use of liposomes, using the Freeze-Thaw technique in liquid nitrogen. These liposomes were separatedly prepared, using commercially available lipids. Furthermore, to

augment the specific and active targeting of the system towards pancreatic cancer cells, CKAAKN peptide was inserted into the lipidic shell.

2.5.1.Preparation of Liposomes

The first step in the preparation of the liposomes was the obtention of the lipids' stock. The precise volume of DOPC (1,2-dioleoyl-sn-glycero-3-phosphocholine, Avanti Polar Lipids Inc.) solution in chloroform, which corresponded to 2.5 mg of lipids, was collocated into a glass test tube under chemical hood for enough time till complete chloroform evaporation. Subsequently, the dried lipids were dissolved in 400 µl of pure ethanol and 600 µl of bidistilled water, obtaining a 2.5 mg/ml DOPC solution. The presence of ethanol enabled the lipids' monomeric configuration, preventing their assembly into liposomes.

Once the stock was obtained, two types of liposomes were prepared, as reported in Figure 2.12. The first one consisted of merely DOPC, and the second one composed of DOPC coupled with a target ligand compound, consisting of DSPE-PEG(2000) Maleimide (Avanti Polar Lipids Inc.) linked to the CKAAKN target peptide.

The preparation process was based on a solvent-exchange method. The DOPC lipid stock was diluted by a 1:10 factor in bidistilled water in an Eppendorf tube. Lipids naturally changed their configuration from monomers to self-assembled liposomes, due to the increased amount of water. Solely DOPC liposomes' preparation was completed.

In order to obtain the second type of liposomes, the previous protocol was repeated, adding the target peptide compound to the so-formed liposomes, in a molar ratio of 99.5:0.5 mole % (DOPC:DSPE-PEG(2000)-Maleimide-CKAAKN). The stock of the target peptide compound had a concentration of 20.375 mg/ml and was obtained by the optimization of an existing protocol; the molecular weight was 3688.6 g/mol.

For the calculus of the exact amount of peptide to be added to the liposomes' solution, the corresponding moles of 25 µl of DOPC stock lipids were estimated. The stock's concentration was 2.5 mg/ml and the molecular weight was 786.113 g/mol. Therefore, 25 µl of solution amounted to 0.0004 moles. To respect the molar ratio, the needed volume of functional lipids linked to the target ligand was computed as 0.08 µl. As handling such a small volume could easily carry the risk of error, stocks of 10 µl of DSPE-

PEG-CKAAKN lipids diluted by a 1:10 factor in ethanol were prepared, making the manipulation of such small quantities more accessible.

Once both liposomes' samples were prepared, an incubation period of 8 hours, optimized by a research group member, was performed in an orbital shaker (VWR Incubating orbital shaker, Professional 3500) at 200 rpm and 37 ºC. This process aimed at the stabilization of the so-formed liposomes in both cases, and the correct incorporation of the peptide compound into the lipidic shell for the peptide-containing sample.

Ultimately, the samples were dialyzed. The dialysis process, previously optimized, allowed the remotion of the unbounded peptide but was performed on both samples to obtain a uniform protocol. SnakeSkin Dialysis Tubing (3.5K MWCO, 16 mm dry I.D., 35 feet, Thermofisher Scientific) was cut into 10 cm pieces. A handmade tight knot was performed at one end of the membrane, previously soaked in bidistilled water for easier handling. The knot was then sealed with Parafilm and a plastic clip, to avoid leakage. The sample was added from the open end, and an equal procedure of knotting was performed to close the dialysis bag. Dialysis was carried out putting the samples into a jar containing a magnet and the amount of bidistilled water to reach a ratio of 1 litre or water for each ml of liposomes' solution. The jar was then closed and positioned for 18 hours over a stirring plate, at 70/80 rpm.

The above-described samples were stable for 7 to 10 days after their preparation if kept at room temperature in a cool and dark place. Depending on the experiments needed, different volumes were prepared to be used subsequently, always respecting the proportions previously described. When the samples were to be used for cell treatments, all the above-mentioned procedures were developed in sterile conditions under a biological hood.

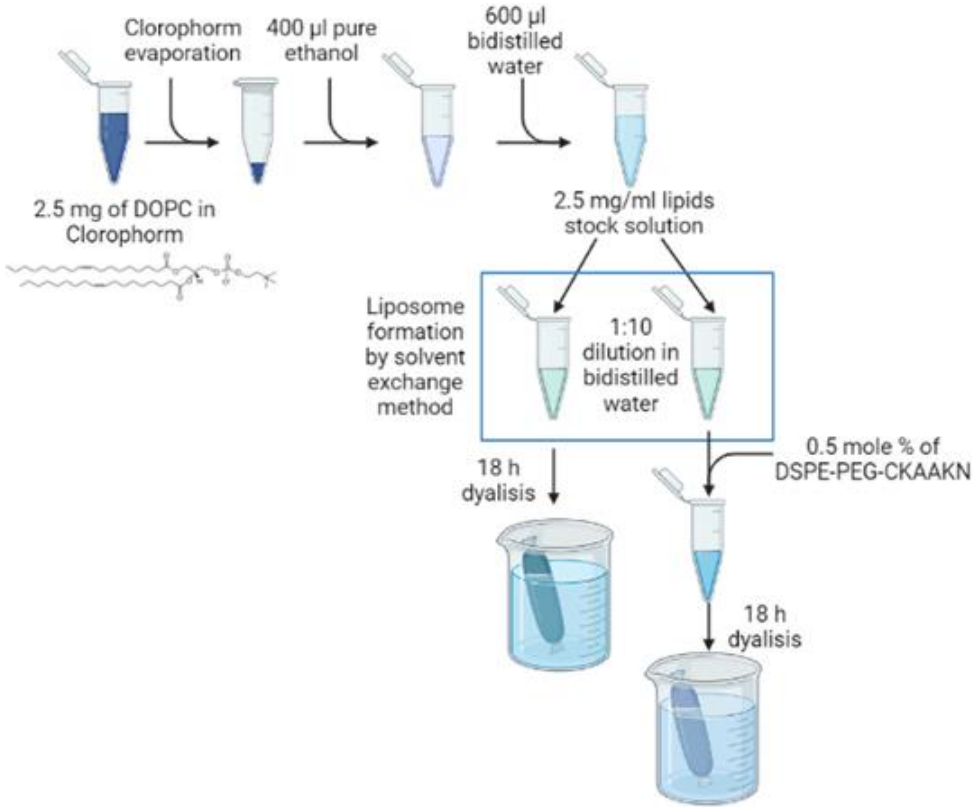

Figure 2.12: Preparation of DOPC solution and protocol for DOPC and DOPC:DSPE-PEG-CKAAKN liposomes

2.5.2.Lipid Coating of NanoCrystals

The lipid coating of the NCs was executed by exploiting the freeze-thaw technique. It consists in freezing the samples using liquid nitrogen, at -196ºC, and thawing them at room temperature. The liposomes' membrane suffers from disruption, reorganization (also in terms of lamellarity) and fusion, allowing the shell formation around the NCs.

The desired amount of drug-unloaded NCs was collected from the stock colloidal suspension and put into an Eppendorf tube. Centrifugation at 14000 RCF for 10 minutes was performed and the ethanol supernatant was removed. The obtained pellet was resuspended in a proportion of 1 µl of bidistilled water for each 10 µg of NCs, and vigorously mixed; the dispersion of the pellet in bidistilled water using this ratio was assessed by an optimization process previously developed.

The drug-loaded NCs pellets, which were kept at -20ºC overnight (see section 2.4.5), were put at room temperature before being suspended in bidistilled water using the same above-mentioned proportions.

Therefore, all stocks obtained had a proportion of 1 µl water for 10 µg NCs. The needed amount of NCs could be easily calculated and taken in order to prepare the different samples needed for the cell treatments and characterization processes.

The freeze-thaw technique protocol was optimized by another research team member. The selected number of cycles was 6 and a volume:volume:weight ratio was determined as 1:0.5:0.5; 1 referred to the corresponding volume (µl) of the only DOPC liposomes, 0.5 to the DOPC-peptide solution (µl) and 0.5 to the nanocrystals weight (µg).

Samples were obtained by sonication and vortexing (1 minute each) of the liposomes' stock solution. The corresponding volume of DOPC liposomes' sample was added in a Cryovial, considered as 1 ratio. Then, the required DOPC-peptide liposomes were added, in a ratio of 0.5 in volume, and finally, NCs dispersed in water were taken from the previously developed samples, for a 0.5 ratio in weight, added to the cryovial, and vigorously mixed with a pipette.

The Freeze-Thaw technique was applied. Samples were immersed in liquid nitrogen for 3 minutes until frozen. The thaw process was carried out at room temperature for a sample dependent time (approximately 30 minutes per ml of sample). The consecutive freeze and thaw sequence represents one complete cycle of the process. Therefore, it was repeated 6 times.

After the 6^{th} cycle, and once the sample was completely thawed, the so-obtained nanoconstructs were stabilized by one hour of shaking under incubation conditions (200 rpm at 37 ºC). The whole process is depicted in Figure 2.13.

When LNCs were developed for the in-vitro studies, the samples' procedures were carried out in sterile conditions, under a biological hood. Freezing and thawing procedures were developed taking care of the conservation of the sterility of the sample.

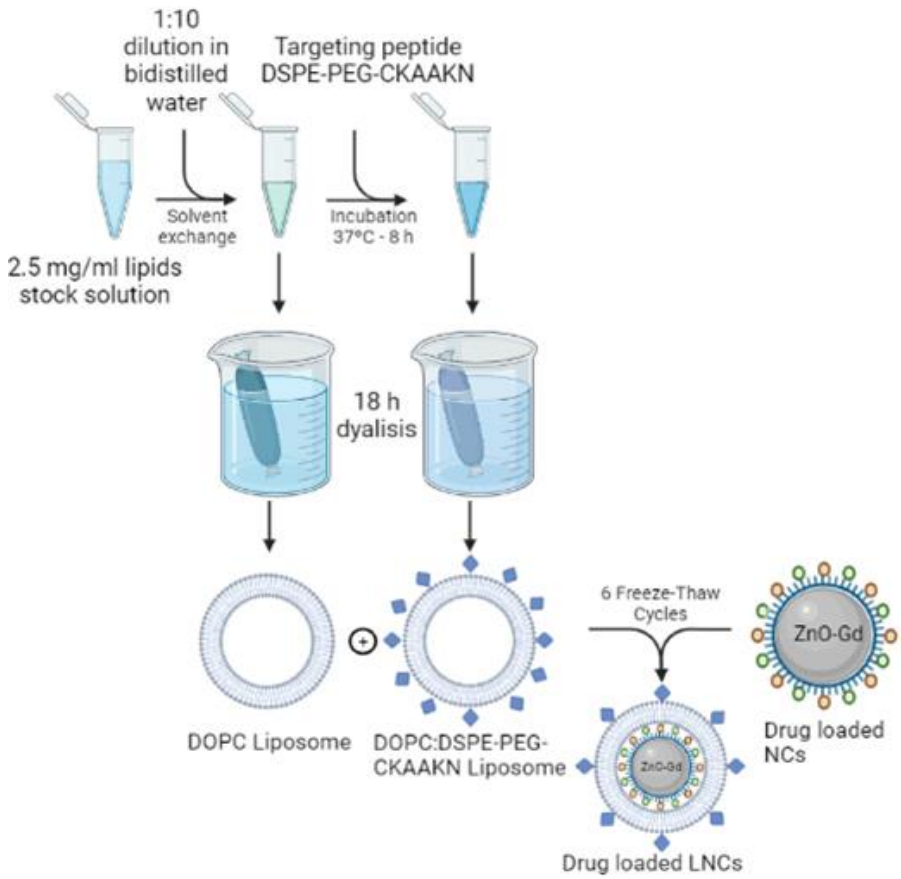

Figure 2.13: DOPC and DOPC:DSPE-PEG-CKAAKN liposomes' and LNCs preparation with F-T technique

2.5.3. Microscopy and Fluorescence Microscopy

Fluorescence microscopy allowed to monitor the correct lipidic encapsulation of the NCs, by the detection of multiple fluorescence indicators (fluorophores) which specifically label single target molecules.

Fluorophores' activity is based on the phenomenon of fluorescence; emission of light is provoked in the indicator when excited by an emitted ray, presenting specific absorption and emission wavelength bands.

The technique consists of the illumination of the whole specimen analyzed by a parallel beam of light (or wide-field of view), consisting in a specific band of wavelengths, of high intensity. The effect is the excitation, via the filter block, of the fluorophores contained in the sample. The resulting fluorescence is captured electronically by a camera. The ultimate goal is the separation of the emitted light from the excitation light, by the use of optical filters and their correct selection in terms of the indicators used. The latter should preferably present high emission quantum yields (high ratio of the

number of photons emitted to that absorbed), and their efficiency is expressed by an extinction coefficient, namely the likelihood of absorbing the light at the given wavelength per mass density.

Fluorescence microscopy was performed with a wide-field fluorescence inverted microscope (Nikon Eclipse Ti-E), equipped with a high-resolution camera (Zyla 4.2 Plus, 4098×3264 pixels, Andor Technology) using a 60× and 100x immersion oil objective (Apo 1.40, Nikon), with a super bright wide-spectrum source (Shutter Lambda XL), operating with NIS-element software.

Liposomes were labelled by linking the target ligand to FITC dye (excitation peak 495 nm, emission peak 519 nm), and images were obtained with the green channel; while NCs were tagged with Atto 550 NHS ester (excitation peak 544 nm, emission peak 576 nm), being images obtained with the red channel. Both resulting images were merged by means of the co-localization tool of the NIS-Element Software, to assess the encapsulation of the nanocrystals inside the lipidic shell.

For the preparation of the samples, firstly NCs were labelled with Atto 550. To this aim, the corresponding volume of NCs needed were collected from the stock and put into an Eppendorf tube, previously coated with an aluminium foil to prevent the dye's degradation because of the entering of light. Subsequently, Atto 550 NHS ester (Sigma Aldrich) was added in a volume:weight ratio of 1 µl per 500 µg of NCs. A little magnet was cleaned with ethanol and put into the tube, which was consecutively closed and positioned over a stirring plate, at 200rpm, to perform the labelling process overnight.

Once finished, the magnet was taken out, centrifuge was performed (at 14000 RCF for 10 minutes), and the supernatant containing not linked dye was removed and thrown away, always in dark conditions and taking care to not let light pass through the tube. Afterwards, two washing steps were performed by adding the quantity of pure ethanol needed to reach a 1 mg of NCS/ml concentration. Completed the washing procedures, the obtained pellet of dyed NCs was resuspended into bi-distilled water, following the protocol mentioned in paragraph 2.5.2, so as to maintain the reproducibility and consistency of the samples for following characterization processes and cell treatments.

For the labelling of the liposomes for the microscopy nanoconstruct samples, the procedure explained in section 2.5.1 was carried out with some

modifications. The CKAAKN peptide (DSPE-PEG-CKAAKN) was first linked to the FITC dye and then added to the DOPC liposomes' solution before carrying out 8 hours of incubation and 18 hours of dialysis. All procedures were developed under dark conditions, covering first the Eppendorf tube and then the jar for the dialysis process with aluminium foil.

Finally, the nanoconstructs with the labelled components were obtained following the encapsulation process reported in section 2.5.2.

1 µl of the nanoconstructs' solution was diluted in a ratio 1:20 in volume in bidistilled water. 2 µl of the obtained sample were put onto a microscope slide and covered with a cover glass, fixing it with nail polish drops. The slide was then turned upside-down and put onto the appropriate instrument's glass holder, where the sample's settlement was achieved by waiting a couple of minutes. The objective was oiled and juxtaposed with the glass, for the performance of the analysis by the illumination of the sample with the microscope objective.

Subsequently, different pictures of the samples were acquired, and the colocalization tool of the instrument was used for the evaluation of the encapsulation efficiency; setting a threshold between 0.1 and 1 µm, to avoid the consideration of larger aggregates. The spots in the red and green channel, for NCs and liposomes respectively, were counted. Images obtained were overlapped and merged so as to assess the encapsulation process, using the following equation for the calculation of the percentage of colocalized correctly encapsulated nanoconstructs:

$$\%\ coloc.\, NCs = \frac{(n^{\circ}\ coloc.\, spots)}{(tot\ n^{\circ}\ red\ spots)}$$

The successful encapsulation process was therefore measured by the quantity of ATTO550-labelled NCs that were effectively coated by the FITC-labeled liposomes' membrane (colocalized spots) with respect to only the red channel spots. In this work, a reduced amount of empty lipidic shells were considered acceptable.

2.5.4.Dynamic Light Scattering - Size

Liposomes alone, Nanoconstructs and Drug-loaded Nanoconstructs were characterized by DLS size and Z-Potential measurements. The procedures were equal to those previously described (sections 2.3.1 and 2.3.2), with only a modification. The prepared samples were vortexed and put into another

type of cuvette (ZEN0118), where 50 µl were sufficient, so as to avoid the waste of material.

2.5.5. Nanoparticle Tracking Analysis (NTA)

Nanoparticle Tracking Analysis (NTA) was exploited for the evaluation of the nanoconstructs' development, in terms of the hydrodynamic diameter, size distribution and concentration.

The instrument utilized was NanoSight NS300 (Malvern Panalytical). It consists of a chamber where a minimum volume of 500 µl of sample is put to be analyzed. This chamber is then irradiated with a laser beam that suffers from scattering when encountering nanoparticles. The detection is carried out by a 20x magnification microscope, which is connected to a camera that tracks the Brownian motion, and therefore all calculations are carried out, using the same principles as described in section 2.3.1. Detection measurements are reliable within a concentration of the sample in the range of 20-80 particles/frame.

Samples were prepared as previously described. Afterwards, dilutions of small volumes (50 µl) of the nanoconstructs' solutions in double-distilled water (500 µl) were obtained. Measurements were carried out, checking on the quality criteria above-mentioned; if the sample did not meet such requirements, successive dilutions were performed until reaching the expected values.

2.6 Drug Release in RPMI

Drug release experiments into cell culture media (RPMI) was performed. The aim of these analyses was to assess the retention of the drug previously loaded on the NCs surface, in both pristine and lipid-coated configurations, when exposed to cell culture media before arriving to their ultimate target.

Sorafenib and Vismodegib uptakes were developed on naked NCs, which were then used both as drug-loaded pristine NCs, and drug-loaded lipid coated LNCs, obtained after performing the previously reported protocols. The same drug-unloaded samples, both in pristine and LNCs configurations, were taken as control. All samples were monitored for 96 hours of RPMI culture, being the data collected at different time points.

In order to analyze the quantity of drug being released in RPMI media, calibration curves had to be created for both Sorafenib and Vismodegib. Although the hydrophobicity of the drugs, the dilution in this media was

possible because of the presence of salts. The standard samples, with known concentrations of each drug in RPMI were obtained and analyzed in the same way as depicted in section 2.4.3, including one additional sample with a concentration of 0.001 µM. 100 µl of each solution were analyzed in the UV-Vis reader, the absorbance spectra were obtained, the data was linearly fitted and the calibration curves' interception and slope values were collected.

The protocol developed for assessing the RPMI release was the same for both Sorafenib and Vismodegib and is the following described. For each drug, the corresponding colloidal solution volume for obtaining 350 µg of NCs was collected and put into 4 different Eppendorf tubes. Centrifugation at 14000 RCF for 10 minutes was performed, and pellets were obtained by removing the supernatant.

For Sorafenib samples, two pellets were redispersed in Sorafenib solution (1mM) in ethanol. The other two pellets were instead dispersed in the drug's solvent, in this case, pure ethanol.

For Vismodegib samples, two pellets were dispersed in Vismodegib in DMSO (1mM) solution, and the other two in DMSO alone.

Samples followed the described uptake protocol (paragraph 2.4.4), being the stirring time of 2 hours for Sorafenib samples and 3.5 hours for Vismodegib samples. After the absorbance analysis, all pellets were stored in the freezer (-20^{o}C) overnight.

Afterwards, one drug-loaded and one drug-unloaded sample went through the lipid coating process (explained in section 2.5.2), while the other two remained stored in the freezer without following treatments. Once obtained the LNCs, and as depicted in Figure 2.14, all four pelleted samples containing 350 µg of NCs and LNCs, drug unloaded and loaded, were resuspended into 700 µl of RPMI (ratio 1:2 weight in volume). For obtaining significantly statistical results, triplicate experiments were carried out. 3 Eppendorf tubes containing 800 µl of RPMI were filled with 200 µl of the previously obtained solutions, having each a concentration of 100 µg of NCs per 1 ml of RPMI.

As blank control samples, 1 ml of RPMI was put in 3 different Eppendorf tubes.

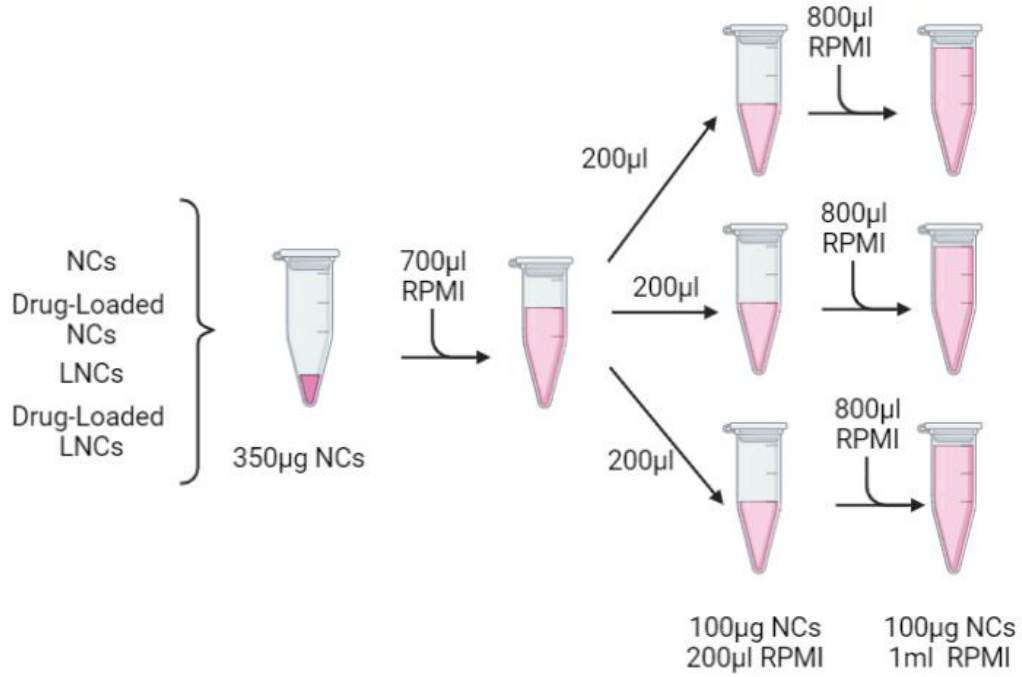

Figure 2.14: Sample preparation for drug release experiment in RPMI.

Consequently, 15 samples were obtained for each drug. They were put in an orbital shaker at 200 rpm, at 37 ºC. The concentration of drug release was assessed at different time points (0.5, 2, 24, 48, 72, and 96 hours), by performing a centrifuge of all samples at 10000 RCF for 5 minutes and collecting 3 aliquots of 100 µl of supernatant of each sample and filling the Quartz glass microplate's wells. Because of the centrifuge process, a pellet in the bottom of each tube was obtained, so special care was taken in order not to collect NCs, avoiding touching the pellet or making it disperse. Control samples were subjected to the same protocol for uniformity of the treatment. UV-Vis absorbance measurements were performed, at the corresponding wavelength used for the calculus of the calibration curve.

Once the needed supernatant had been carefully taken out of the samples, the pellets were redispersed in the remaining 700 µl of RPMI, mixing with the pipette and vortexing. All samples were put again into the orbital shaker until the development of the reading.

Once the reading was done, the 300 µl of each sample were put back into the corresponding tubes, vigorously mixed and vortexed again for homogenization, to continue with the release experiment.

Drug release was evaluated at each time step. The absorbance value for each sample was taken. The respective control absorbance was subtracted,

to remove the background; in the case of NCs the background consisted of RPMI and NCs, whereas for LNCs, it was RPMI and LNCs.

After this process, the concentration of each drug was calculated, using the respective calibration curve obtained in previous experiments.

2.7 In-Vitro Assays

The aim of this Master's Thesis work was the development of nanoconstructs consisting of lipid-coated dual drug-loaded NCs, which could specifically target and kill pancreatic cancer cells, not provoking toxic effects on the healthy cells surrounding the tumour.

For this aim, the drug-loaded LNCs were tested on three different cell lines: BxPC-3 (a human pancreatic cancer cell line), AsPC-1 (a human pancreas adenocarcinoma ascites metastasis cell line) and HPDE (human pancreatic duct epithelial cells).

The nanoconstructs were tested on the above-mentioned cells. Cellular uptake was assessed by fluorescence microscopy, cytotoxicity of the compounds was evaluated with WST-1 assay, and apoptotic events were checked through the apoptosis/necrosis assay.

2.7.1. Fluorescence Microscopy

Cellular uptake of the nanoconstructs into the pancreatic cancer cells was assessed through fluorescence microscopy, explained in paragraph 2.5.3.

For the development of the experiment, liposomes were labelled by linking the target peptide with FITC, as explained in section 2.5.5, while cell membranes with Wheat Germ Agglutinin, Alexa Fluor™ 647 Conjugate (WGA647, Thermo Fisher) (excitation peak at 650 nm, emission peak at 668 nm). Afterwards, drug-unloaded LNCs were obtained, as reported in section 2.5.2, and AsPC-1 and BxPC-3 cells were treated using a concentration of 30 µg/ml, for 20 hours.

2.7.2. Cell Viability Assay

To assess the cytotoxicity of the drug-loaded LNCs, drug unloaded, single drug loaded and dual drug-loaded samples were prepared as explained in section 2.5.2.

Firstly, both pancreatic cancer cell lines (i.e. AsPC-1 and BxPC-3) were treated with Sorafenib-loaded LNCs in concentrations of 10, 20, 30, 40, and 50 µg/ml (µg of NCs/ml of RPMI). The cells were also treated with the same concentration of drug-unloaded LNCs, and free Sorafenib at the same concentration that the uptake obtained on the surface of the NCs.

Further experiments were performed with the use of single Sorafenib and Vismodegib loaded LNCs and dual drug-loaded LNCs. In this case, the nanocontructs were prepared following the procedure explained in Section 2.5.2, and administered to the cells with a concentration of 20 µg/ml for 48 hours. Two different initial conditions of the cells were considered. The first one was untreated cells, that were then treated with the drug-loaded LNCs; whereas the second group was pre-treated for 24 hours with 10 µM Gemcitabine and then treated as the first one.

The same experiment was developed with HPDE cells, only in non-Gemcitabine-pretreated conditions. These cells were treated with Sorafenib, Vismodegib and dual drug-loaded LNCs for 48 hours using a concentration of 20 µg/ml.

After each of the treatments, cells were exposed to WST-1, a cell proliferation reagent, in order to analyze the cytotoxicity of the LNCs. Cells' mitochondrial dehydrogenases can convert tetrazolium salt WST-1 to formazan, being the latter a dye, whose absorbance can be measured using a microplate reader. If cells are viable, a higher concentration of the dye will be present, as mitochondrial activity would be maintained, therefore causing high values of absorbance of the reading.

2.7.3. Apoptosis/Necrosis Assay

The conjunction of the effects of the drugs and the LNCs should direct the cell into apoptotic phenomena; being apoptosis the programmed cell death through particular signalling pathways.

The evaluation of the presence of this process, and therefore the efficiency of the treatment, was assessed by the apoptosis/necrosis assays. These experiments exploit the cells' characteristic processes during their death. The externalization of phosphatidylserine (PS) to the cell surface happens when cells go through the apoptotic process in early stages; whereas the cells' membrane degradation is an event present in late apoptosis stages or necrosis.

For these analyses, the final constructs (Sorafenib and Vismodegib single and dual drug-loaded LNCs) were prepared as reported in paragraph 2.5.2, and administered to the cells with a concentration of 20 µg/ml. In parallel, the same amount of drugs contained in the NCs surface was administered as free drugs.

Once the treatments were developed, cells were exposed to a specific reagent (Guava® Nexin Reagent). This reagent permits the distinction of the molecules of PS, and therefore the apoptotic process, due to its content of labelled Annexin V protein. It also allows determining the necrotic or late apoptotic effects, because it contains 7-AAD, a dye used as an indicator of the cell's membrane integrity. At this point, apoptotic events caused by the administration of the nanoconstructs were evaluated through flow cytometric analyses.

3 Results and Discussion

This chapter presents the results achieved in this Master Thesis work.

Zinc oxide nanocrystals are primarily characterized in their undoped configuration and after being doped with the rare earth element Gadolinium. XRD diffractogram and FESEM images are presented.

Upon functionalization of the Gadolinium-doped NCs with amino propyl functional groups, further characterizations are developed, in terms of hydrodynamic size and zeta potential, chemical and physical composition, and surface properties.

3.1 Characterization of Ol-ZnO-Gd NCs

In the first place, the freshly synthesized Zinc Oxide nanocrystals, in their undoped (undoped NCs) and Gd-doped (Gd-doped NCs) configurations were characterized in terms of their crystalline structure and morphology.

To proceed to such subsequent analyses, the very first step was knowing the concentration of the colloidal suspension obtained. Both samples underwent the protocol explained in paragraph 2.2, and the resulting concentrations are shown in Table 3.1. This information was later used for calculating the precise amount of nanocrystals needed for the different characterization methods.

NCs	Concentration
Undoped NCs	4.2 mg/ml
Gd-doped NCs	2.5 mg/ml

Table 3.1: Concentrations of synthetized pristine and Gd-doped Ol-ZnO-NCs

3.1.1. X-Ray Diffraction (XRD)

X-ray diffractometry (XRD) was performed to obtain details about the crystalline structure of the NCs and exclude the presence of unwanted secondary phases due to the doping reaction.

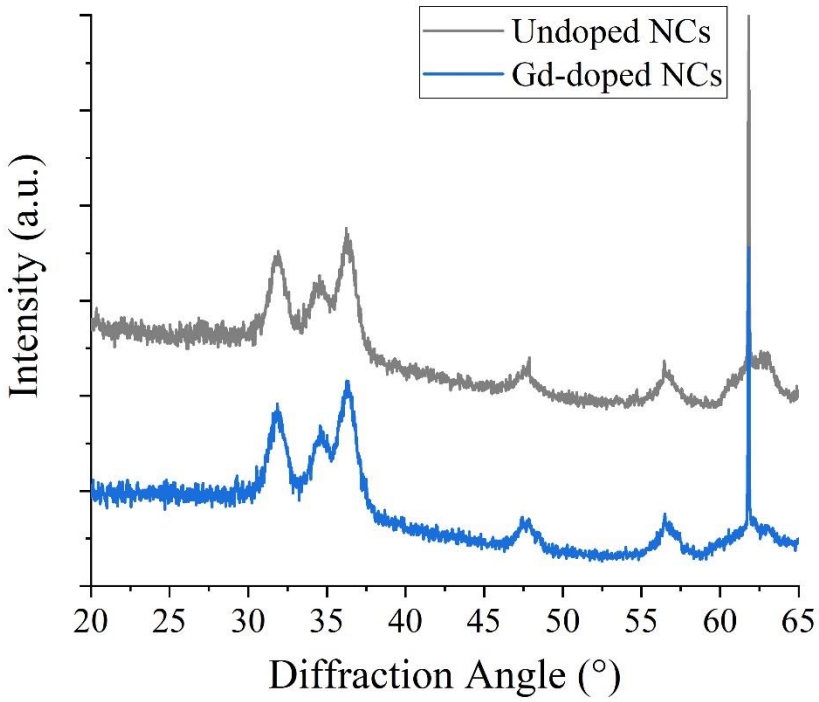

Figure 3.1: X-ray diffractograms of undoped and Gd-doped Ol-ZnO-NCs.

Crystallographic plane	Diffraction angle Undoped NCs	Diffraction angle Gd-doped NCs
(100)	31.9º	31.8º
(002)	34.4º	34.5º
(101)	36.4º	36.3º
(102)	47.6º	47.5º
(110)	56.7º	56.5º

Table 3.2: XRD diffraction angles of undoped and Gd-doped Ol-ZnO-NCs, and relative crystallographic planes.

The XRD patterns obtained from both samples, shown in Figure 3.1: X-ray diffractograms of undoped and Gd-doped Ol-ZnO-NCs., do not display considerable differences. Table 3.2 reports the diffraction angles obtained, that correspond to the wurtzite crystalline structure characteristic peaks according to the standard XRD pattern of ZnO (JCPDS card n. 36-11451), thus confirming the absence of undesired oxides due to the reaction phase and doping elements. Moreover, Gd-doped NCs showed unvaried lattice parameters upon doping with Gd, confirmed by the absence of any significant peak shifts.

3.1.2. Field Emission Scanning Electron Microscope (FESEM)

Field Emission Scanning Electron Microscope (FESEM) was used for the analysis of the shape and morphology of the NCs.

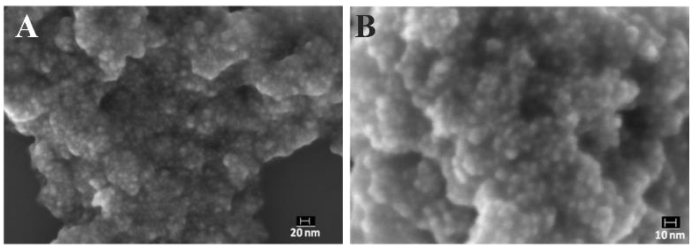

Figure 3.2: Field emission scanning electron microscopy (FESEM) image of undoped (A) and Gd-doped (B) Ol-ZnO-NCs.

The FESEM analysis, reported in Figure 3.2, showed spherical-shaped morphology of the nanocrystals, with average diameters ranging from 5 to 8 nm. These results were comparable to those previously described by Dr. Sugata Barui [39]. The content of Gd dopant was estimated by EDX, confirming a doping level of 0.37 at%, in line with the previously reported results.

3.2 Characterization of functionalized Ol-ZnO-Gd NCs

Once the functionalization reaction was completed, as detailed in paragraph 2.2, the functionalized Gd-doped Ol-ZnO nanocrystals (in the following called only NCs) underwent the protocol for concentration calculation, as previously described. Table 3.3 summarizes the results obtained, which were then used to prepare the NCs in specific amount, for further characterization in terms of chemical composition, physical and surface properties, as well as for subsequent drug uptake.

Sample	Concentration
NCs-unfunc	2.5 mg/ml
NCs	3.28 mg/ml

Table 3.3: Concentration of suspension of pristine and functionalized NCs

3.2.1. Dynamic Light Scattering – Size

The hydrodynamic size distribution of the nanocrystals was evaluated by DLS measurements right after the functionalization. Pristine and functionalized NCs were analyzed in two different dispersants: ethanol (EtOH), in which they were synthesized and stored, owing to an optimal dispersion in this media, and water, in which they were to be dispersed for applicative purposes, as their final aim was to circulate into biological fluids.

As reported in Figure 3.3a and 3.3b, all the samples showed a monodispersed size distribution, ranging between 180 and 195 nm in both ethanol and water. These narrow distributions were confirmed by the low values of the Polydispersity Index (PDI) reported in Table 3.4, not exceeding the value of 0.2, characteristic of monodispersed samples.

The results in terms of PDI confirm the monodispersed distribution and the stability of the nanocrystals in both media. The higher value of hydrodynamic diameters obtained by this technique than those described by FESEM measurements are due to the high number of ions adsorbed at the NCs surface. The surface chemical functionalization of the NCs with aminopropyl groups does not seem to affect the size distribution significantly.

Sample	Z-average	PDI
NCs-unfunc_EtOH	191 nm	0.166
NCs_EtOH	182.6 nm	0.168
NCs-unfunc_Water	189.4 nm	0.142
NCs_Water	191.8 nm	0.141

Table 3.4: Values of the average size of pristine and functionalized Gd-doped NCs

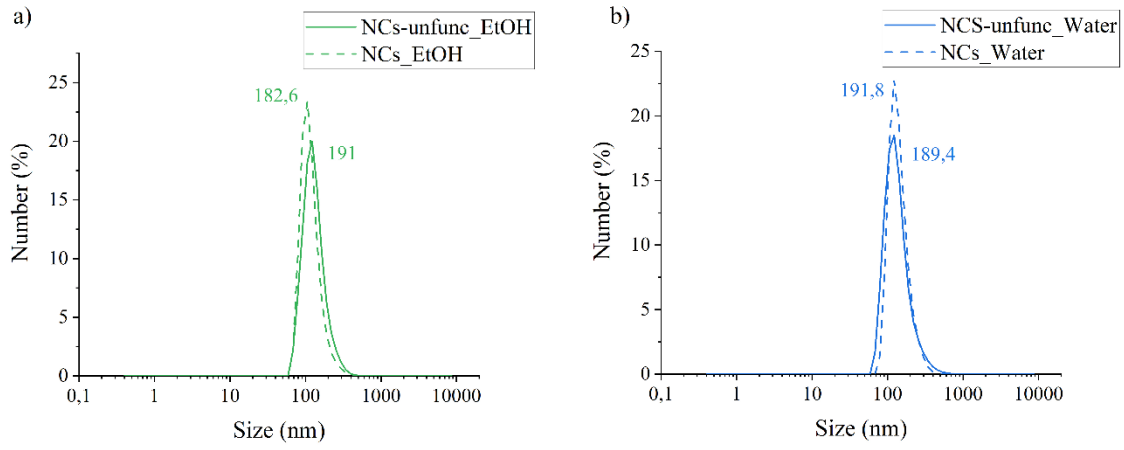

Figure 3.3: DLS measurements (number%) of unfunctionalized and functionalized NCs dispersed in Ethanol (a), and in bi-distilled water (b).

3.2.2.Zeta Potential measurements

The samples were dispersed in pure double-distilled water, to compare the zeta potential distribution between pristine and functionalized NCs at neutral pH. As shown in Table 3.5 and Figure 3.4, both samples exposed positively charged surfaces. The presence of -NH_2 groups in the functionalized sample determined an increase of the zeta potential value in comparison to the pristine one, as expected, resulting in increased stability in water. This fact can be explained by the positive charges exposed by the amine groups at pH 7 (i.e. -NH_3^+ group), as previously reported in the literature [27].

Sample	Z-Potential	St Dv
NCs-unfunc_Water	25.1 mV	0.1
NCs_Water	27.8 mV	0.458

Table 3.5: Z-Potential values of unfunctionalized and functionalized NCs

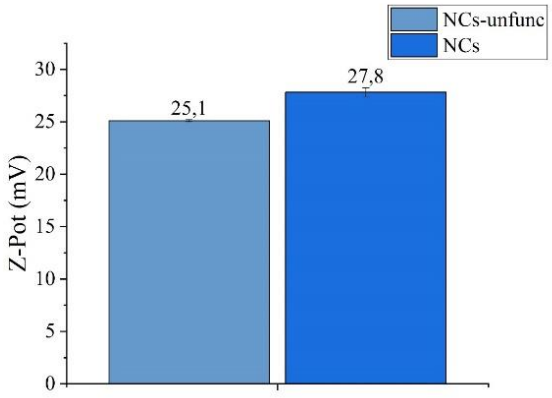

Figure 3.4: Z-Potential values of pristine and functionalized NCs in bi-distilled water.

3.2.3.Fourier-Transform Infrared Spectroscopy (FTIR)

The Fourier-Transform Infrared Spectroscopy (FTIR) measurement was carried out for both functionalized and unfunctionalized nanocrystals.

The spectra reported in Figure 3.5 display common features in both cases. A wideband from 3600 to 3200 cm^{-1} corresponds to the stretching vibration of hydroxyl (-OH) groups on the surface of ZnO. The highest peak, positioned at 440 cm^{-1}, is related to ZnO vibration in the fingerprint region. The peaks at 2925 cm^{-1} and 2860 cm^{-1} are attributed to asymmetric and symmetric stretching vibrations of methylene (CH_2) and methyl (-CH_3) groups derived from both oleic acid capping and amino-propyl functionalization, while those at 1570 cm^{-1} and 1420 cm^{-1} characterize residual acetate groups derived

from the synthesis (C=O and C-O vibrations), thus confirming the presence of the oleic acid.

Particularly, no significant differences arise when comparing functionalized and unfunctionalized NCs, as the peaks corresponding to the presence of amino (-NH_2) groups are almost not detectable. This could probably be due to the presence of the oleic acid signal, whose peaks cover the expected -NH_2 vibration peaks. Specifically, according to the literature [40], primary amine peaks should be located in the range from 1640 cm^{-1} to 1590 cm^{-1}, which in the FTIR spectra obtained, is occupied by the peaks corresponding to C=O bands due to the presence of the Oleic Acid.

Furthermore, the absence of the amino peaks could also be a consequence of the low amount of functional moiety APTMS used to carry out the functionalization (nominally just 10mol% with respect to the molar amount of ZnO NCs in the post-synthesis grafting). This result has also been obtained in the literature [41], where it was shown that the number of amino-propyl groups attached to the surface of the nanocrystals was very low. Nevertheless, and as it will be shown below, this tiny amount of such groups is sufficient for the efficient dye labelling of the NCs.

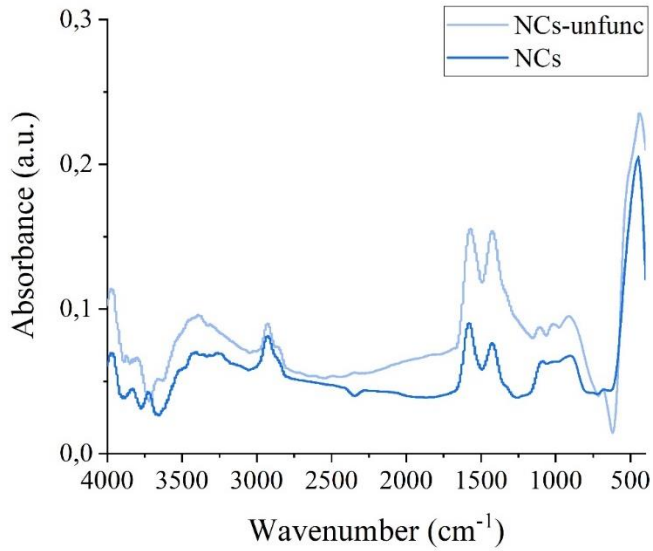

Figure 3.5: Fourier-transform infrared spectroscopy (FTIR) spectra comparison between unfunctionalized and functionalized (NCs) samples.

3.3 Drug Uptake

3.3.1. Calibration Curves

The absorbance spectra of Sorafenib in Ethanol and Vismodegib in DMSO were obtained by UV-Vis spectroscopy. The aim was to analyze the absorbance spectrum to identify, for each drug in each respective solvent, a particular wavelength in which an evident peak was shown for each concentration. Using the data contained at this wavelength, a calibration curve was plotted by reporting the absorbance versus the concentration of the drug. This curve was therefore used to calculate the amount of drug that was loaded on the NCs, by subtracting the remaining concentration of the drug in the solvent after the uptake process, from the initial drug concentration.

SORAFENIB IN ETHANOL

For the studies carried out with Sorafenib in Ethanol, which absorption spectrum is shown in Figure 3.6a, a strong peak could be differentiated at 265 nm. This was taken as the wavelength used for identifying the values of absorbance that were then taken into account for the plotting of the calibration curve, shown in Figure 3.6b.

However, as shown by the absorption spectra, concentrations of the drug equal to or higher than 500 μM, led to the saturation of the measurement, making the detection of a peak impossible to achieve. Therefore, the calibration curve was constructed taking into account the lower concentrations, up to 250μM, and the obtained curve was linearly fitted, achieving an R-square close to 1.

For the above-mentioned reason, and to maximize the drug loading, minimizing the saturation of the instrument, the following protocol was carried out. The uptake of the drug was performed with 1mM solutions, whereas the absorbance analysis to calculate the actual uptake was executed using a 1:4 dilution of the supernatant, obtaining a 250 μM solution that could be analyzed with the calibration curve. The calculated drug concentrations were then multiplied by a factor of 4, to recover the real concentration of drug uptake.

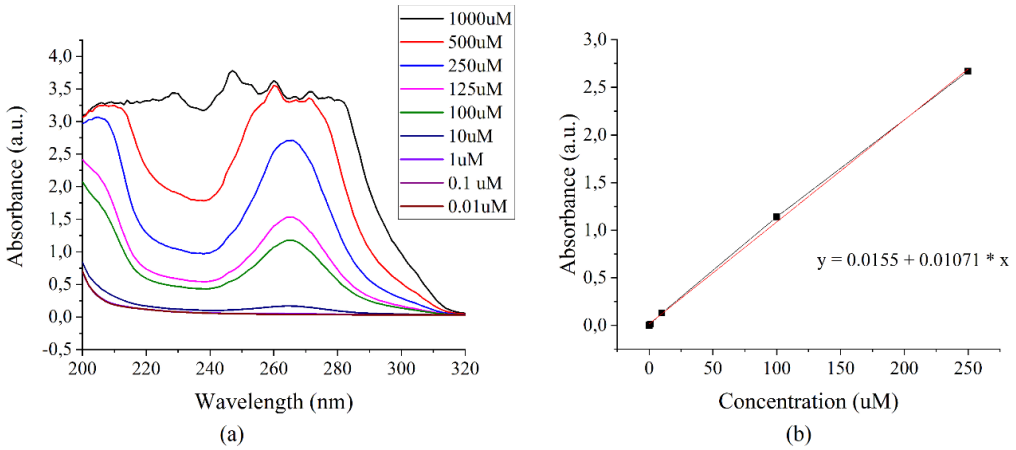

Figure 3.6: Sorafenib in ethanol. (a) Absorption spectra reported from 200 to 800 nm. (b) Calibration curve at 265 nm and fitting values.

VISMODEGIB IN DMSO

The absorbance analysis was also carried out for Vismodegib in DMSO. From the obtained spectrum (Figure 3.7), a narrow peak could not be identified for wavelengths higher than 260 nm. However, a small absorbance increase was detected around 280 nm for low concentrations, so this wavelength was chosen for the construction of the calibration curve, as it provided quite spaced values of absorbance at different concentrations.

The saturation of the instrument was again detectable for high concentrations, such as 1mM. However, and in contrast with the previous drug analysis, the saturation did not turn up to be a problem when using 500 µM concentrations. Thereafter, the standard curve was constructed with this maximum concentration, and a linear fitting was applied, obtaining an R-square value close to 1. To maximize the drug loading, 1mM solution was put in contact with the NCs, whereas the absorption reading of the drug uptake was executed using a 1:2 dilution of the supernatant obtained, corresponding to a concentration of 500 µM to avoid saturation of the reading. The obtained concentration was multiplied by a factor of 2 to recover the original value.

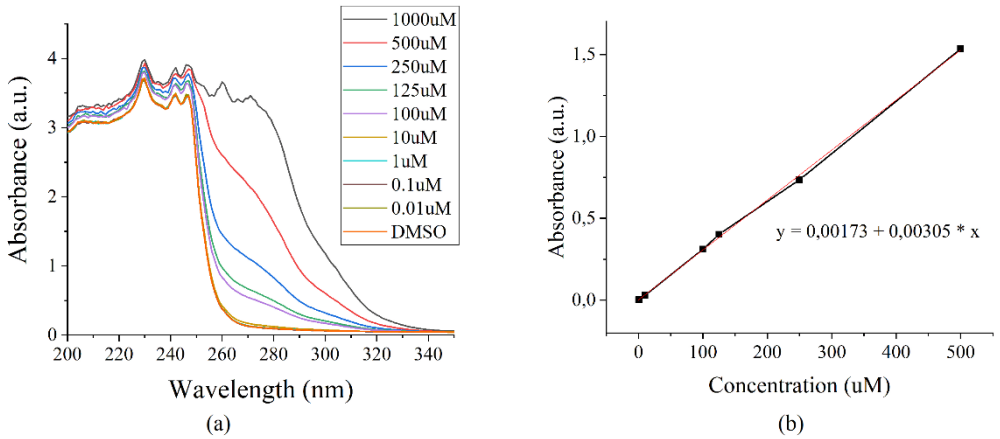

Figure 3.7: Vismodegib in DMSO. (a) Absorption spectra reported from 200 to 800 nm. (b) Calibration curve at 280 nm and fitting values.

SORAFENIB IN RPMI

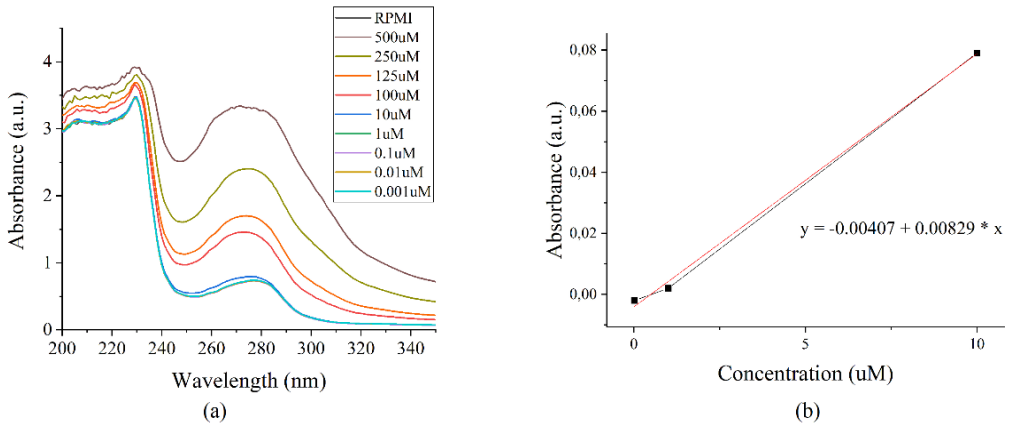

Figure 3.8: Sorafenib in RPMI. (a) Absorption spectra, from 200nm to 350nm. (b) Calibration curve, at 275nm, used concentrations: 0.01, 1, and 10 µM.

VISMODEGIB IN RPMI

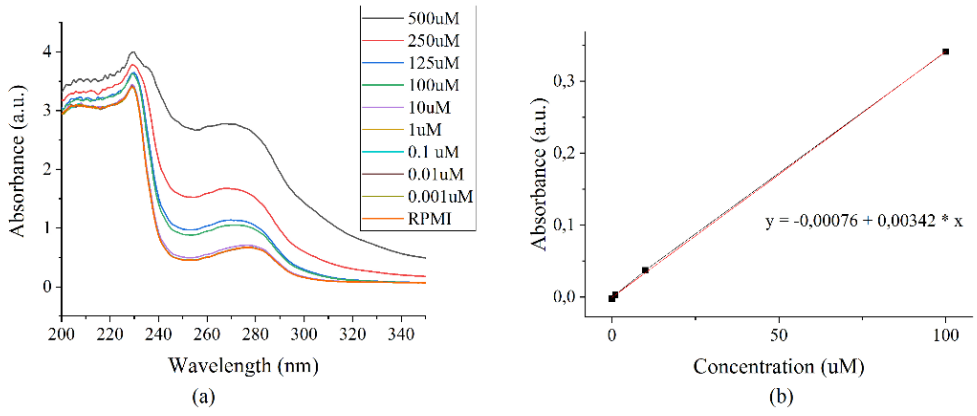

Figure 3.9: Vismodegib in RPMI. (a) Absorption spectra, from 200nm to 350nm. (b) Calibration curve, at 278nm, used concentrations: 0.001, 0.01, 1, 10, 100 µM

Sorafenib and Vismodegib absorption spectrum in RPMI were studied for the measurement of the drug released in culture media. For both drugs, the obtained spectrum showed saturation of the instrument at a concentration of 1mM, so this value was not considered.

For Sorafenib in RPMI, and as reported in Figure 3.8a, a peak at 275 nm was noticeable, thus this wavelength was selected for the creation of the calibration curve. Previous experiments carried out by laboratory members revealed that the quantity of drug released by the NCs in this media had concentration values around 1 μM. Thus a higher and a lower point were considered for the construction of the calibration curve (specifically 0.01, 1, and 10 μM), to reduce the polarization error that high concentrations might introduce. By executing the linear fitting of the curve, seen in Figure 3.8b, an R-square value of 0.99786 was obtained.

For Vismodegib in RPMI, which spectrum is reported in Figure 3.9a, the evident peak wavelength selected for the calculation of the curve was 278 nm. In the case of this drug, previous experiments demonstrated that the concentration released remained around 10 μM. Hence, the selected concentrations for the construction of the curve were 0.001, 0.01, 1, 10, and 100 μM. After the linear fitting, the R-square value obtained was 0.9979.

The values of intercept and slope were calculated and extracted from the linear fitting of the obtained curves, as summarized in Table 3.6. These values were then used to determine the concentration of the drugs in the test samples, using the data of the absorbance readings and making the calculations explained in Paragraph 2.4.4.

Sample	Wavelength	Intercept	Slope
Sorafenib in EtOH	265	0.0155	0.01071
Vismodegib in DMSO	280	0.00173	0.00305
Sorafenib in RPMI	275	-0.00407	0.00829
Vismodegib in RPMI	278	-0.00076	0.00342

Table 3.6: Wavelength of analysis and extraction of intercept and slope values for each drug solution.

3.3.2.Drugs Uptake Studies

The following studies aimed to find the time step of adsorption required for a meaningful quantity of each drug to be loaded on the NCs. Therefore, for each drug and its solvent, 5 different uptake time steps were considered,

as explained in paragraph 2.4.4, the uptake curve was gathered and the results were evaluated.

The uptake curve of Sorafenib is shown in Figure 3.10a. As it can be seen, a considerable uptake was obtained on the NCs surface after the first two hours, continuing to increment for the consecutive two hours (time steps 3 and 4), before decreasing by the 6th hour. This last fact can be hypothesized to be a consequence of the release of the drug into the solvent after such a period because the linking of the NCs to the surface takes place by adsorption and not by a covalent or strong boundary.

The time step of 2 hours was selected as the optimal one because it permits to reach a good compromise between the quantity of time required and the amount of drug-loaded on the surface of the NCs.

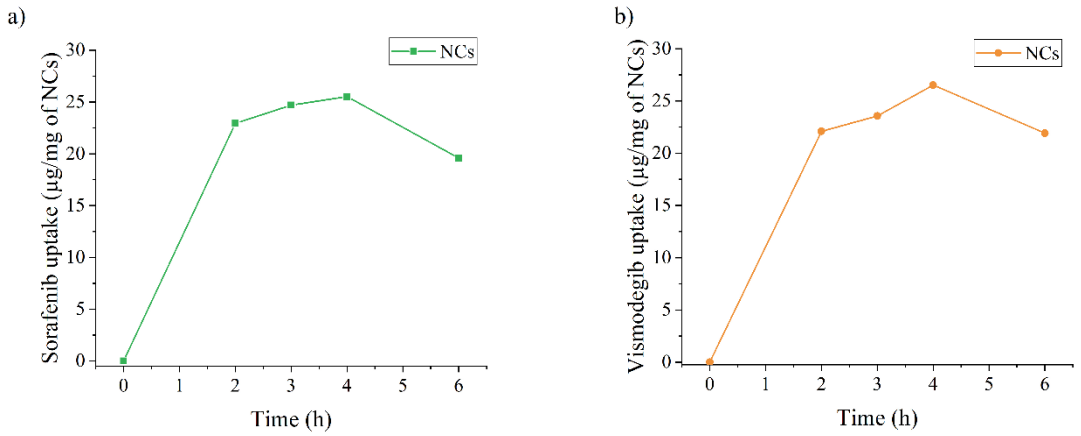

Figure 3.10: Drug uptake in NCs (µg drug/mg of NCs) for Sorafenib (a) and Vismodegib (b).

For the uptake of Vismodegib, as shown in Figure 3.10b, the highest value of uptake took place after 3.5-4 hours followed by a slow release.

As a result of these studies, and previous ones obtained by the research group, the time for the uptake of each drug, and their order when developing the dual drug loading were established. Firstly, 3.5 h of uptake of Vismodegib had to be carried out, followed by 2 h of Sorafenib uptake. Vismodegib was thus selected to be the first uptaken drug because it does not suffer any relevant leakage from the NCs surface once immersed in ethanol, i.e. during the following Sorafenib uptake.

Reaching these conclusions, the dual drug loading experiments were performed, and the uptaken drug was measured after each single drug uptake, as detailed in Figure 3.11. Results of the single drug uptake into the dual drug loaded NCs, are shown in Figure 3.12.

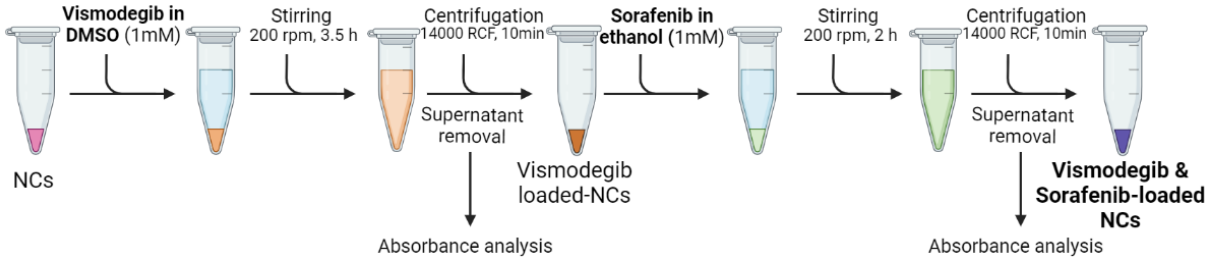

Figure 3.11: Schematic process of dual drug loading of NCs and uptake reading

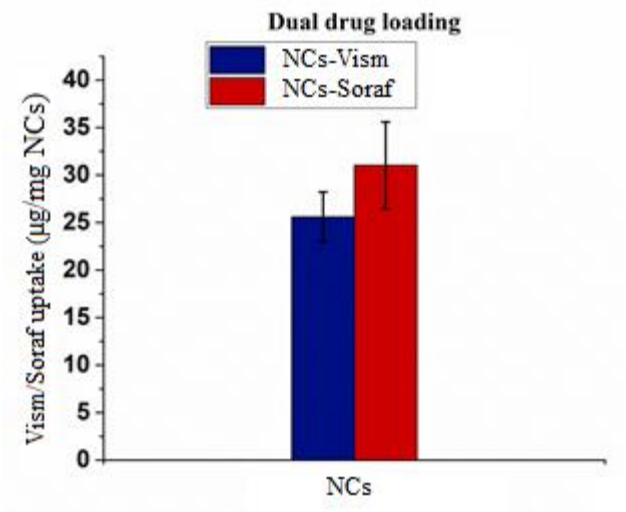

Figure 3.12: Drug uptake values of Sorafenib and Vismodegib (µg/mg of NCs), in dual-drug loaded samples.

3.3.1. Single and dual drug uptake

DLS - Size

The size distribution of the NCs was evaluated after the drug uptake, as described in paragraph 2.3.1. This experiment was aimed to understand if there were substantial differences in the size distribution values that could determine the presence of the drugs, not only in their single absorption but also in the dual drug-loaded sample. Figure 3.13 reports the size values after the single and dual drug uptake. Drug-loaded NCs exhibit an increase in the average size and also in PDI, in comparison with unloaded ones, as shown in Table 3.7. This increase could probably be due to the interaction between the NCs surface and the hydrophobic drugs. When the latter are adsorbed on the surface, the interactions between ions become weaker, increasing the hydrodynamic diameter measured by the DLS instrument. Results thus suggest the correct adsorption of all single and dual-drugs on the NCs' surface.

Sample	Z-average	PDI
NCs	191.8 nm	0.141
NCs-Soraf	393.8 nm	0.199
NCs-Vism	272.3 nm	0.15
NCs-Dual	294.8nm	0.238

Table 3.7: Values of the size of drug-loaded NCs

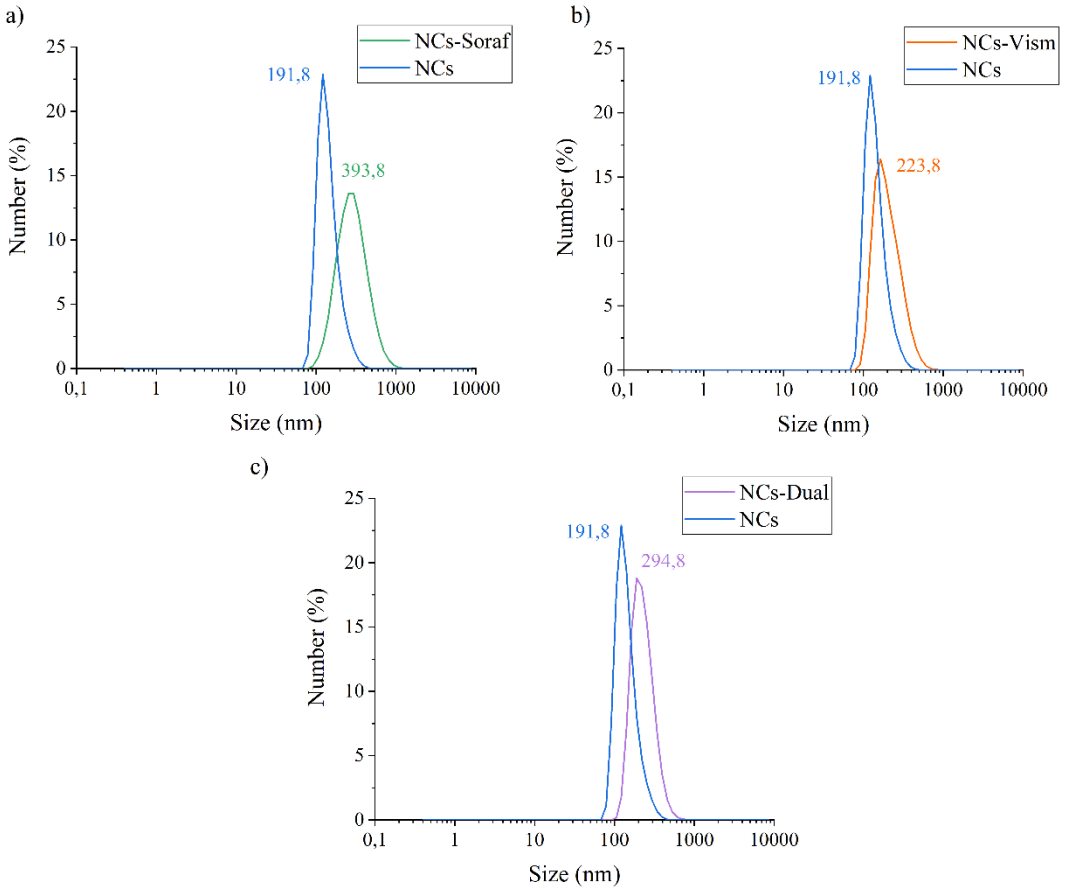

Figure 3.13: DLS measurements of drug loaded NCs, in comparison with NCs. (a) Sorafenib, (b)Vismodegib, and (c) dual drug-loaded NCs.

Zeta Potential

Dual drug loaded NCs sample was also characterized in terms of their Z-Potential and compared with the unloaded one. As reported in Table 3.8 and Figure 3.14 no significant differences were detected after the dual drug

adsorption, maintaining the positively charged surface characteristics, and allowing the correct successive coating with liposomes.

Sample	Z-Potential	St Dv
NCs	27.8 mV	0.458
NCs-Dual	25.8 mV	0.378

Table 3.8: Z-Potential measurements of dual drug loaded and unloaded NCs.

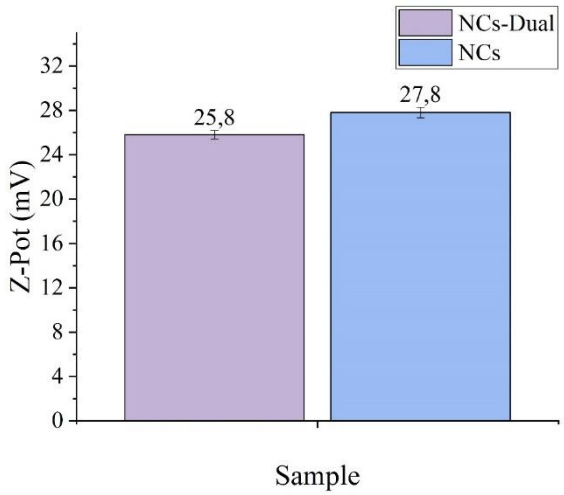

Figure 3.14: Z-Potential of dual drug loaded and unloaded NCs.

FTIR

The following analysis was carried out to evaluate the presence of the drugs on the surface of the nanoparticles.

No significant differences were noticed between the single and dual drug loaded, and the unloaded NCs. This could be explained by the fact that very low amounts of drugs were uptaken on the surface of the nanocrystals, whose peaks were not high enough to be comparable to the NCs ones.

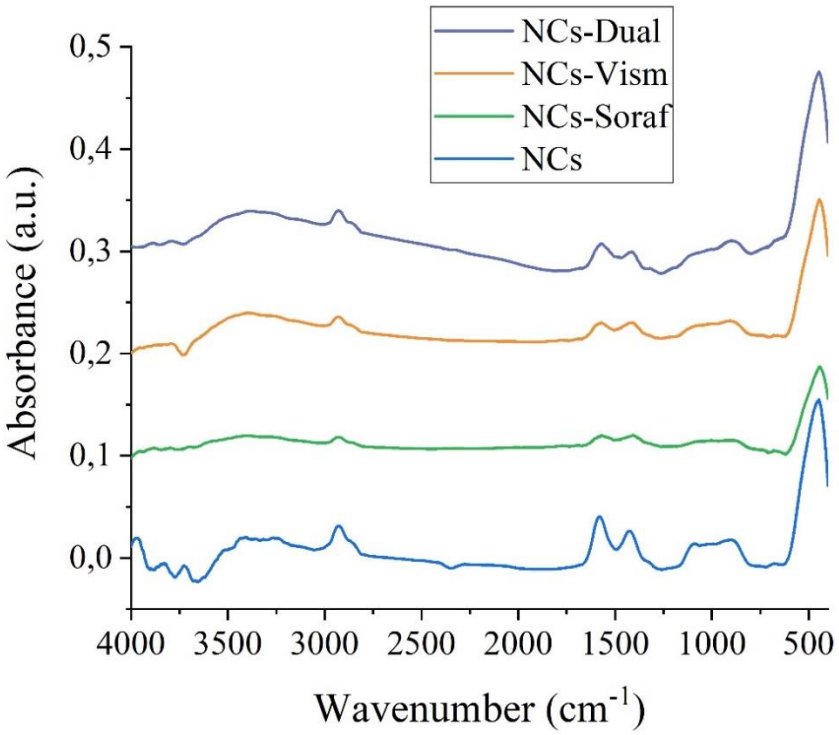

Figure 3.15: FTIR analysis of drug loaded and unloaded NCs.

3.4 Nanoconstruct Design

The following section regards the nanoconstructs development, and the characterization results obtained in the different processes needed to prepare them.

The main elements analyzed are the liposomes, obtained with commercially available lipid DOPC, and the conjugation with the specific targeting peptide DSPE-PEG-CKAAKN.

The characterizations were made in terms of size distribution with NTA techniques, and Z-Potential.

Finally, the coating of the nanocrystals with the lipid shell and the efficacy of the procedures were assessed.

3.4.1. Liposomes (DOPC and DOPC:DSPE-PEG-CKAAKN)

The functionalized Gd-doped ZnO NCs were coated with a lipidic bilayer derived from two different liposome formulations made with DOPC and DOPC: DSPE-PEG-CKAAKN, to generate the final nanoconstructs. Such

liposomes were obtained by a solvent-exchange method, and their size distribution characterization was carried out right after being formed, through NTA measurements.

The results obtained, shown in Figure 3.16 exhibit optimal stability of the liposomes and narrow size distribution, with average values of 138 nm for DOPC, and 147 nm for DOPC:DSPE-PEG-CKAAKN. This slight increase in size may be due to the presence of the target peptide component in the structure of the liposome.

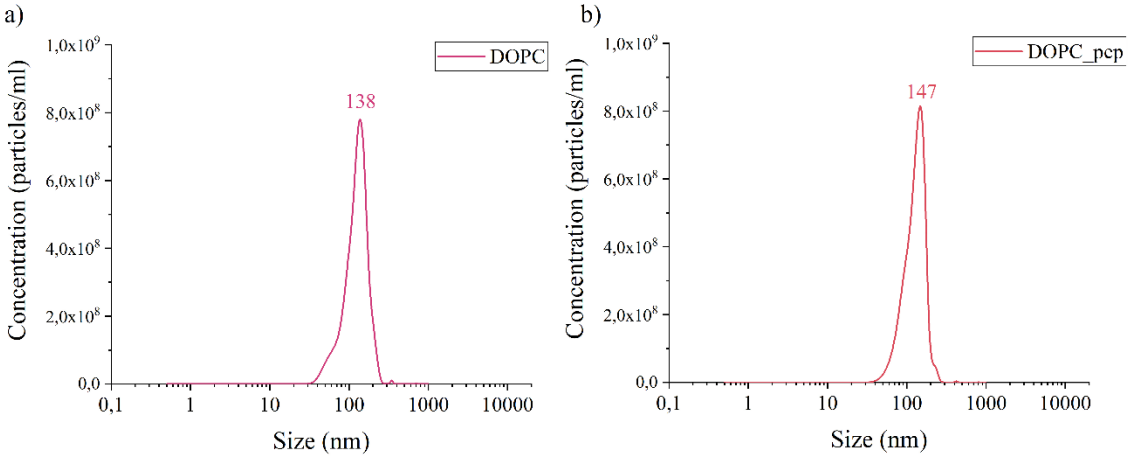

Figure 3.16: NTA analysis. DOPC (a) and DOPC-peptide (b) liposomes

The following coating of the NCs with the so obtained liposomes was achieved using the freeze-thaw procedure. Therefore, the technique was previously evaluated.

A mix of both types of liposomes was obtained using the proportions for the final nanoconstructs of 1:0.5 in volume between DOPC liposomes and DOPC:DSPE-PEG-CKAAKN liposomes. In absence of the NCs, this mixture was exposed to 6 consecutive cycles of 3 minutes of freezing in liquid nitrogen and the necessary time, i.e. approximately 15 minutes for 500 µl samples, of thawing at room temperature. The sample, obtained by the fusion of the membranes of the liposomes, was analyzed to determine the process effects on the so-formed DOPC-DOPC:DSPE-PEG-CKAAKN liposomes. Their size distribution is shown in Figure 3.17. It is noticeable that this type of process reduces the monodispersity of the sample size distribution, in comparison to the solvent exchange method previously analyzed, increasing not only the mean size values of the liposomes obtained but also the standard deviation, as reported in Table 3.9.

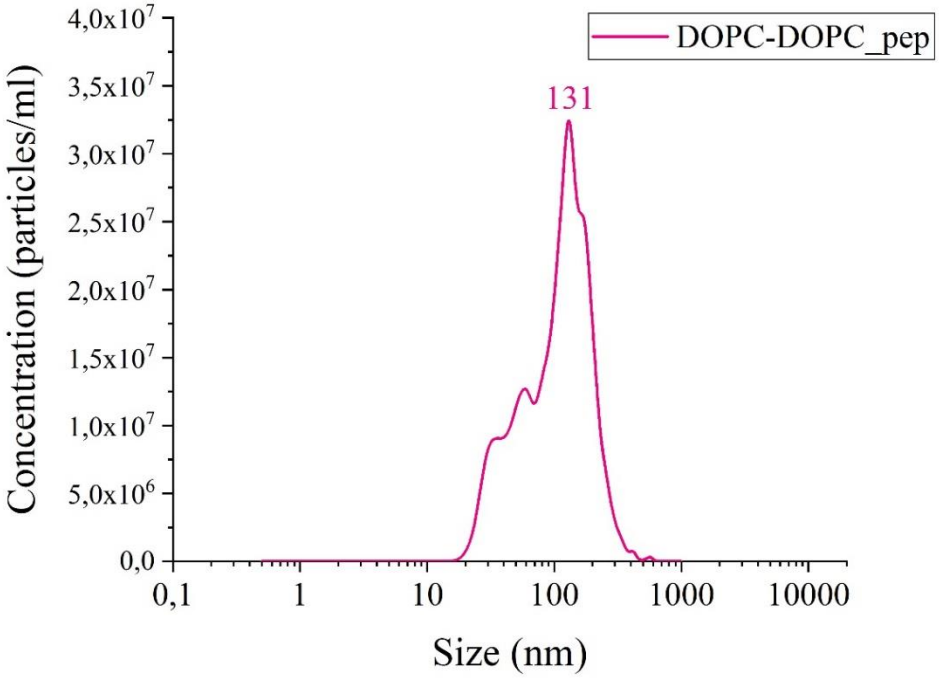

Figure 3.17: NTA measurement of DOPC-DOPC_peptide liposomes obtained with Freeze-Thaw Technique

Liposomes	Mean Size	St Dv
DOPC	140.8 nm	41.7 nm
DOPC:DSPE-PEG-CKAAKN	141.4 nm	40 nm
DOPC-DOPC:DSPE-PEG-CKAAKN	158 nm	78.8 nm

Table 3.9: NTA size measurements of DOPC, DOPC:DSPE-PEG-CKAAKN and DOPC-DOPC:DSPE-PEG-CKAAKN (1:0.5) liposomes.

Each type of liposome was characterized in terms of Z-potential, the results are reported in Figure 3.18. As it can be distinguished, all liposomal membranes showed a negatively charged surface, with the highest absolute value being that of DOPC:DSPE-PEG-CKAAKN, probably as a result of the presence of the target peptide. As expected, the freeze thaw DOPC-DOPC:DSPE-PEG-CKAAKN liposomes show an intermediate Z-potential value between those of DOPC only liposomes and DOPC:DSPE-PEG-CKAAKN ones. This result evidences the fact that the sample obtained with the freeze-thaw procedure was a fusion between both samples, reaching an intermediate value.

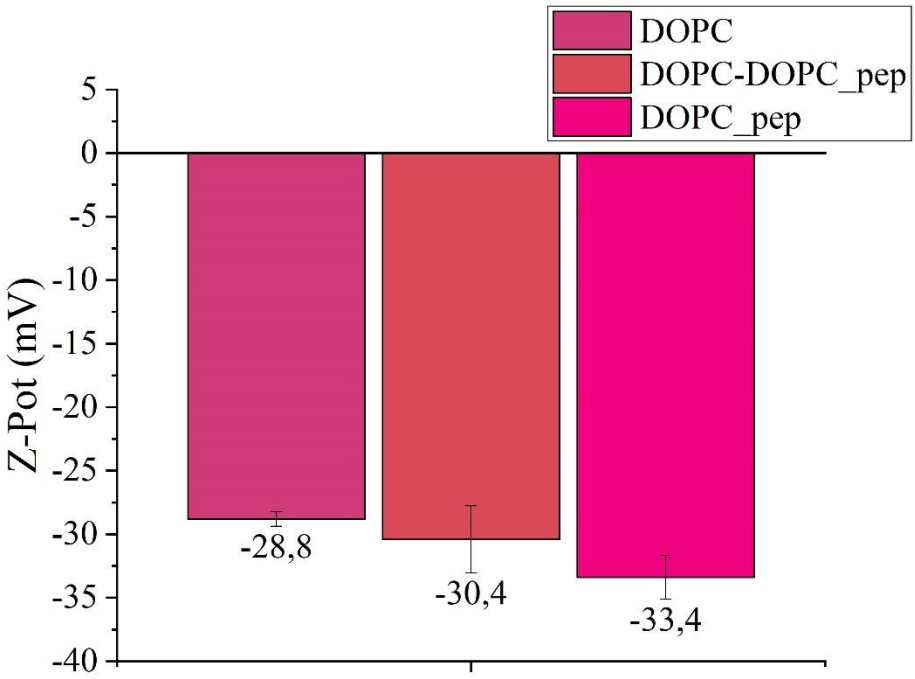

Figure 3.18: Z-potential values of DOPC, DOPC:DSPE-PEG-CKAAKN and DOPC-DOPC:DSPE-PEG-CKAAKN (1:0.5) liposomes.

3.4.2. Liposome Coating of NanoCrystals

Optimization studies were previously developed by members of the research team, regarding the achievement of desirable levels of encapsulation. Different ratios between the amounts of liposomes and NCs were studied, and the number of cycles for the freeze-thaw technique was assessed, to optimize the entire procedure.

A ratio of 1:0.5:0.5 (volume:volume:weight) between the volume of the DOPC, of DOPC:DSPE-PEG-CKAAKN liposomes solution, and the mass in µg of NCs was selected.

The optimization process also analyzed the quantity of freeze-thaw cycles needed for improving the size distribution of the final nanoconstruct, reaching the best results with the accomplishment of 6 cycles. The NTA results of the so-obtained Lipo-coated NanoCrystals (LNCs), consisting of NCs coated by DOPC-DOPC:DSPE-PEG-CKAAKN liposomes, are shown in Figure 3.19 and are characterized by a quite monodispersed size distribution, showing a central peak centered at 105 nm.

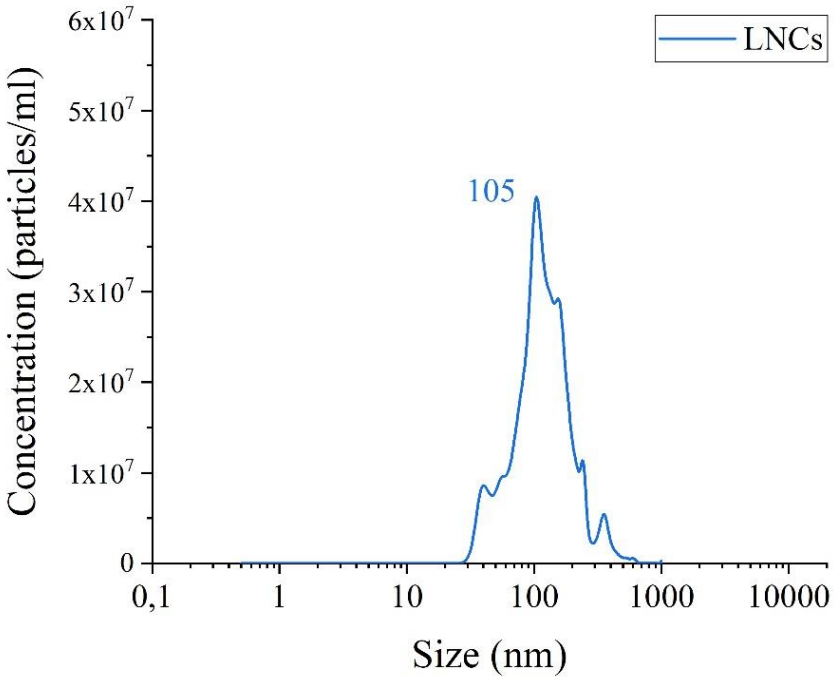

Figure 3.19: NTA Size distribution of LNCs

Characterization in terms of Z-potential was then carried out. As reported in Figure 3.20, the decrease in z-potential value was remarkable; naked NCs displayed a Z-potential of +27,8 mV, whereas the value obtained for LNCs was -20.8 mV, close to the Z-potential value of -30.4 mV obtained for freeze-thaw liposome DOPC-DOPC:DSPE-PEG-CKAAKN, without NCs.
As a whole, these results nicely suggest the success of the NCs encapsulation process by the liposome using the freeze-thaw method, as the Z-potential of the final LNCs nanconstruct is negative and the size distribution similar to the DOPC-DOPC:DSPE-PEG-CKAAKN liposome.

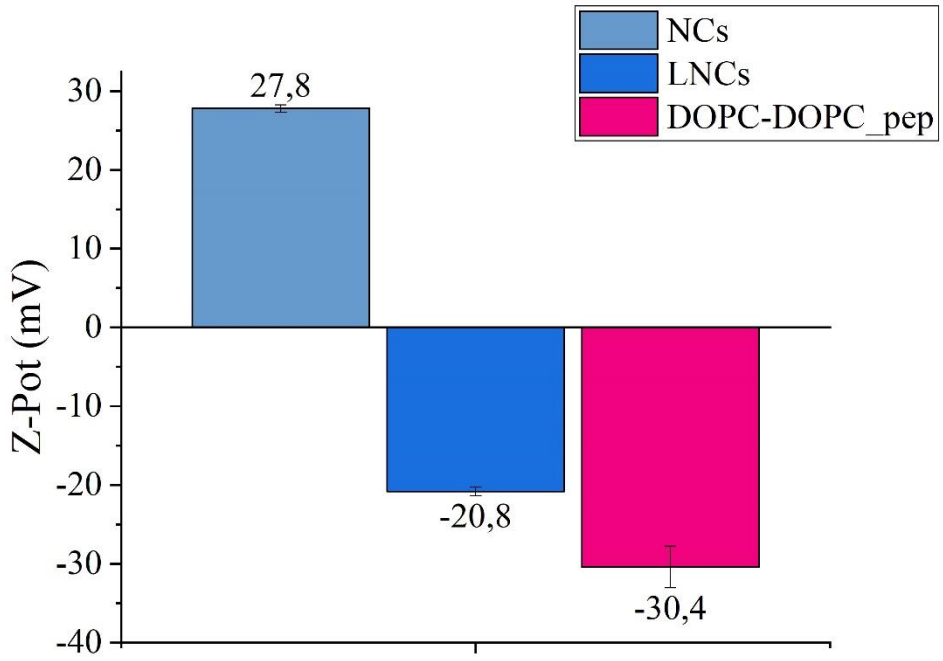

Figure 3.20: Z-Potential of NCs, LNCs and DOPC_pep

The NTA technique retuned a size distribution composed of different peaks after the preparation of the LNCs nanoconstruct by freeze-thaw technique, as can be seen in Figure 3.21. Some hypotheses regarding this distribution were the presence of naked NCs, which were not correctly encapsulated in the liposome during the process, thus generating peaks at lower sizes, and that the presence of NCs coated with different liposome sizes could generate distinctive peaks at higher values. Therefore, to confirm the results obtained with the z-potential characterization, the fluorescence microscopy technique was exploited to get accurate information about the LNCs sample.

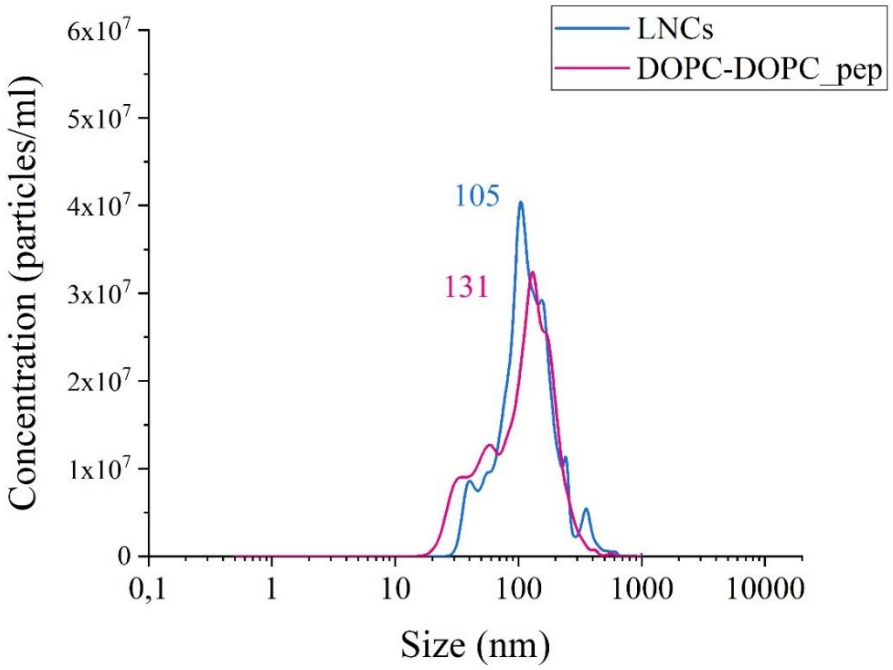

Figure 3.21: NTA of LNCs with respect to DOPC-DOPC_pep. Both obtained by Freeze-Thaw technique

The NCs were labelled with the Atto 550 dye, imaged in the red channel, whereas the liposomes' synthetic peptide was bound with the FITC dye, thus being imaged in the green channel. Microscope images, reported in Figure 3.22, demonstrate good levels of colocalization of the two dyes for the LNCs sample after the freeze-thaw cycles; the colocalization percentage was equal to 92%. Therefore, it was assumed that the diverse peaks shown in the NTA graphs were caused by the encapsulation of the NCs by different lipidic shell sizes, and not because of the presence of naked NCs. In addition, some green spots alone can be detected, thus indicating the possible presence of some empty liposomes formed.

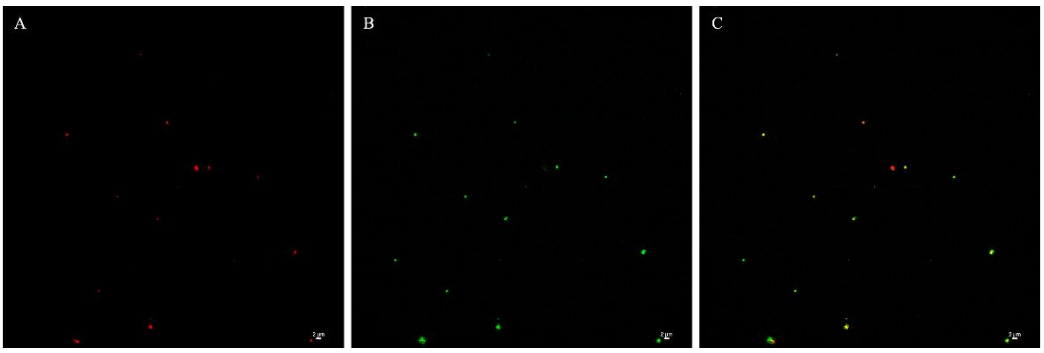

Figure 3.22: Fluorescence microscopy images of the DOPC-DOPC:DSPE-PEG-CKAAKN-FITC-ZnO-Gd- NH2-ATTO550 nanoconstruct. Red channel (A), green channel (B) and merged images (C)

All these data were used for the development of the simple and dual drug loaded nanoconstructs for the treatment and diagnosis of pancreatic cancer cells, such as BxPC-3 and a metastatic cell line AsPC-1.

3.4.3.Lipid Coating of Drug loaded nanocrystals

The next step in the characterization of the nanoconstructs, was the analysis of the properties of the nanoconstructs obtained with the simple and dual drug loaded LNCs. Size distribution was assessed, not only by DLS but also by NTA techniques. Besides, the so-obtained samples were characterized by their zeta potential.

DLS and NTA

Figure 3.23 reports the results of the DLS measurements of the unloaded LNCs, in comparison with the single and dual drug-loaded lipid nanocrystals. All drug-loaded samples show an increase in their mean average size. This can be explained by the incorporation of the drug on the surface of the NCs, which can diminish the original superficial properties, causing aggregation of the NCs. Sorafenib loaded sample showed a higher average size (954 nm), whereas that of Vismodegib was moderately lower. The most similar size distribution to the unloaded LNCs was that of the dual drug-loaded LNCs, which suggests the fact that the mix of both drugs stabilized the lipid coating better than their single drug counterparts. In all cases, the PDI values in Table 3.10 report a non-monodispersed size distribution of the LNCs without and with drugs.

The high concentration of lipid-coated NCs used for the measurements may have led to the formation of small aggregates, therefore all outcomes show a little peak around 1000 nm.

Sample	Z-average	PDI
LNCs	826,9	0,389
LNCs-Soraf	954	0,514
LNCs-Vism	801,4	0,458
LNCs-Dual	843,9	0,445

Table 3.10: Size average and PDI of LCNs, unloaded and drug loaded samples

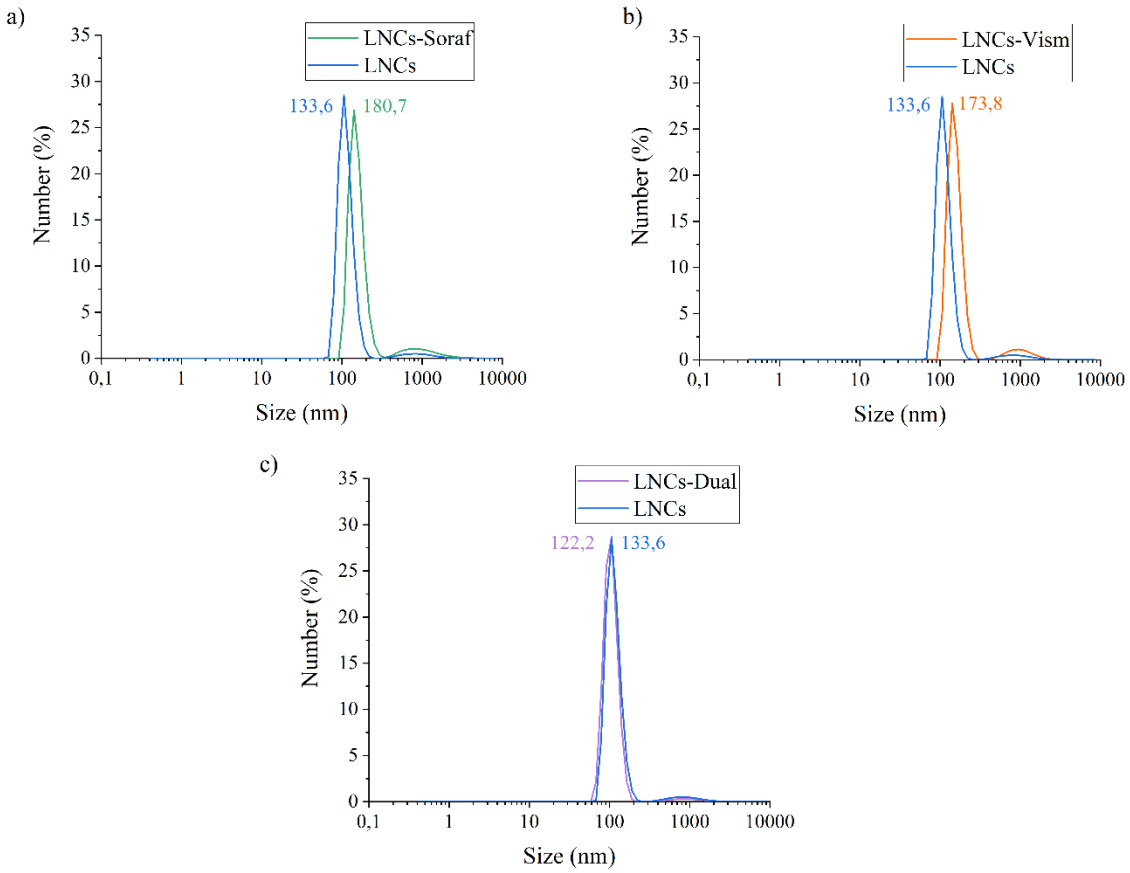

Figure 3.23: DLS measurements. Unloaded and drug loaded comparison. (a) Sorafenib, (b) Vismodegib, and (c) dual.

NTA analyses were also carried out, resuspending the NCs using a 1:50 dilution factor. The results obtained, shown in Figure 3.24 exhibit a polymodal behaviour, showing in each case different narrow peaks, being for Sorafenib 142 nm, for Vismodegib 109 nm, and dual-drug NCs 121 nm, similarly to the results obtained with the DLS technique.

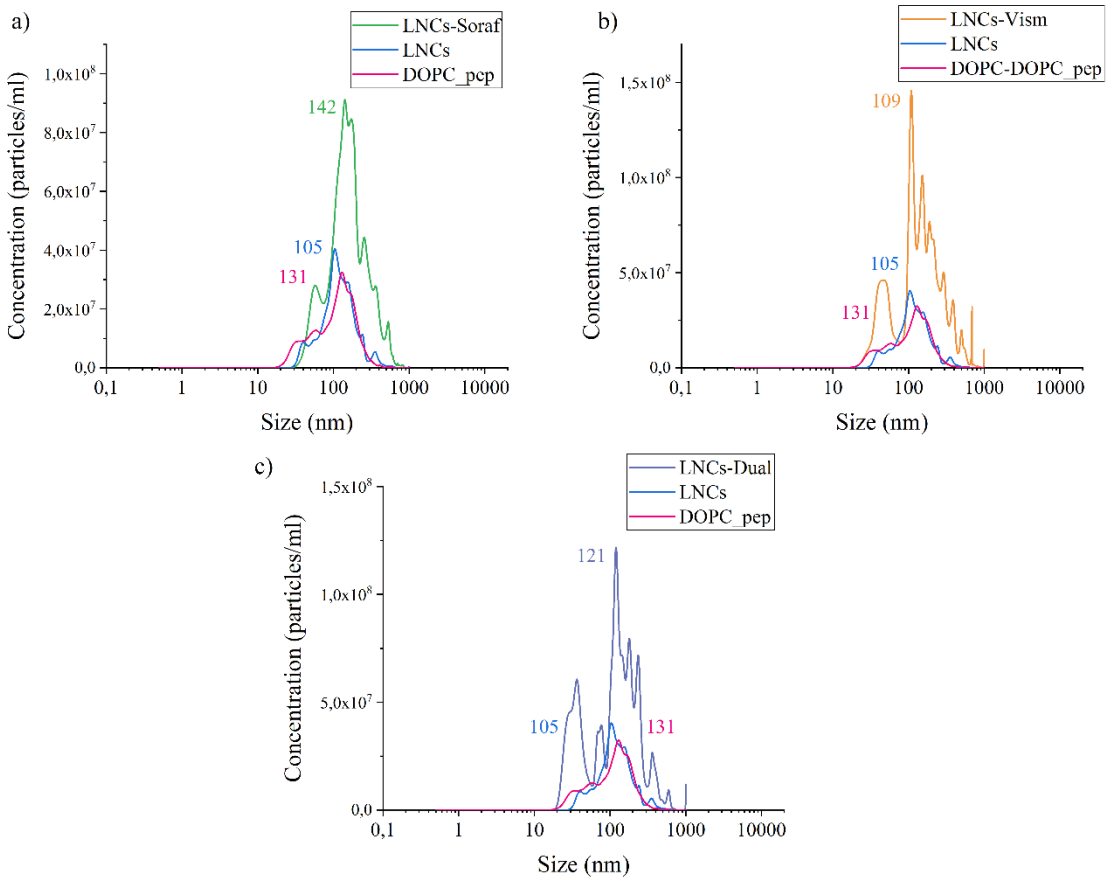

Figure 3.24: NTA measurements, comparison between LNCs, DOPC-DOPC_pep and drug loaded LNCs.

Zeta-Potential

Further zeta potential measurements were carried out, with the dual drug loaded LNCs sample. The results, shown in Table 3.11 and Figure 3.25: Z-potential measurements of drug-unloaded and dual drug loaded LNCs, demonstrate slightly reduced surface charges, which indicate that the incorporation of both drugs did not carry significant alterations on the superficial properties of LNCs, thus permitting the correct and complete encapsulation of the NCs by the lipid coating.

Sample	Z-Potential	St Dv
LNCs	-20.8 mV	0.1
LNCs-Dual	-20.6 mV	0.666

Table 3.11: Z-potential values of unloaded and dual drug-loaded LNCS.

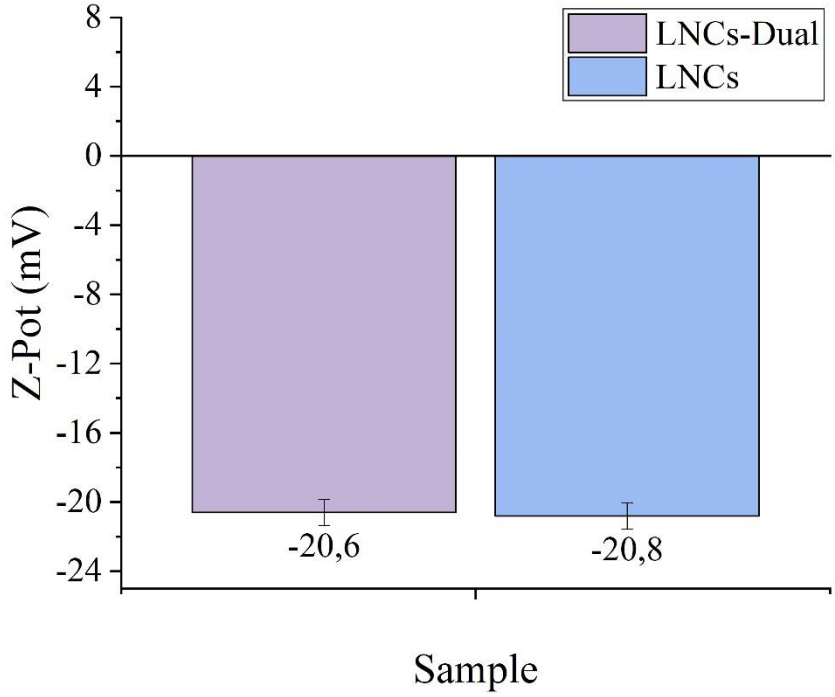

Figure 3.25: Z-potential measurements of drug-unloaded and dual drug loaded LNCs

The above-mentioned characterizations, in terms of size distribution and zeta potential, seem to suggest the correct and complete formation of the drug loaded LNCs. The obtained nanoconstructs, were then tested on pancreatic cancer cells, specifically on BxPC-3 and AsPC-1 cells, to evaluate and assess their therapeutic effects.

3.5 Drug Release in RPMI

The obtained nanoconstructs were evaluated in terms of their ability to guarantee a specific drug delivery kinetics to the target cells, without the loss of their drug content while in circulation before reaching it. This experiment aimed to check the good retention of the drug at the surface of the ZnO NCs, to prove the shielding effect of the lipid coating of the LNCs, and assess the release profile over time.

Both vismodegib and sorafenib drug release were evaluated in cell culture medium (RPMI) for 96 hours, in conditions of continuous stirring (200 rpm) at 37 °C. The unit of measure was selected as µg of drug released with respect to mg of NCs.

As it can be observed from the release profile of Figure 3.26 of both drugs, NCs without the lipid coating have an uncontrolled and rapid release, in comparison with their LNCs counterparts.

The Sorafenib release profile demonstrates a sustained release in a long time setting from the LNCs, whereas Vismodegib release kinetics from LNCs shows a rapidly increasing delivery in the first 48 hours. This behaviour is hypothesized to be optimal, as the more rapid release of Vismodegib out of the nanoconstruct could be useful for the depletion of tumour stroma by inhibiting HH signalling pathway, whereas the moderate but sustained release of sorafenib over time, having anti-angiogenic effect, is necessary to maintain long-lasting therapeutic conditions in the tumour microenvironment.

Therefore, the lipid bilayer coating acts as a shield against the rapid and uncontrolled drug release, preventing high quantities of both drugs to be immediately delivered, as in the case of lipid-uncoated NCs. The results, combined with the good colloidal stability in solution of LNCs and the cell viability and uptake results reported below, confirm that the developed nanoconstructs have improved performances, in comparison with the NCs alone, to carry out a specifically targeted delivery.

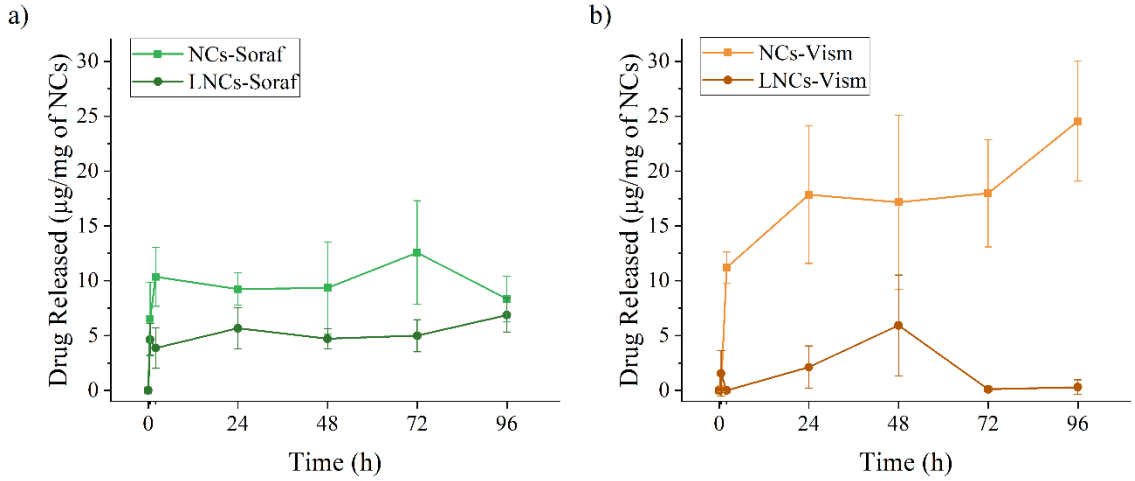

Figure 3.26: Drug release of (a) Sorafenib and (b) Vismodegib in RPMI.

3.6 In-Vitro Assays

The nanoconstructs obtained were tested on two different cell lines, BxPC-3 and AsPC-2, which were treated with single and dual drug-loaded LNCs and as a comparison, with free drugs, both as single and dual drug administration, by the Co-Supervisor of this Master's Thesis work. The aim was to study the cellular uptake, understand the cytotoxicity of the drug-loaded nanoconstructs in comparison with their free drug counterparts, and assess the type of cell killing mechanism.

Sorafenib, Vismodegib, and their dual combination were first uptaken into the NCs, then the lipid coating with targeting peptide was performed and drug loaded LNCs were obtained. All stages of the process were performed under sterile conditions, ensuring the sterility of the samples. The same amount of the drugs uptaken on the nanoconstructs was used as free drugs administered to the cells.

For the WST-1 and the apoptosis/necrosis assays, the uptaken drug on the surface of the NCs was approximately 25 µg/mg of NCs for Sorafenib, and 30 µg/mg of NCs for Vismodegib, as previously evidenced in Figure 3.12. The low quantity of drug uptaken can be a result of the hydrophobic molecules' interaction with the NCs surface, but as will be following described, these quantities were sufficient for demonstrating therapeutic effects.

3.6.1. Fluorescence Microscopy

For the evaluation of the internalization of the final nanoconstructs into the two different cell lines BxPC-3 and AsPC-1, fluorescence microscopy analysis was performed. This experiment aimed to understand whether the internalization of LNCs was enhanced by the presence of the specific targeting ligand.

Different dyes were used for labelling each of the LNCs components. For cellular membranes, WGA647 was used, thus fluorescing in the pink channel of Figure 3.27; whereas the lipidic shell could be recognized in the green channel, thanks to the FITC dye bound to the targeting peptide. The treatment was carried out with a concentration of LNCs corresponding to 30 µg/ml of NCs, for 20 hours. Figure 3.27a. reports the results obtained on AsPC-1, while those on BxPC-3 are shown in Figure 3.27b. The two rows display different points of the analyzed samples, each one including the labelling of the membrane alone in the purple channel, the liposome with the

target peptide in the green channel and their merged image. When analyzing the merged channel (panels on the right column), a complete internalization of the LNCs could be recognized, especially for BxPC-3, as essentially all liposomes were located inside the cellular membranes.

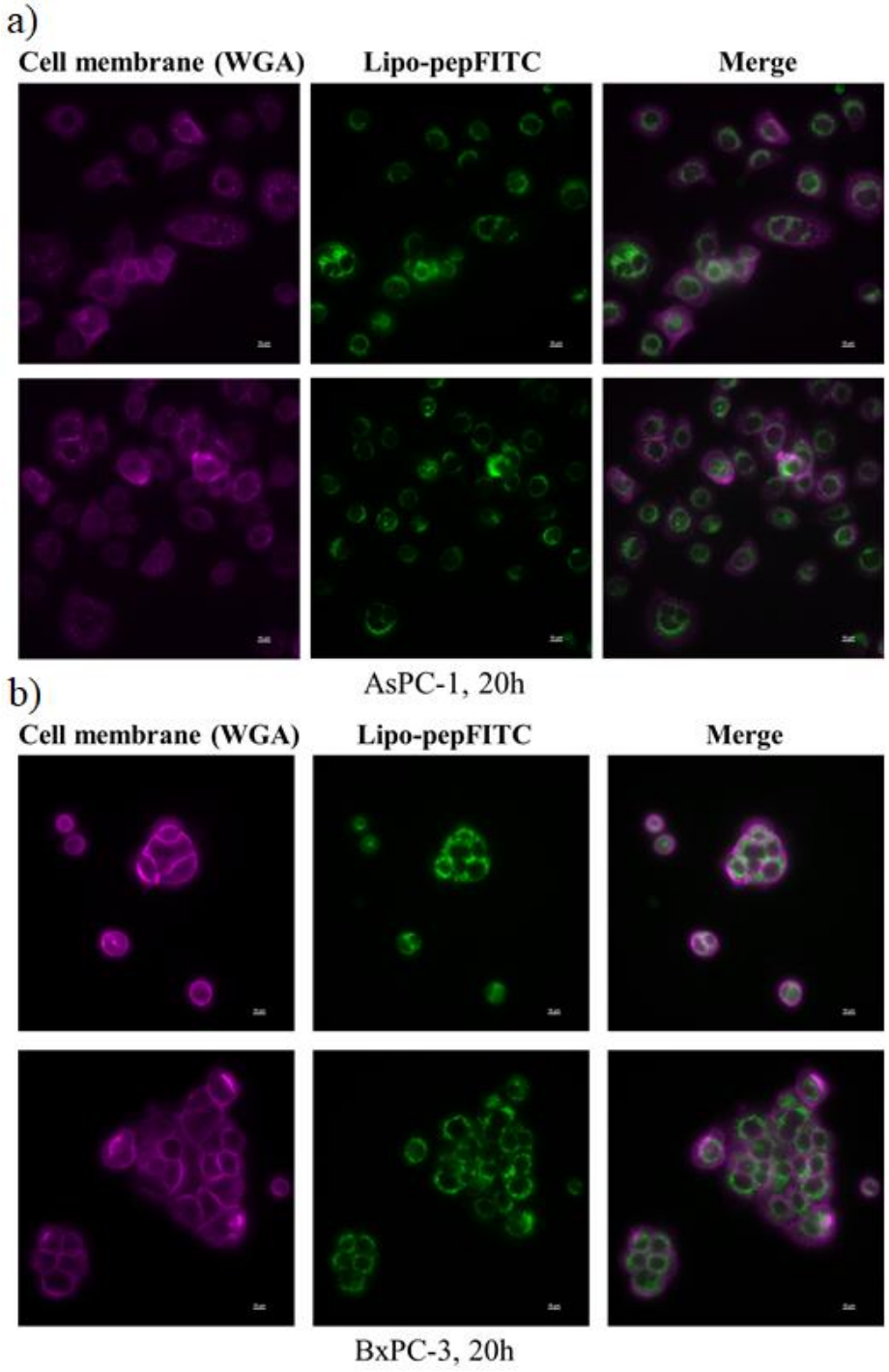

Figure 3.27: Fluorescence microscopy images. (a) AsPC-1 cell line, (b) Bx-PC cell line

3.6.2. Cell Viability Assays

The final nanoconstructs, consisting of unloaded and drug loaded NCs, covered with the lipidic shell containing the targeting peptide, had to be tested in order to assess their effects on living cells. Therefore, using the WST-1 technique, cytotoxic effects of different concentrations of LNCs alone and Sorafenib loaded LNCs were evaluated on a human metastatic pancreatic cell line (AsPC-1) and a human pancreatic cancer cell line (BxPC-3). The uptaken drug on the surface of the NCs was 30 μg/mg of NCs for Sorafenib, and 40 μg/mg of NCs for Vismodegib.

Figure 3.28a and Figure 3.28b report the experiment's outcome, showing the percentage of cell viability after 48 h of incubation with different concentrations of LNCs alone and Sorafenib loaded LNCs, specifically 10, 20, 30 and 40 μg of NCs/ml of RPMI solution. Results are expressed as percentage with respect to untreated cells (0 μg of NCs/ml). In order to evaluate the effects of the nanocarried drug with its free configuration, cells were also treated with Sorafenib alone, using the corresponding amount of drug that has been uptaken on the surface of the LNCs. The aim was to find the citotoxic threshold, and select the optimal LNCs concentration to be used in the following experiments.

As displayed in the resulting graphs, for AsPC-1 cell lines, the metabolic activities when testing a concentration of 10 μg of LNCs/ml remained unvaried concerning untreated cells, with all testing solutions (LNCs, LNCs-Soraf and Free Soraf). Similar results were obtained at the following concentration of 20 μg of LNCs/ml, and with the minimum concentration in the BxPC-3 cells.

In contrast, both AsPC-1 and BxPC-3 cells showed a very reduced vitality when considering the Sorafenib loaded LNCs with a concentration of 30 and 40 μg/ml, being the result obtained at 30 μg of LNCs/ml for AsPC-1 and 20 μg of LNCs/ml for BxPc-3 the most interesting ones. At this concentrations, for each assay, it can be observed that nor the presence of the LNCs alone, nor that of the Sorafenib as a free drug affect the cell viability, remaining larger than 90% in all cases. The drug loaded LNCs are demonstrated to be significantly toxic, causing reduced viability of 75% for BxPC-3 cells, and only 30% for AsPC-1 with respect to the untreated cells.

Furthermore, LNCs alone showed little cytotoxic effects within lower concentrations, thus proving good biocompatibility of the LNCs, and that the incorporation of the targeting peptide did not increase toxicity either. Yet,

when analyzing higher concentrations, the toxicity increased, reaching a vitality of less than 50% at a 40 µg of LNCs/ml concentration for AcPC-1 cells, and less than 20% for the same concentration used on BxPC-3. A moderate cytotoxic behaviour can be observed when carrying out the free drug treatment.

Therefore, in order to observe the toxic effect of the Sorafenib LNCs without reaching low cell viability, 20 µg/ml was chosen as the optimal concentration to be used in the following in-vitro experiments, as it reflected the optimum cytotoxicity of Sorafenib to check the effect of the combined drug therapy. A concentration of 30 ug/mL could not be selected it demonstrated a high cell killing effect (almost 90% in BxPC-3 cell lines).

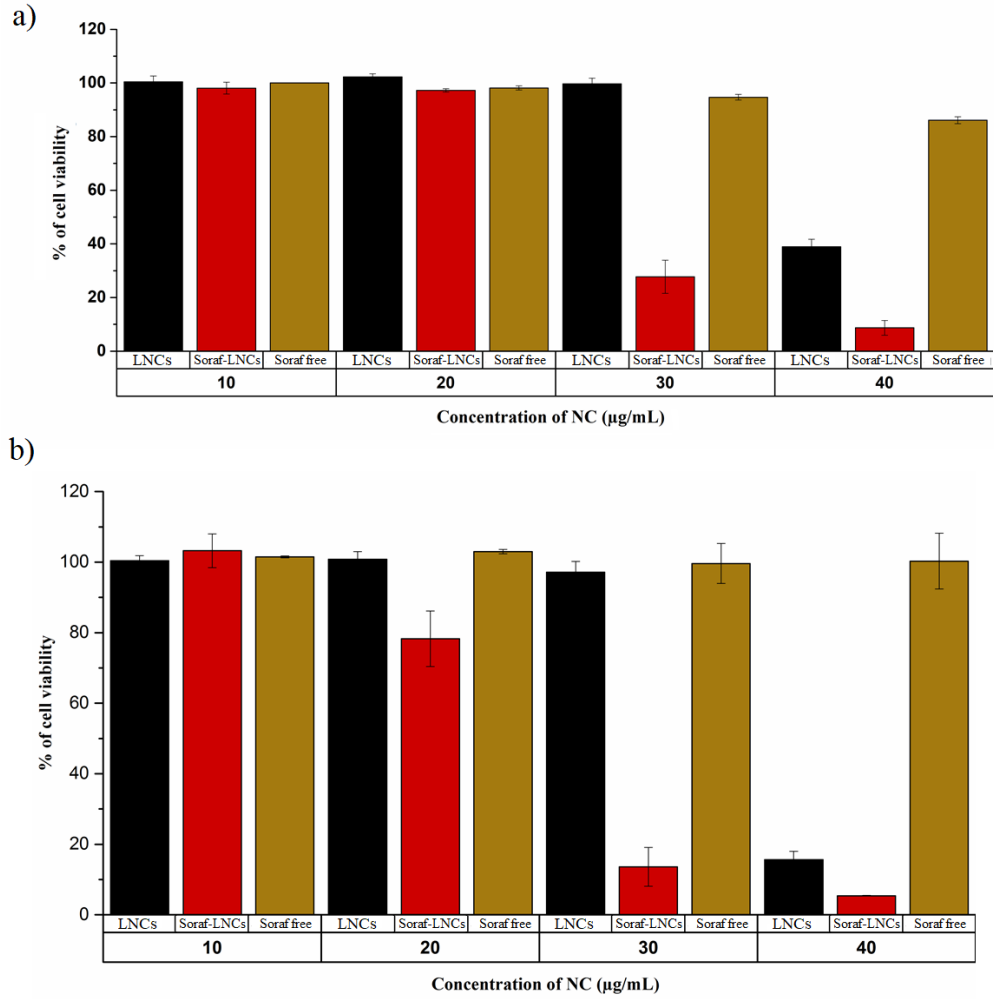

Figure 3.28: Citotoxicity of the Sorafenib-loaded LNCs, compared to the drug-unloaded nanoconstruct and the free drug, on the (a) AsPC-1 and (b) BxPC-3 cell line after 48 hours.

Remarkably, the highest cytotoxic effects of Sorafenib are observed when the drug is nanocarried, with respect to the free drug treatment, thus remarking the improved efficacy of the treatment when encapsulating the drug.

The nanoparticle-carrying drug approach is more appealing not only for the multiple action of the nanoconstruct but also for the larger effectiveness with respect to the conventional treatments used in clinics.

AsPC-1 and BxPC-3 cell lines were then pre-treated with a conventional chemotherapeutic drug, Gemcitabine, for 24 hours at a 10 µM concentration. The therapeutic effects of LNCs nanoconstructs were then assessed, not only on the previously mentioned cell lines, pretreated and not, but also on a healthy pancreatic cell line HPDE (Primary Human Pancreatic Epithelial), without Gemcitabine pretreatment.

Dual-drug loaded LNCs were used for treatment in comparison with both single Sorafenib and Vismodegib drug-loaded LNCs, always using a 20 ug/ml concentration. The metabolic activity was evaluated after 48 hours, employing the WST-1 assay. The outcome of the experiment, reported in Figure 3.29a and Figure 3.29b, shows increased efficiency of therapy in both AsPC-1 and BxPc-3 cell lines once using the dual-drug loaded LNCs nanoconstruct and a remarkable therapeutic efficacy once both cell lines are pre-treated with Gemcitabine. In particular, a reduction of cell viability of approximately 20% is favoured in the Gem-pretreated cell groups with respect to the non-pretreated cells.

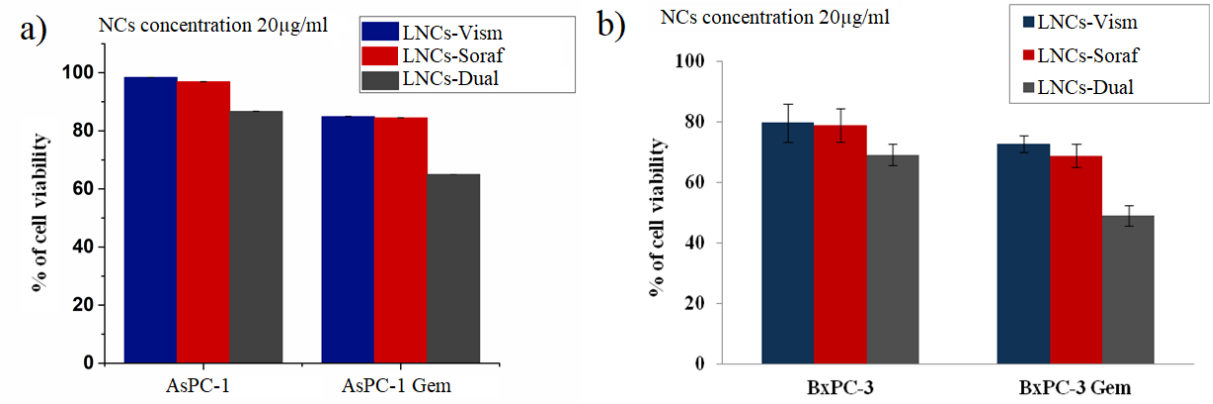

Figure 3.29: WST-1 assay. (a) AsPC-1 cell line, (b) BxPC-3 cell line

Results obtained with the healthy HPDE cell line, Figure 3.30, show that the cell viability was not compromised by the use of the dual-drug loaded LNCs and, as a comparison, by the single-drug loaded LNCs. This can be a

consequence of the active targeting action of the nanoconstructs, which permits the killing of only cancerous and metastatic cell lines, not influencing the vitality of healthy pancreatic cells. These results are therefore very promising, as an aim of the development of these nanoconstructs was the limitation of the toxicity to healthy surrounding tissue around the tumour.

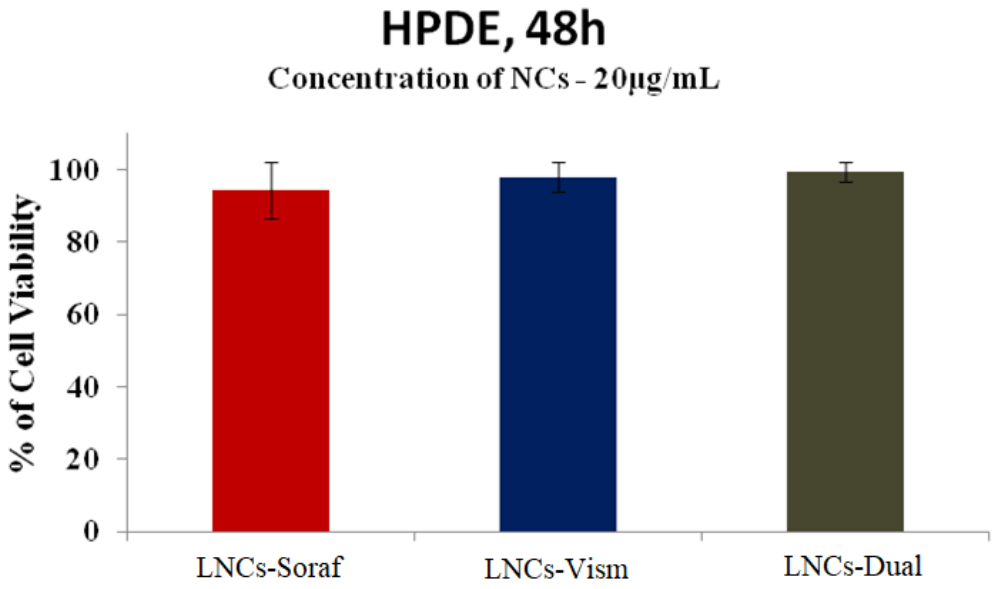

Figure 3.30: WST-1. HPDE cell line

All these results are proof that the nanoconstructs are not toxic by themselves, up to a certain concentration. Besides, the nanocarried drugs show a better and more efficient therapeutic action than their free drug counterparts, and they show limited toxicity towards healthy tissue in the surrounding environment of the tumour when maintained at a 20 µg of LNCs/ml concentration.

3.6.3. Apoptosis/Necrosis Assays

Cytotoxicity of the drug-loaded constructs was proven in the previous section with a concentration of 20 µg of LNCs/ml.
Further studies were carried out to investigate the cell-killing mechanism, in both AsPC-1 and BxPC-3 cell lines. Apoptosis/necrosis analyses were executed, treating the cells with the same concentration of 20 µg/ml of drug-

loaded LNCs, and their corresponding free drug, i.e. Sorafenib alone, Vismodegib alone, or the combination of both free drugs. The treatment duration was 24 hours, after which results were collected and evaluated.
Samples obtained were examined under flowcytometry, as the basis of the apoptosis/necrosis assay is the fluorescence emission. When cells suffer a necrotic death, their genetic material can be bound to a fluorescent intercalator of DNA, Propydium Iodide (PI) which is unable to cross the cell membrane, unless cell is dying by necrosis. Differently, apoptotic processes can be distinguished by the labelling with Annexin V of the PS molecules which becomes exposed on the external side of the membrane due to this type of death.
Two experiments were carried out. In both cases, the population of untreated cells was set. The first set of experiments regarded a direct treatment of the cells with both the drug loaded LNCs and the corresponding free drug concentrations. The second set of experiments was carried out with a pretreatment with Gemcitabine.
Figure 3.31a reports the results obtained on AsPC-1 cell lines, when treated only with a single drug, i.e. Sorafenib and Vismodegib, loaded LNCs and their corresponding free drug concentrations. The therapeutic effects of the drug-loaded LNCs were significantly higher than the single drug counterpart, obtaining for Sorafenib-loaded LNCs 7.8% of necrotic cells compared to 1.83% with free drug treatment, and for Vismodegib-loaded LNCs 6.87% with respect to 1.18% with free drug.
For the BxPC-3 cell line results were also promising, as shown in Figure 3.31b, as the efficacy of the drug loaded LNCs was noticeably high, being the necrotic events for Sorafenib loaded LNCs 11.68% in comparison with 3.49% with free drug, whereas for Vismodegib loaded LNCs 11.07% with respect to 2.65% of free drug. Similarly, the apoptotic events were higher when deliverying the drugs with the LNCs nanocarriers with respect to the free drugs.
The above results confirm that, when delivered through the nanoconstruct, both drug inhibitors show enhanced efficacy using the same mechanism of action, leading to apoptosis of the treated cells. These results evidenced an important potential of the nanoconstructs in the treatment of pancreatic cancer, showing greater effects on BxPC-3 cancer cells than on metastatic AsPC-1 cells.

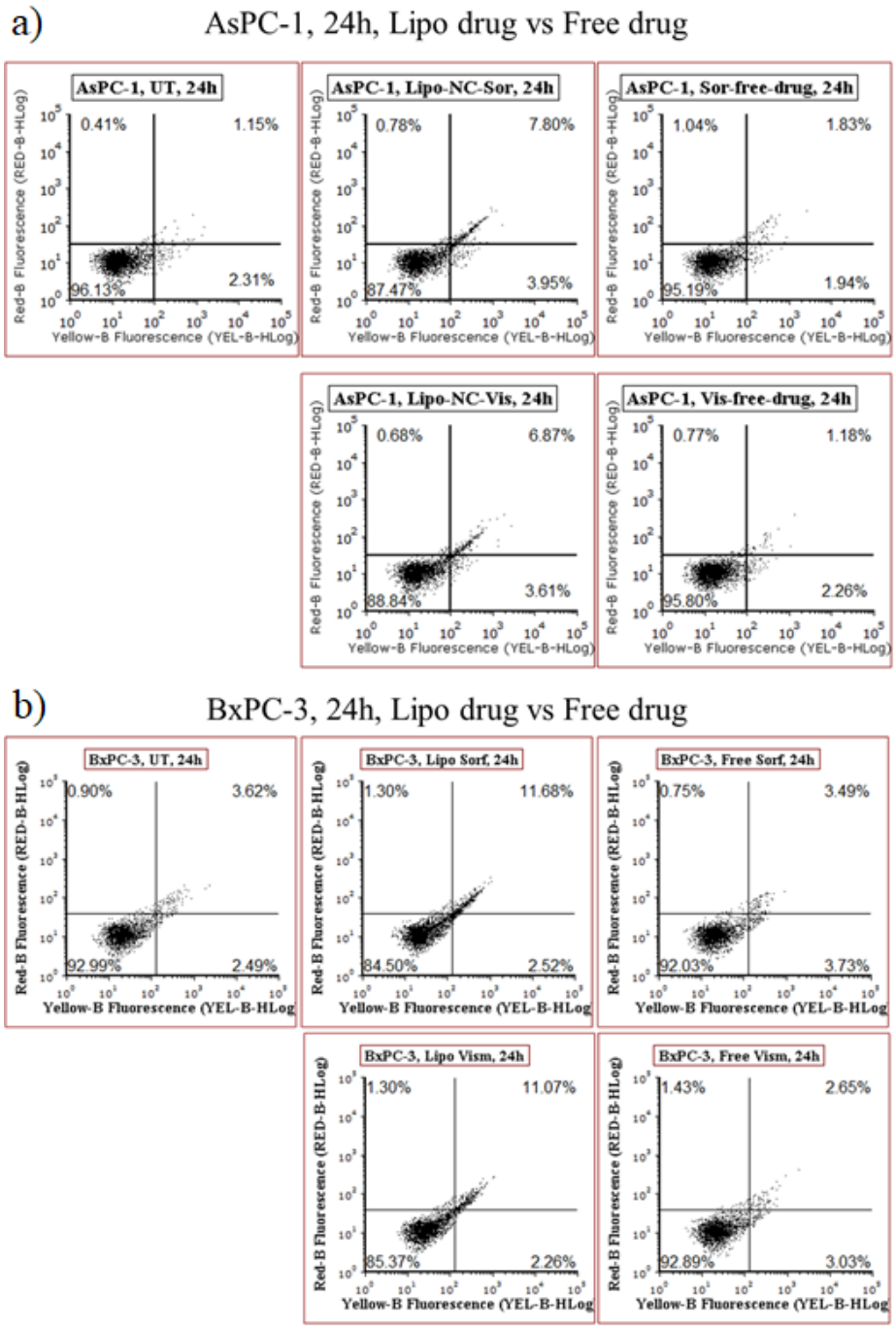

Figure 3.31: Apoptosis/necrosis study. (a) AsPC-1, (b) BxPC-3

The second set of experiments regards the evaluation of the performance of the dual-drug loaded nanoconstruct, in both cancer cell lines subjected to pretreatment with Gemcitabine for 24 hours and then exposed to the single

and dual-drug loaded LNCs. The apoptosis/necrosis assay was then performed 24h after the incubation with LNCs, and results are shown in Figure 3.32.

Gemcitabine-pretreated AsPC-1 cells show a 15.47% of necrosis when treated with the nanoconstructs, in comparison to an 11.67% with free drugs. Apoptotic events were almost similar in Gemcitabine-pretreated AsPC-1 cells with the use of LNCs (10.98%) with respect to 10.90% of apoptosis with free dual drug.

AsPC-1 cells, not pretreated with Gemcitabine, were also evaluated for comparison: when treated with dual-drug loaded LNCs, cells show an increase of necrosis events with respect to free-drug treatment (10.13% to 5.42%), whereas similar apoptotic events were recorded (5.17% with LNCs versus 6.62% with free drugs).

BxPC-3 cell line reports also promising results once pretreated with Gemcitabine and using LNCs. In particular, necrotic events were increased up to 62.11% when using the dual-drug loaded LNCs in comparison with 27.14% when using free drugs, thus underlining the efficacy of the LNCs nanoconstruct delivery in the therapeutic effects on pancreatic cancer. In the case of apoptotic events, the use of LNCs (5.75%) versus free drugs (8.46%) was not remarkable.

More modest cell death values were obtained if BxPC-3 cell are not pretreated with Gemcitabine: necrotic events are 11.87% when using the dual-drug loaded LNCs with respect to 6.11% reported for the free drugs. Here also apoptotic events are not remarkable and no difference is observed when using nano-carried drugs (3.46%) with respect to the free molecules (4.55%).

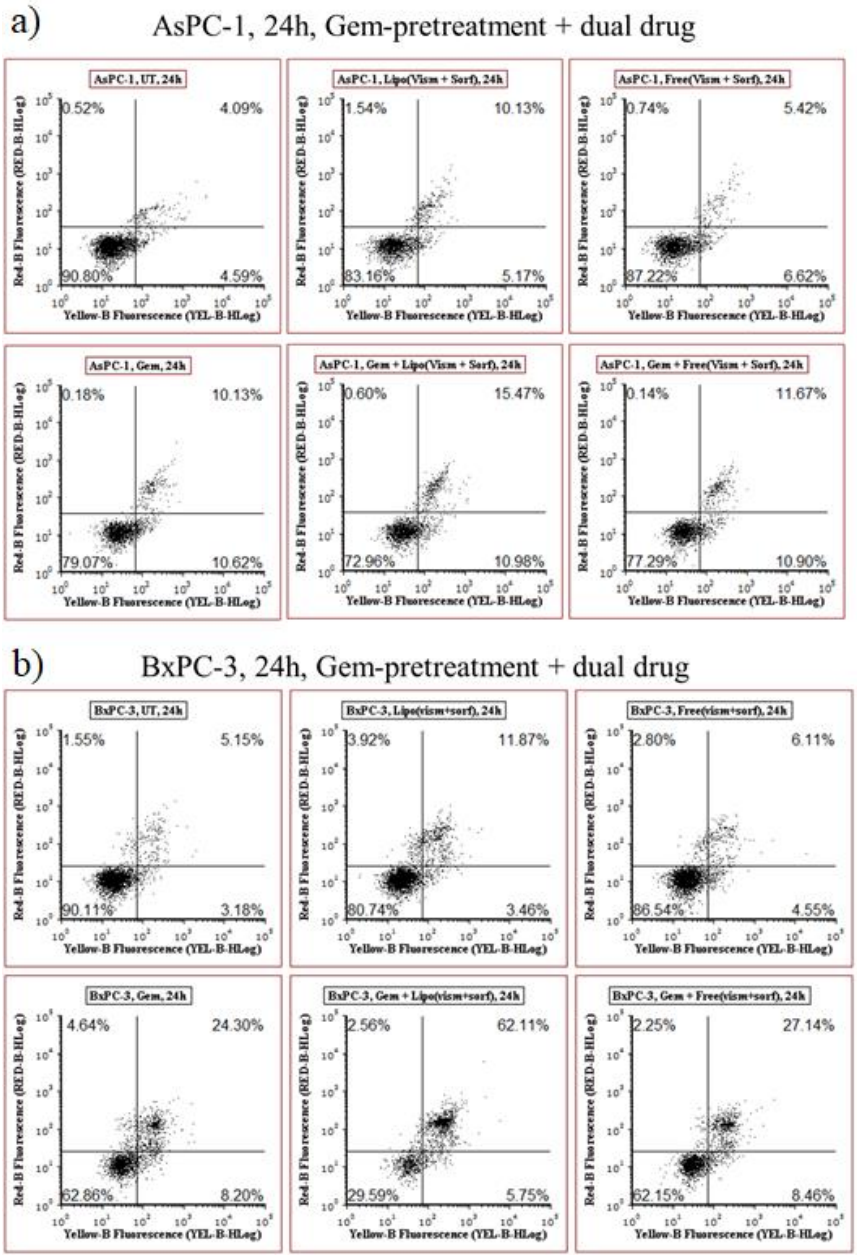

Figure 3.32: Apoptosis/Necrosis assay. (a)AsPC-1, (b)BxPC-3

From all the above-mentioned results, it is clear that the LNCs nanoconstructs have achieved efficient and highly effective performances in comparison with the free drug counterparts. Better outcomes were seen with the BxPC-3 cancer cells than with the AsPC-1 metastatic ones, thus suggesting that this kind of treatment could be promising for the proposed pancreatic ductal adenocarcinoma in not metastatic stages.

4 Conclusions

This Master Thesis was focused on the development of an innovative, dual drug-loaded nanotheranostic and biomimetic platform, containing dual inhibitor therapeutic agents, namely Sorafenib and Vismodegib, uploaded on the surface of aminopropyl-functionalized Gd-doped zinc oxide nanocrystals. The whole nanoparticle was coated with a lipidic bilayer, consisting of liposomes, and finally functionalized with a specific targeting peptide, namely CKAAKN, for active pancreatic cell targeting. The studies developed consisted on optimization and characterization processes, concluding with the in-vitro test of the nanoconstructs obtained on three different pancreatic cell lines, including both healthy and cancerous types.

The synthesis of ZnO nanocrystals was successfully performed by wet chemical co-precipitation method, in both undoped and Gadolinium doped versions. Characterization results corresponded to those depicted by Dr. Barui, thus proving the reproducibility of the method. The samples were able to be stored in ethanol and water, remaining stable in both media.

The successful functionalization of the Gd-doped nanocrystals with aminopropyl groups (NCs) was confirmed by DLS, Z-potential and FTIR characterizations.

The drug loading process was evaluated. The time and the order of the dual drug uptake were validated to be first Vismodegib in DMSO for 3.5 hours and then Sorafenib in ethanol for 2 hours. The so-obtained dual drug-loaded Nanocrystals and their single drug counterparts were characterized in terms of size distribution, Z-potential and FTIR analysis, to assess on their correct adsorption.

The next step was the proper nanoconstruct development, by coating the so obtained NCs with two different types of liposomes. The first one consisted of commercially available lipids, namely DOPC. The second one consisted on the same DOPC liposomes with the addition of one synthetic target peptide, CKAAKN, successfully linked to DSPE-PEG(2000)Maleimide lipids, for the active targeting of pancreatic cancer cells. The encapsulation procedure of the NCs with both DOPC and DOPC:DSPE-PEG-CKNAAKN liposomes was developed by 6 Freeze-Thaw cycles, thus obtaining lipid-coated NCs (LNCs) nanoconstructs. Characterization procedures of the obtained nanoplatforms included NTA analyses, Z-Potential and DLS measurements, and fluorescence microscopy analysis.

All results obtained were validated for the correct creation of the simple and dual drug-loaded theranostic nanoplatforms.

In-vitro testing of the obtained nanoconstructs was carried out for three different cell lines: a human pancreatic cell line (BxPC-3), its human metastatic counterpart (AsPC-1) and a healthy pancreatic duct epithelial cell line (HPDE). Firstly, internalization process was confirmed by fluorescence images, showing the presence of the nanoconstructs inside the cellular membranes of both the cell lines.

Afterwards, cell viability assays were carried out. Promising results were obtained when considering an optimized concentration of 20 µg/ml. Drug-unloaded LNCs were not cytotoxic for both cell lines, neither was the equivalent amount of drug loaded on the NCs when administered as free drug. However, when drugs were carried by means of the nanoconstructs, the cytotoxic effect became evident, mostly on BxPC-3 cell line, confirming the efficacy of the nanoplatforms obtained on cancer cells. Furthermore, optimal results were obtained when analyzing the performance of the nanoconstructs towards healthy HPDE cells as no cytotoxicity was shown, thus highlighting the specific targeting towards cancer cells and showing no damage to healthy surrounding tissue.

The last cell experiments were developed in order to understand the mechanism of cell death when treated with nanoconstructs. Optimal results were obtained, as apoptosis pathways were highly active in the presence of the final nanotheranostics platforms.

All collected data constitute a solid database proving the efficacy of the innovative dual drug loaded nanotheranostics platform, specifically towards cancer cells. It represents a promising alternative or complementary tool to the traditional treatments of pancreatic cancer, exploiting the synergic effects of dual drug inhibitors, the active targeting and the absence of damages towards the healthy tissues, overcoming the actual limits of pancreatic cancer treatments.

5 Bibliography

[1] World Cancer Research Fund, "Cancer Facts and Figures 2021," *World Cancer Research Fund International*. pp. 1–4, 2021, [Online]. Available: http://www.wcrf.org/int/cancer-facts-figures/worldwide-data.

[2] J. D. Mizrahi, R. Surana, J. W. Valle, and R. T. Shroff, "Pancreatic cancer," *Lancet*, vol. 395, no. 10242, pp. 2008–2020, 2020, doi: 10.1016/S0140-6736(20)30974-0.

[3] W. C. R. Fund, "Cancer Facts and Figures 2022." 2022.

[4] C. Leroux and G. Konstantinidou, "Targeted therapies for pancreatic cancer: Overview of current treatments and new opportunities for personalized oncology," *Cancers (Basel).*, vol. 13, no. 4, pp. 1–28, 2021, doi: 10.3390/cancers13040799.

[5] J. Zhao *et al.*, "Simultaneous inhibition of hedgehog signaling and tumor proliferation remodels stroma and enhances pancreatic cancer therapy," *Biomaterials*, vol. 159, pp. 215–228, 2018, doi: 10.1016/j.biomaterials.2018.01.014.

[6] R. K. Jain, "Normalizing tumor microenvironment to treat cancer: Bench to bedside to biomarkers," *J. Clin. Oncol.*, vol. 31, no. 17, pp. 2205–2218, 2013, doi: 10.1200/JCO.2012.46.3653.

[7] Z. Y. Zhao and W. Liu, "Pancreatic Cancer: A Review of Risk Factors, Diagnosis, and Treatment," *Technol. Cancer Res. Treat.*, vol. 19, pp. 1–13, 2020, doi: 10.1177/1533033820962117.

[8] Y. Xue, Y. Gao, F. Meng, and L. Luo, "Recent progress of nanotechnology-based theranostic systems in cancer treatments," *Cancer Biol. Med.*, vol. 18, no. 2, pp. 336–351, 2021, doi: 10.20892/j.issn.2095-3941.2020.0510.

[9] J. K. Patel and A. P. Patel, "Passive Targeting of Nanoparticles to Cancer," pp. 125–143.

[10] N. Alasvand *et al.*, *Therapeutic Nanoparticles for Targeted Delivery of Anticancer Drugs*, no. 2011. Elsevier Inc., 2017.

[11] X. Liu, J. Jiang, and H. Meng, "Transcytosis - An effective targeting strategy that is complementary to 'EPR effect' for pancreatic cancer nano drug delivery," *Theranostics*, vol. 9, no. 26, pp. 8018–8025, 2019, doi: 10.7150/thno.38587.

[12] T. D. Clemons, R. Singh, A. Sorolla, A. Hubbard, and K. S. Iyer,

"The Distinction Between Active and Passive Targeting of Nanoparticles Dictate Their Overall Therapeutic Efficacy .," 2018, doi: 10.1021/acs.langmuir.8b02946.

[13] W. jin Jeong, J. Bu, L. J. Kubiatowicz, S. S. Chen, Y. S. Kim, and S. Hong, "Peptide–nanoparticle conjugates: a next generation of diagnostic and therapeutic platforms?," *Nano Converg.*, vol. 5, no. 1, pp. 1–18, 2018, doi: 10.1186/s40580-018-0170-1.

[14] P. Sapra and T. M. Allen, "Ligand-targeted liposomal anticancer drugs," *Prog. Lipid Res.*, vol. 42, no. 5, pp. 439–462, 2003, doi: 10.1016/S0163-7827(03)00032-8.

[15] Z. Shi, Y. Zhou, T. Fan, Y. Lin, H. Zhang, and L. Mei, "Inorganic nano-carriers based smart drug delivery systems for tumor therapy," *Smart Mater. Med.*, vol. 1, pp. 32–47, 2020, doi: 10.1016/j.smaim.2020.05.002.

[16] J. Jiang, J. Pi, and J. Cai, "The Advancing of Zinc Oxide Nanoparticles for Biomedical Applications[1] J. Jiang, J. Pi, and J. Cai, 'The Advancing of Zinc Oxide Nanoparticles for Biomedical Applications,' vol. 2018, 2018.," *Bioinorg. Chem. Appl.*, vol. 2018, p. 18, 2018.

[17] M. Canta and V. Cauda, "Biomaterials Science The investigation of the parameters a ff ecting the ZnO nanoparticle cytotoxicity behaviour : a tutorial review," 2020, doi: 10.1039/d0bm01086c.

[18] A. Ancona *et al.*, "Lipid-Coated Zinc Oxide Nanoparticles as Innovative ROS-Generators for Photodynamic Therapy in Cancer Cells," doi: 10.3390/nano8030143.

[19] P. Taylor, Y. T. Chung, M. M. Ba-abbad, and A. W. Mohammad, "Functionalization of zinc oxide (ZnO) nanoparticles and its effects on polysulfone-ZnO membranes," no. July 2015, doi: 10.1080/19443994.2015.1067168.

[20] S. Ghaffari, M. Sarrafzadeh, and Z. Fakhroueian, "Functionalization of ZnO nanoparticles by 3-mercaptopropionic acid for aqueous curcumin delivery : Synthesis , characterization , and anticancer assessment," *Mater. Sci. Eng. C*, vol. 79, pp. 465–472, 2017, doi: 10.1016/j.msec.2017.05.065.

[21] P. Saravanan, K. Jayamoorthy, and S. Anandakumar, "Ac ce p te d cr t," *Sensors Actuators B. Chem.*, 2015, doi: 10.1016/j.snb.2015.05.069.

[22] Y. Liao, Z. Hu, Q. Gu, and C. Xue, "Amine-Functionalized ZnO Nanosheets for Efficient CO2 Capture and Photoreduction," pp. 18847–18855, 2015, doi: 10.3390/molecules201018847.

[23] X. Yang, C. Zhang, A. Li, J. Wang, and X. Cai, "PT SC," *Mater. Sci. Eng. C*, p. #pagerange#, 2018, doi: 10.1016/j.msec.2018.10.066.

[24] A. Luchini and G. Vitiello, "Understanding the Nano-bio Interfaces : Lipid-Coatings for Inorganic Nanoparticles as Promising Strategy for Biomedical Applications," vol. 7, no. May, pp. 1–16, 2019, doi: 10.3389/fchem.2019.00343.

[25] J. Liu, A. Stace-naughton, X. Jiang, and C. J. Brinker, "Porous Nanoparticle Supported Lipid Bilayers (Protocells) as Delivery Vehicles," pp. 1354–1355, 2009.

[26] K. Zeng, J. Li, Z. Zhang, M. Yan, Y. Liao, and X. Zhang, "targeted drug carriers : study on cell-specific toxicity in vitro and lymphatic targeting in vivo," *J. Mater. Chem. B*, 2015, doi: 10.1039/C5TB00486A.

[27] B. Dumontel *et al.*, "Enhanced biostability and cellular uptake of zinc oxide nanocrystals shielded with a phospholipid," *J. Mater. Chem. B*, 2017, doi: 10.1039/c7tb02229h.

[28] "Exosomes_ biogenesis, biologic function and clinical potential _ Cell & Bioscience _ Full Text." .

[29] F. Susa, T. Limongi, B. Dumontel, V. Vighetto, and V. Cauda, "Engineered Extracellular Vesicles as a Reliable Tool in Cancer Nanomedicine," 2019.

[30] Y. T. Sato *et al.*, "Engineering hybrid exosomes by membrane fusion with liposomes," *Nat. Publ. Gr.*, no. February, pp. 1–11, 2016, doi: 10.1038/srep21933.

[31] R. van der Meel, E. Sulheim, Y. Shi, F. Kiessling, W. J. M. Mulder, and T. Lammers, "Smart cancer nanomedicine," *Nat. Nanotechnol.*, vol. 14, no. 11, pp. 1007–1017, Nov. 2019, doi: 10.1038/s41565-019-0567-y.

[32] J. Ferlay *et al.*, "Cancer statistics for the year 2020: An overview," *Int. J. Cancer*, vol. 149, no. 4, pp. 778–789, 2021, doi: 10.1002/ijc.33588.

[33] C. Li, H. Zhang, X. Gong, Q. Li, and X. Zhao, "Graphical abstract," *Colloids Surfaces B Biointerfaces*, 2018, doi: 10.1016/j.colsurfb.2018.11.043.

[34] T. A. Singh, J. Das, and P. C. Sil, *Jo ur l P re of.* Elsevier B.V, 2020.

[35] L. Tan, C. He, X. Chu, Y. Chu, and Y. Ding, "Charge-reversal ZnO-based nanospheres for stimuli-responsive release of multiple agents towards synergistic cancer therapy," *Chem. Eng. J.*, vol. 395, p. 125177, 2020, doi: 10.1016/j.cej.2020.125177.

[36] D. Warther *et al.*, "Porous silicon based intravitreal platform for dual-drug loading and controlled release towards synergistic therapy," *Drug Deliv.*, vol. 25, no. 1, pp. 1537–1545, 2018, doi: 10.1080/10717544.2018.1486474.

[37] P. P. Nanoparticles, G. Babos, E. Bir, M. Meiczinger, and T. Feczk, "Dual Drug Delivery of Sorafenib and Doxorubicin," pp. 1–12, 2018, doi: 10.3390/polym10080895.

[38] K. I. David, L. R. Jaidev, S. Sethuraman, and U. M. Krishnan, "DUAL DRUG LOADED CHITOSAN NANOPARTICLES – SUGAR-COATED ARSENAL AGAINST PANCREATIC CANCER," *Elsevier B.V.*, 2015, doi: 10.1016/j.colsurfb.2015.08.038.

[39] S. Barui, R. Gerbaldo, N. Garino, R. Brescia, F. Laviano, and V. Cauda, "Facile chemical synthesis of doped ZnO nanocrystals exploiting oleic acid," *Nanomaterials*, vol. 10, no. 6, pp. 1–15, 2020, doi: 10.3390/nano10061150.

[40] J. Coates, "Encyclopedia of Analytical Chemistry -Interpretation of Infrared Spectra, A Practical Approach," *Encycl. Anal. Chem.* pp. 1–23, 2004.

[41] M. Carofiglio, S. Barui, V. Cauda, and M. Laurenti, "Doped zinc oxide nanoparticles: Synthesis, characterization and potential use in nanomedicine," *Appl. Sci.*, vol. 10, no. 15, 2020, doi: 10.3390/app10155194.